

Cross-Frequency Phase-Amplitude Coupling in Brain Oscillations

Soheila Samiee

Doctor of Philosophy

Integrated Program in Neuroscience,
Department of Neurology and Neurosurgery,

McGill University, Montreal, Quebec, Canada
2019



A thesis submitted to McGill University in partial fulfillment of the requirements
for the degree of Doctor of Philosophy.

©Soheila Samiee, 2019

Abstract

The brain is a complex biological system with different capabilities from responding to environmental stimuli in a fraction of a second, to information integration, creative processing, decision making, learning and memory. It is composed of numerous interconnected neural circuits, at multiple scales, forming the static and dynamical substrate of brain functions and behavior. The static properties of brain networks are essentially those of the anatomical structure of the brain, with anatomical connections between brain regions and neural ensembles. The dynamical aspect is related to the neurophysiological activity of neural circuits and of their interactions in real time. Brain rhythmic fluctuations represent a significant portion of these dynamical aspects. Interactions between oscillatory rhythms are thought to be involved in the spatial and temporal integration of information by the brain. Recent findings have provided strong evidence of such interactions with different brain functions but the actual mechanisms remain unclear. Hence, in-depth studies of this phenomenon will improve our knowledge of the dynamical aspects of brain neural networks in health and disease.

The main objective of my dissertation was to study cross-frequency interactions between neural oscillations at different rhythms, with an emphasis on phase-amplitude coupling. One of the first challenging issues in studying cross-frequency phase-amplitude coupling is in obtaining accurate measurements from electrophysiological recordings. My first study was dedicated to proposing an analytical approach for improved identification and measurement of phase-amplitude coupling in a time-resolved manner for a variety of experimental designs. In a second study, I further analyzed how cross-frequency phase-amplitude coupling was related to the epileptic phenotype of a rodent model of mesial temporal lobe epilepsy. We found expressions of excessive coupling between the phase of slow non-REM sleep oscillations – reflecting excitability cycles – and the amplitude of high-frequency oscillations in the seizure onset zone of the epileptic animals. We also observed a positive linear relationship between this abnormally elevated phase-amplitude coupling and the number of epileptic seizures per day. In my

last study, I investigated the phase-amplitude coupling signatures of healthy brain functions with auditory pitch discrimination as a model. Using magnetoencephalography (MEG) source imaging, we found that delta-phase to beta-amplitude coupling significantly increased during task performance compared to baseline resting state in auditory cortex and inferior frontal gyrus regions. This physiological coupling was over-expressed in individuals affected by a tone deafness syndrome called amusia. Our findings highlight the regions, the nature of their activity and their interactions that are crucial to auditory pitch perception, which is involved in higher-order brain functions such as music appreciation and natural speech processing in language.

Overall, the present research body of work confirms that cross-frequency phase-amplitude coupling improves the characterization of the nature of brain activity, and how it is compromised in certain pathological changes. Future research will look into the translation potential of the measure in detecting and monitoring the progression of brain disorders.

Résumé

Le cerveau est un système biologique complexe aux capacités multiples, de la réponse aux stimuli environnementaux en une fraction de seconde à l'intégration d'informations sensorielles multimodales, au processus créatif, la prise de décision, l'apprentissage et à la mémoire et le langage. Il est composé de nombreux circuits neuronaux interconnectés, à plusieurs échelles, formant le substrat structurel et dynamique des fonctions cérébrales et du comportement.

L'architecture des réseaux cérébraux est essentiellement celle de la structure anatomique des connexions cérébrales reliant régions et ensembles neuronaux. L'aspect dynamique est lié à l'activité neurophysiologique des circuits neuronaux et leurs interactions en temps réel. Les fluctuations rythmiques du cerveau représentent une partie importante de ces aspects dynamiques. On fait l'hypothèse que les interactions entre rythmes oscillatoires à différentes fréquences sont impliquées dans l'intégration spatiale et temporelle de l'information par le cerveau. Des découvertes récentes ont fourni de solides preuves de telles interactions dans différentes fonctions cérébrales, mais la connaissance des mécanismes impliqués est encore bien incomplète. Par conséquent, des études approfondies des phénomènes associés sont nécessaires pour éclaircir la nature des manifestations dynamiques saines et pathologiques au sein des réseaux cérébraux.

L'objectif principal de ma thèse a été d'étudier les interactions entre oscillations neuronales à différents rythmes, en mettant l'accent sur le couplage phase-amplitude. L'obtention de mesures précises à partir d'enregistrements électrophysiologiques est nécessaire à l'étude du couplage phase-amplitude. Ma première étude visait donc à proposer une approche analytique pour une identification et des mesures améliorées du couplage phase-amplitude résolues dans le temps, qui soient également valides dans diverses conditions expérimentales. Dans une seconde étude, j'ai analysé le lien entre le couplage phase-amplitude et le phénotype épileptique d'un modèle rongeur d'épilepsie du lobe temporal médian. J'ai découvert des expressions de couplage excessif entre la phase d'oscillations lentes du sommeil non REM - rythmées par les cycles d'excitabilité neuronale - et l'amplitude d'oscillations hautes-fréquences dans la zone de dé-

clenchement des crises. J'ai également observé une corrélation positive entre ce couplage phase-amplitude anormalement élevé et le nombre de crises d'épilepsie par jour vécues par chaque animal. Dans ma dernière étude, j'ai mis en évidence les signatures de couplage phase-amplitude dans un modèle de fonction cérébrale saine, la discrimination auditive de la hauteur tonale. En utilisant l'imagerie des sources magnétoencéphalographiques (MEG), j'ai pu constater que le couplage de la phase des ondes delta avec l'amplitude des oscillations bêta augmentait considérablement au cours de l'exécution de la tâche par rapport à l'état initial de repos, dans le cortex auditif et les régions du gyrus frontal inférieur. Ce couplage physiologique était surexprimé chez les individus atteints du syndrome de surdité tonale appelé amusie. Mes résultats mettent en évidence les régions, ainsi que la nature de leur activité et de leurs interactions, qui sont essentielles à la perception auditive tonale, et qui sont également impliquées dans des fonctions cérébrales avancées telles que l'appréciation de la musique et le traitement naturel de la parole dans le langage.

Ainsi, mes travaux de recherche montrent que le couplage inter-fréquentiel phase-amplitude caractérise de manière plus détaillée la nature de l'activité cérébrale et la manière dont elle est compromise par certains changements pathologiques. Des recherches futures examineront le potentiel de telles mesures dans la détection et le suivi de la progression des troubles cérébraux.

Acknowledgements

Firstly, I would like to express my sincere gratitude and appreciation to my supervisor Prof. Sylvain Baillet for his continuous support, patience, motivation and encouragements. His constant guidance helped me in all steps of my PhD research. I am truly grateful for his unwavering help, dedication, and enthusiasm.

I am grateful to my committee members, Dr. Jean Gotman and Dr. Etienne de-villers-Sidani for their invaluable time, consultation, and assistance throughout my research; not only for their insightful comments and encouragement, but also for the hard questions which incited me to widen my research from various perspectives.

I would like to express my thanks to my co-authors and collaborators, especially Dr. Peretz and Dr. Avoli for their valuable comments and suggestions, and also Dr. Florin and Dr. Levesque for providing data. I would also like to thank my friends and colleagues, especially Elizabeth Bock for all her help in data collection and analysis as the MEG system manager, Francois Tadel for all helps related to Brainstorm, and my good friends in the lab Peter, Jie, Jeremy, Jason, and Justine. I will never forget our lunch times and social events.

Last but not least, I would like to express my very profound gratitude to my family: my mother, who supported me in every single step of this journey despite our geographical distance; and my husband, Mehdi, for his continuous encouragement, support and patience during this period. This accomplishment would not have been possible without them. My special thanks goes to my little princess, Kowsar, who brought a lot of joy, fun and happiness to our life, and also made me work more efficiently to be able to spend enough time with her at home.

I also gratefully acknowledge the funding sources that made my PhD work possible. This work was supported by a grant from National Science and Engineering Research Council of Canada (NSERC), and a studentship from the Integrated Program in Neuroscience of McGill University.

Contents

1	Introduction	1
1.1	Motivation	1
1.2	Overview of the thesis	4
1.3	Contribution of Authors	5
1.4	Contribution to original knowledge	6
2	Chapter 2: Literature review	8
2.1	Brain oscillations	8
2.2	Cross-frequency coupling	11
2.2.1	Network architecture and CFC types	13
2.2.2	CFC functions	17
2.2.3	CFC in health and disease	23
2.2.4	Methods for PAC calculation	26
2.3	Epilepsy	29
2.3.1	Introduction and definitions	29
2.3.2	Treatment	30
2.3.3	Pathophysiology	31
2.3.4	Mesial temporal lobe epilepsy (MTLE)	33
2.3.5	Summary	33
2.4	Pitch discrimination	34
2.4.1	Anatomy of pitch perception	34
2.4.2	Brain dynamics of pitch discrimination	35
2.4.3	Congenital amusia	36
2.4.4	Summary	37
2.5	Conclusion	37
3	Chapter 3: Time-resolved phase-amplitude coupling in neural oscillations	38
3.1	Preface	38
3.2	Abstract	40
3.3	Introduction	41

3.4	Material and Methods	43
3.4.1	Principles	43
3.4.2	Sparse estimation of time-resolved PAC	47
3.4.3	Statistical tests for tPAC	48
3.4.4	Experimental data	48
3.5	Results	51
3.5.1	Time-resolved estimation of PAC properties: frequency for phase, amplitude and coupling strength	51
3.5.2	Methods comparison study	53
3.5.3	Electrophysiological data	58
3.6	Discussion	62
3.7	Conclusion	63
3.8	Supporting information	65
3.8.1	Asymmetric synthesized data	65
3.8.2	Interpolation of the coupling maps	66
4	Chapter 4: Phase-amplitude coupling and epileptogenesis in an animal model of MTL	67
4.1	Preface	67
4.2	Abstract	70
4.3	Introduction	72
4.4	Material and methods	73
4.4.1	Animal Preparations	73
4.4.2	Analysis of seizures and seizure onset zones	74
4.4.3	Extraction of NREM sleep epochs	74
4.4.4	Phase-amplitude coupling analysis	77
4.4.5	Statistical analysis	78
4.5	Results	79
4.5.1	Seizures and interictal spikes	79
4.5.2	Power effect: slow-wave oscillations and ripple band	80
4.5.3	Phase-amplitude coupling	81
4.6	Discussion	86
5	Chapter 5: Neurophysiological network dynamics for pitch discrimination	91
5.1	Preface	91
5.2	Abstract	93
5.3	Introduction	95

5.4	Material and Methods	97
5.4.1	Participants	97
5.4.2	Experimental design	97
5.4.3	Data acquisition	99
5.4.4	Data preprocessing and source modeling	99
5.4.5	Event-related responses	100
5.4.6	Regions of interest	100
5.4.7	Monitoring of vigilance: posterior alpha-band activity	101
5.4.8	Phase-amplitude coupling	101
5.4.9	Stimulus-brain response coupling	102
5.4.10	Effective connectivity estimation with directed phase-transfer entropy	102
5.4.11	Statistical analyses	103
5.5	Results	103
5.5.1	Behavior	103
5.5.2	Event-related responses	105
5.5.3	Posterior alpha power	106
5.5.4	Phase-amplitude coupling	106
5.5.5	Directed functional connectivity	110
5.6	Discussion	113
6	General discussion & conclusion	120
6.1	Summary of findings and discussions	120
6.2	Future research	124
6.2.1	Mechanisms	124
6.2.2	Inter-regional coupling	125
6.2.3	PAC and epilepsy	126
6.3	Conclusion	127
	List of Publications	128
	Bibliography	129

List of Figures

2.1	Cross frequency coupling neural architecture.	15
2.2	Cross frequency coupling types.	16
2.3	Cross frequency coupling functions.	19
2.4	Hypothetical models of cross-frequency coupling in health and schizophrenia.	24
2.5	Obtaining cross-frequency phase-amplitude coupling.	27
2.6	Role of dis-inhibition in seizure-generating neuronal networks.	32
3.1	tPAC procedure	43
3.2	Illustrations of the effect of the coupling strength parameter	50
3.3	Illustration of tPAC analysis outcome on a synthesized data set.	52
3.4	Performance comparisons of selected PAC methods against tPAC	55
3.5	Phase-amplitude coupling from LFP data recorded in the third layer of a rat entorhinal cortex	59
3.6	Time-resolved tPAC parameters related to behavior	60
3.7	A sample of synthesized data with phase-amplitude coupling generated using asymmetric duty cycle model for frequency for phase.	65
4.1	Typical recordings from control and epileptic animals.	76
4.2	Seizure onset zone and interictal spikes in epileptic animals.	80
4.3	Phase-amplitude coupling in EEG recordings.	82
4.4	PAC coupling strength.	84
4.5	Distributions of the phase of fast oscillatory activity coupled to slow-wave oscillations.	85
5.1	Experimental design, and regions of interest	98
5.2	Behavioral performances, vigilance and event-related EEG responses.	105
5.3	Phase-amplitude coupling analyses.	107
5.4	Directed functional connectivity analyses and summary of findings.	111

List of Tables

2.1 Brain oscillations in neural networks	10
-----------------------------------------------------	----

List of Acronyms

AAC	Amplitude amplitude coupling
AD	Alzheimer's disease
ADHD	Attention-deficit hyper activity disorder
AF	Arcuate fasciculus
CFC	Cross frequency coupling
EEG	Electroencephalography
ERP	Event-related potential
fMRI	Functional magnetic resonance imaging
GABA	Gamma amino butyric acid
GLM	General linear model
HFO	High frequency oscillations
HYP	Hypersynchronous-onset
IFG	Inferior frontal gyurs
IRCFC	Inter-regional cross-frequency coupling
LFP	Local field potential
LVF	Low-voltage fast-onset
ILAE	International League Against Epilepsy
MBEA	Montreal battery of evaluation of amusia
MEG	Magnetoencephalography
MRI	Magnetic resonance imaging
MTLE	Mesial temporal lobe epilepsy
NDPAC	normalized direct phase-amplitude coupling
OCS	Obsessive-compulsive disorder
PAC	Phase amplitude coupling
PFC	Phase frequency coupling

PPC	Phase phase coupling
PET	positron emission tomography
PING	Pyramidal interneuron gamma
PD	Parkinson's disease
PV+	Parvalbumin-positive
SPECT	Single photon emission computed tomography
SOZ	Seizure-onset zone
STDP	Spike timing dependent plasticity
TPAC	time-resolved phase amplitude coupling

1

Introduction

"Clocks tick, bridges and skyscrapers vibrate, neuronal networks oscillate. Are neuronal oscillations an inevitable by-product, similar to bridge vibrations, or an essential part of the brain's design?"

Buzsáki and Draguhn [2004]

1.1 Motivation

Neurons and other nerve cells are considered to be the fundamental units of the nervous system. The neuron is an electrically excitable cell which connect with other cells via synapses; and synapses are specialized structures, which let neurons communicate through electrical or chemical signals. Synaptic signals can be either excitatory or inhibitory, increasing or reducing the net voltage of the target cell, respectively. A typical neuron consists of three main components: a soma (i.e. the cell body), an axon, and several dendrites. From the computational standpoint, the neuron is thought to be the basic processing unit of the brain [McCulloch and Pitts, 1943]. It receives and integrates inputs from other neurons, and discharge a spike if the integrated inputs exceed a critical level of excitation. These spikes, also called action potentials, are providing a medium for communication between cells.

Introduction

Brain functions and behavior are not enabled by single neural cells; they emerge from cell assemblies and network circuits, as the outcome of complex interactions between neural cells [Gerstein and Kirkland, 2001]. Through development and learning, these interactions contribute to shaping the actual connections and wiring between neurons in circuits and assemblies that typically work together. Principal cells (i.e. neurons) also wire with inhibitory interneurons, which play an important role in enabling sophisticated computational processes [Buzsaki, 2006; Friedrich et al., 2013]. The synchronized cellular activity within neural ensembles produce rhythmic fluctuations also called *brain rhythms* or *neural oscillations*, that are observed at multiple scales of neurophysiological recording. There is a vast literature of empirical observations of these oscillations in different species both *in vivo* and *in vitro* (e.g. in mice [Buhl et al., 1998], rats [Chrobak and Buzsáki, 1998], monkeys [Kreiter and Singer, 1992], cats [Gray and Singer, 1989] and human being [Hari and Salmelin, 1997; Bragin et al., 1999]), and basic research on their signal origins and their functional characteristics across the frequency spectrum [Steriade et al., 1993; Freeman, 2004; Buzsáki and Draguhn, 2004; Buzsáki et al., 2012]. These oscillations are shown to be related to the interdependent dynamics of excitatory principal cells and inhibitory interneurons [Buzsaki, 2006], and are widely studied markers of brain functions and dysfunctions.

The synaptic weights in connected neural assemblies are plastic and they can change through short-term and long-term potentiations. The functional role of brain oscillations expressed in various frequency ranges is widely researched. My thesis intends to contribute to such clarification effort. So far, oscillations are thought to bind neurons into assemblies with transient synchronization of cells through dynamic connections [Engel et al., 2001; Varela et al., 2001]. Such mechanism would facilitate synaptic plasticity and bias input selection [Buzsaki, 2006]. Synchronous oscillations are also involved in the production and enhancement of neuronal temporal correlation [Harris et al., 2003], which is necessary for spike timing dependent plasticity (STDP) [Wang, 2010]. Symmetrically, neuronal synchronization patterns can be influenced by STDP [Izhikevich, 2006; Cassenaer and Laurent, 2007; Nowotny et al., 2008; Thivierge and

Introduction

Cisek, 2008; Fründ et al., 2009]. Therefore, oscillations are at minimum signal markers of neuroplasticity of the brain. They are also suggested to contribute to the temporal representation and long-term consolidation of information ([Buzsáki and Draguhn, 2004; Jacobs et al., 2007]).

Overall, brain oscillations are actively studied as signal markers for bridging the neural dynamics of brain systems and circuits to complex behavior [Somers and Kopell, 1993; Engel et al., 2001; Steriade, 2001; Hasselmo et al., 2002; Whittington and Traub, 2003; Niell and Stryker, 2010; Buschman et al., 2012], including network formation and processing for sensory perception, memory, and even consciousness [Gray et al., 1989; Kahana et al., 2001; Engel et al., 2001; Canolty and Knight, 2010]. While we have made considerable progress in the understanding of the cellular and molecular machinery of neural cells and their environment, major knowledge and technical gaps remain to comprehend the emergence of complex behaviors from brain circuits, and the diverse and profound phenotypes of brain disorders. For all the reasons we have just briefly reviewed, studying neural oscillations can contribute to our better understanding of integrating mechanisms relating the dynamics of neural circuits to behavior in health and disease [Buzsaki, 2006; Baillet, 2017].

Most electrophysiological studies in the field have used different forms of power spectral decompositions of electrophysiological signals in one or several empirically-defined frequency bands of interest [Buzsáki and Draguhn, 2004; Baillet, 2017]. More recently, strong interest has emerged about the study of interdependencies between oscillatory signals at distinct frequencies. As we will review below, such manifestations of cross-frequency coupling (CFC) are associated with complex brain functions. For instance, in the conceptual framework of active inference in brain functions [Rao and Ballard, 1999; Friston, 2005], it is hypothesized that brain oscillations may enable distinct channels for feedforward and feedback communication between brain regions and systems [Buzsáki and Draguhn, 2004; Fontolan et al., 2014]. Dynamic interactions between oscillations are also associated with items registration and manipulation in working memory tasks [Axmacher et al., 2010], or information segregation in the hippocampus

Introduction

[Colgin et al., 2009]. Hence, methods for identifying and characterizing interactions between oscillating rhythms are essential to advance the understanding of the biological mechanisms of brain functions and dysfunctions.

The main purpose of this thesis was to contribute to the relatively new field of research on interdependencies between brain oscillatory fluctuations at different frequencies. My goals were 1) to contribute a new versatile and time-resolved approach to measuring cross-frequency interactions, and to validate the approach in (2) an animal model of partial epilepsy and (3) the brain networks of human auditory pitch processing, using different modalities of electrophysiology, to demonstrate the flexibility and generalizability of the approach and tools.

1.2 Overview of the thesis

The rest of this dissertation is organized as follows. Chapter 2 provides a detailed literature review on neural oscillations, cross-frequency coupling (its definition, brain network architectures, types and functions, known patterns in health and disease, and associated signal processing methods), epilepsy (as a disease model investigated with cross-frequency coupling subsequently in the thesis), and auditory pitch discrimination (a brain function also studied with CFC measures in our third work).

A novel method for cross-frequency phase-amplitude coupling calculation is proposed and presented in Chapter 3. This technique is demonstrated first with synthesized data, and compared to existing methods. Chapter 4 details a study on how phase-amplitude coupling is affected in a rodent model of mesial temporal lobe epilepsy. Investigation of phase-amplitude coupling in human auditory pitch discrimination in normal hearing and amusia – a neurological disorder affecting pitch processing and music perception and appreciation – are presented in Chapter 5. Chapter 6 concludes the thesis with a general discussion about my contributions and suggests future research directions in the field.

1.3 Contribution of Authors

I am the first author of all three manuscripts included in this dissertation. In all experiments, I performed the methodological developments, software implementations, data processing, and analysis of the results. The contributions of the co-authors include supervision of the research, providing data, technical discussions, funding and review of manuscripts. The summary of contributions of the co-authors of each manuscript is provided in the following:

Manuscript 1: Samiee, S. and Baillet, S. Time-resolved phase-amplitude coupling in neural oscillations. *NeuroImage*, 159:270–279, 2017

- Soheila Samiee introduced a new algorithm for time-resolved phase-amplitude coupling analysis that is presented in this manuscript. This involved identifying the problem, suggesting a solution with mathematical formulation, and software implementation. The method was evaluated with ground-truth simulated data and empirical local field potential (LFP) data. The initial draft and final version of the manuscript was written by Soheila Samiee, and she produced all figures of the paper.
- Sylvain Baillet supervised all aspects of this work. He also reviewed and contributed to writing of the manuscript.

Manuscript 2: Samiee, S., Lévesque, M., Avoli, M., and Baillet, S. Phase-amplitude coupling and epileptogenesis in an animal model of mesial temporal lobe epilepsy. *Neurobiology of disease*, 114:111–119, 2018

- Soheila Samiee was responsible for designing the method, writing analysis scripts, performing data analyses, producing all figures and writing drafts and the final version of the manuscript.
- Maxime Levesque collected the data, marked the seizures and helped with interpreting the results and reviewed the manuscript.

Introduction

- Massimo Avoli helped with results interpretation and reviewed the manuscript.
- Sylvain Baillet supervised the project, provided funding, and contributed to the writing of the manuscript.

Manuscript 3: Samiee, S., Florin, E., Vivan, D., Albouy, P., Peretz, I., and Baillet, S. Oscillatory network dynamics for pitch discrimination. *Submitted*

- Soheila Samiee was responsible for designing the analysis method, wrote the codes, performed data analyses, produced all figures and wrote drafts and the final version of the manuscript.
- Esther Florin and Dominique Vuvan were involved in data collection and study design.
- Philippe Albouy contributed to the approach and reviewed the final version of the manuscript.
- Isabelle Peretz was responsible for the study design, co-funding, and reviewed the final version of the manuscript.
- Sylvain Baillet was responsible for supervising the project, co-funding, as well as editing drafts and the final version of the manuscript.

1.4 Contribution to original knowledge

The main original contributions of this thesis are the following:

1. In the study presented in chapter 3, we introduced a novel method for time-resolved phase-amplitude coupling estimation. The algorithm was implemented in *Brainstorm*, which is open-source software, and the Matlab codes are publicly available in *GitHub* (<https://github.com/SoheilaSamiee/Phase-amplitude-coupling-estimation>).
2. In chapter 4, using the same algorithm, we revealed augmented phase-amplitude coupling related to epileptogenesis in an animal model of MTLE. The study featured two original contributions. First, we showed that the coupling of the amplitude of fast oscillations

Introduction

along the phase of NREM-sleep slow oscillations during inter-ictal periods was elevated in the seizure onset zone. Second, our results revealed for the first time that the strength of that coupling was positively correlated to the severity of the phenotype (as by the daily number of seizures).

3. In chapter 5, we analyzed phase-amplitude coupling in a pitch-discrimination study, a common auditory task, in amusics and healthy controls. We found expressions of delta-to-beta PAC in both groups during pitch processing, with greater strengths in amusia. This over-expression accompanied functional disconnection (decreased of effective connectivity in amusic brains).

2

Chapter 2: Literature review

This chapter reviews the literature about neural oscillations, their cross-frequency coupling, with an emphasis on phase-amplitude coupling. I then briefly introduce backgrounds about epilepsy, pitch discrimination and amusia, which are the models I used for transferring my methodological developments to neuroscience applications, in my second and third studies. More details are provided in the introduction parts of each study.

2.1 Brain oscillations

Brain is a complex system that receives and processes sensory inputs from the environment. These inputs need to be encoded and properly registered for actual processing, yielding perception. One possible generic mechanism is that the brain segregates perceptual events by packing (i.e. grouping) information in time. For instance, [Buzsaki \[2006\]](#) proposed that this is achieved via circuits of coupled *neural oscillators*. A beneficial function of such packing function would be in ordering successive events, establishing causation, and deriving predictions concerning future likely events. Another important function is the integration of distributed processes in the brain [[Levine et al., 1999](#)]. Even very simple sensory-motor behaviors require the coordination of several neural assemblies across the brain. The temporal coordination of oscillatory

Chapter 2: Literature review

neural activities has been proposed as a mechanism for information integration [Gray, 1994; Gray et al., 1989]. The mechanisms ruling the local and inter-regional dynamics of brain oscillations remain to be clarified and understood.

Brain oscillations are reflections of rhythmic neural activities, which can be generated through different mechanisms. In individual neurons, they manifest in the form of rhythmic firing which leads to the excitation or inhibition of post-synaptic neurons, or produce sub-threshold (oscillatory) fluctuations of membrane potentials. At a larger scale, oscillations emerge from interactions between neuronal ensembles, which leads to population synchronization and oscillatory wave propagation [Wang, 2010; Lu et al., 2017; Zhang et al., 2018]. Although the spiking of single principal cells in the cortex typically follow Poisson statistics [Bair et al., 1994], oscillations can emerge from neural assemblies [Gray et al., 1989; Laurent, 1996; Destexhe and Sejnowski, 2003; Buzsáki, 2010]. One key reason behind this observation could be related to the specialized mechanisms for grouping principal cells via inhibitory interneurons [Buzsáki and Draguhn, 2004]. These interneurons can achieve this goal by generating a narrow window for effective excitation and rhythmically modulating the firing rate of excitatory neurons [Cardin et al., 2009]. Three basic physiologically-plausible circuit architectures allow neuronal circuits to synchronize spiking activity and generate periodic rhythms: (i) synaptic coupling between inhibitory inter-neurons, (ii) reciprocal loops between inhibitory and excitatory cells, and (iii) electrical synapses via gap junctions [Wang, 2010]. The actual frequency of such oscillations depend on the decay time of inhibition [Börgers and Kopell, 2005].

Neural and brain oscillations are readily observed *in vivo* and *in vitro*, in multiple brain regions, across all recording scales and several species [Buzsáki and Draguhn, 2004]. Some oscillatory components are self-organized (i.e. spontaneous emergence without external trigger) during rest and sleep [Buzsáki, 2006]. Others are evoked (i.e. time- and phase-locked to stimulus onset) or induced (with looser constraints in terms of timing and phase) in response to sensory inputs [Onitsuka et al., 2013]. Local synchronous oscillating cell assemblies at different

Chapter 2: Literature review

Table 2.1: Brain oscillations in neural networks: a brief summary of some observed oscillations in the brain with the associated anatomies and functions. *Adopted form [Uhlhaas and Singer, 2013] under (CC BY-NC-ND 3.0)*

	Theta (4-7 Hz)	Alpha (8-12 Hz)	Beta(13-30 Hz)	Gamma (30-200 Hz)
Anatomy	Hippocampus, prefrontal cortex, sensory cortex, limbic system	All cortical structures, thalamus, hippocampus	All cortical structures, subthalamic nucleus, hippocampus, basal ganglia, olfactory bulb	All cortical structures, hippocampus, retina, olfactory bulb, tectum, basal ganglia
Function	Memory, synaptic plasticity, top-down control, long-range synchronization	Inhibition, attention, long-range synchronization	Sensory gating, attention, perception, motor control, long-range synchronization, top-down control, consciousness	Perception, attention, memory, consciousness, synaptic plasticity, motor control

frequency bands are typically observed in electrophysiology during cognitive task performance, with functions related to cognition, learning and memory process [Ward, 2003; Albouy et al., 2017] (Table 2.1).

These oscillatory activities are reported in different frequency bands – such as delta, theta, alpha, beta, and gamma – and in multiple patterns including sleep spindles and thalamo-cortical oscillations. Oscillations in the theta (4-8 Hz) and gamma (30-145 Hz) frequency bands are associated with memory functions in rodents, human, and non-human primates [Düzel et al., 2010]. Gamma rhythms (30 - 200 Hz) are suggested to mark information processing in cortical networks [Uhlhaas et al., 2011]. However, the study of electrophysiological activity during complex behaviors requires looking into multiple, possibly interrelated frequency bands. For example, although hippocampal theta oscillations were initially thought to be the only key signal marker of memory processes [Winson, 1978; O’Keefe, 1993; Tesche and Karhu, 2000; Jones and Wilson, 2005], interactions between theta and gamma rhythms via cross-frequency

phase-amplitude coupling were found to be key to the organization of memory functions across multiple time scales in episodic memory [Buzsáki and Moser, 2013] and shown to be correlated with memory performance in rodent models [Tort et al., 2009] and human participants [Canolty et al., 2006; Griesmayr et al., 2010]. Furthermore, such coupling may support the retention and manipulation of working memory items [Axmacher et al., 2010], enabling for instance, multiple channels of information transfer between sub-regions of the hippocampus and the enthorinal cortex [Colgin et al., 2009]. Hence, in addition to single band oscillations, analysis of interactions between these rhythms is an important concept, which has been receiving increasing scientific attention in the study of brain functions. I review in details this phenomenon, known as cross-frequency coupling, in the next subsection.

2.2 Cross-frequency coupling

Studies of the possible functional role played by neural oscillations have reported on rhythms in band-limited frequency ranges [Goldman et al., 2002; Klimesch, 1998; Tallon-Baudry and Bertrand, 1999]. They showed how oscillations are related to memory, sensory perception and cognition [Cohen, 2008]. Beyond these numerous and typical single-band effects, signal interactions between frequency bands have also been reported [Buzsáki and Draguhn, 2004; Canolty et al., 2006; Tort et al., 2008; Axmacher et al., 2010]. Such interactions, also known as cross-frequency coupling, represent a phenomenon well observed and investigated in electrophysiology [Buzsaki, 2006].

Recent studies, reporting on cross-frequency coupling in several brain regions, suggest that it could be a marker of functional activation [Canolty and Knight, 2010]. It was also shown that cognitive performance and its load [Tort et al., 2008, 2009], as well as sensory perception and task performance is associated with changes in the intensity of this coupling [Allen et al., 2011; Dimitriadis et al., 2015]. These CFC have been suggested to be mediated by sub-populations of interneurons – with slower and faster dynamics – which are observed in both neocortex

Chapter 2: Literature review

and hippocampus [Tort et al., 2007; Vierling-Claassen et al., 2010; Hyafil et al., 2015b]. For theta-gamma coupling in particular, in vitro studies have revealed the respective cellular and network origins of each oscillatory component and of their interactions. Low-gamma (30-80 Hz) was found to be produced by interactions within GABAergic inhibitory interneuron networks (denoted "interneuron network gamma" or ING), and by interactions between excitatory pyramidal cells and local inhibitory interneuron networks (denoted: "pyramidal-interneuron network gamma" or PING) [Freeman et al., 1975]. Theta activity is suggested to be the frequency resonance peak of local [Bao and Wu, 2003] and remote networks [Whittington and Traub, 2003] consisting of both pyramidal cells and interneurons [Hutcheon and Yarom, 2000]. Theta-gamma coupling is also suggested to be driven by interneuronal sub-populations. Wulff et al. [2009] used genetically modified mice to show that hippocampus theta-gamma coupling is mainly driven by parvalbumin-positive (PV+) inhibitory interneurons. They further showed that ablation of synaptic inhibition in PV+ cells with genetic modification led to strongly altered theta-gamma coupling in the CA1 of freely behaving mice [Wulff et al., 2009].

As explained for hippocampal theta-gamma coupling, there are two main requirements for a circuit to generate CFC: (i) producing oscillations at two distinct frequency bands, and (ii) coupling between the neural populations that generate each of the oscillations [Hyafil et al., 2015b]. Synchronization of spiking activity leading to generation of oscillatory rhythms can be achieved by synaptic coupling between different types of inhibitory and excitatory neurons and gap junctions [Wang, 2010]. The synchronization mechanisms based on chemical synapses are: recurrent excitation between principal neurons (driven by mutual excitation between pyramidal cells), mutual inhibition between interneurons (driven by inhibitory interneuronal network), and feedback inhibition through the excitatory-inhibitory loop (driven by reciprocal interactions between excitatory and inhibitory neural pools). Finally, gap junctions contribute to the synchronization of spiking activity via electrical synapses between neurons (see [Wang, 2010] for more details on these mechanisms). In the next section, we further explain possible types of coupling between neural circuits with various architectures, and how these architectures may

lead to the different known types of CFC.

2.2.1 Network architecture and CFC types

Interactions between neural circuits that each generate individual oscillation can lead to CFC. Depending on the nature of the coupling between neural populations and the architecture of the network, different types of CFC can be observed. The coupled networks can be either intermingled or connected [Hyafil et al., 2015b]. A CFC network is said to be intermingled when the neural populations that generate each oscillation share a common sub-population (Fig. 2.1A), with this common sub-population leading to coupling between the two networks. Intermingled CFC networks are suggested to be the sources of theta-gamma phase-amplitude coupling in hippocampus [Gloveli et al., 2005; Wulff et al., 2009]. An excitatory network is hypothesized to be shared between the fast spiking cells generating gamma oscillations, and oriens-lacunosum moleculare (O-LM) cells that generate theta-band fluctuations [Tort et al., 2007].

In the case of connected networks, the oscillations are generated from two independent neural circuits. However a uni- or bidirectional connection between the two circuits leads to interactions between generated oscillations in the form of CFC. Reciprocally connected networks produce bidirectional coupling (Fig. 2.1B), while a uni-directional coupling (Fig. 2.1C) is the result of one network actively driving and modulating another oscillatory network. Most theoretical models assume that the network generating the slow oscillation drives the other network producing faster oscillatory signals [Hyafil et al., 2015b]. Yet, Jiang et al. [2015] suggested that a reverse mechanism may also exist. The proposed architecture was used to model auditory theta-gamma coupling in speech perception, where two separate inhibitory-excitatory networks generate oscillatory activity, with theta network driving the gamma oscillation's circuit through a unidirectional connection [Hyafil et al., 2015a].

Another architecture is that of a uni-directional CFC with an external sensory rhythmic input driving the network of fast and slow oscillations leading to coupling (Fig. 2.1D). Pre-

Chapter 2: Literature review

vious research has shown that rhythmic external sensory and motor events [Lakatos et al., 2008; Saleh et al., 2010; Luo and Poeppel, 2007] in addition to internal cognitive processes related to learning and memory [Rizzuto et al., 2006] can entrain low-frequency activity. Therefore, co-occurrence of low-frequency phase entrainment and phase-amplitude CFC implies that high-frequency amplitude modulation by CFC can be entrained and coordinated by slower, behaviorally-relevant internal and external events [Canolty and Knight, 2010]. This model has been tested in a non-human primate vision study, reflecting the modulation of thalamic gamma with slower LFP oscillations driven by periodic visual stimuli [Mazzoni et al., 2008].

Another factor that determines the characteristics of the network is the coupling strength between neural populations. This will lead to either continuous or intermittent CFC [Fontolan et al., 2013]. In continuous CFC, fast oscillations are present at all phases of the slow rhythm. It can happen due to a weak connection from slow to fast oscillatory networks which cannot bring fast oscillation out of oscillatory mode in any particular phase of the slow rhythm's cycle. However, in intermittent CFC – which is a form of CFC with stronger connection between the two networks – fast oscillations are only present during a restricted phase interval of slow rhythms. Coupling strength may also reflect the type of CFC coupling. Jensen and Colgin [2007] suggested four main types of coupling between neural oscillations: amplitude-amplitude coupling (AAC), phase-phase coupling (PPC), phase-frequency coupling (PFC), and phase-amplitude coupling (PAC). The relation between coupling strength and CFC type is that when slow- and fast-oscillatory networks are weakly coupled, such that the intrinsic forces driving each of them are stronger than the synaptic conductance between the two, the amplitude modulation of fast rhythms becomes negligible, yielding phase-phase coupling. In turn, strongly connected networks may yield all the above types of coupling, including phase-amplitude coupling, amplitude-amplitude coupling, and phase-frequency coupling [Hyafil et al., 2015b].

In amplitude-amplitude coupling, the amplitude of a slower rhythm modulates the amplitude (or average power) of fast oscillations (Fig. 2.2B). Cross-frequency amplitude-amplitude

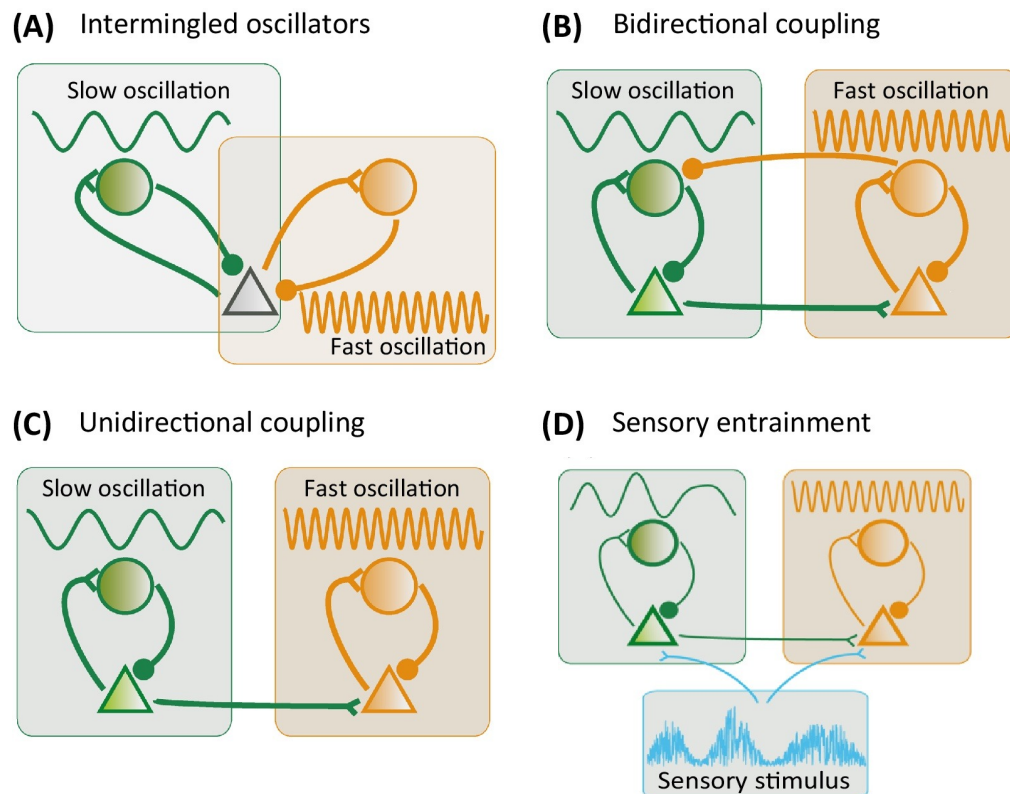


Figure 2.1: Cross frequency coupling neural architecture. A) CFC generated by an intermingled network: the two populations generating the individual oscillations overlap partially. In this example, a sub-population of excitatory neurons (shown with a triangle) contributes to the generation of both slow and fast oscillations, while the inhibitory networks (depicted with circles) generating each oscillation are distinct. B) A reciprocal bidirectional coupling, with two separate inhibitory-excitatory networks for the generation of each oscillation. C) Unidirectional coupling, with two separate networks responsible for the generation of rhythms. Only one network projects onto the other. D) A sub-type of unidirectional network, with sensory stimuli driving the neural population generating the fast and slow oscillations (*original figure from Hyafil et al. [2015b], replicated with permission*)

coupling occurs on top of phase-amplitude coupling when the slow oscillation is asymmetric (the ascending phase has a different duration than the descending phase – duty cycle $\neq 0.5$) [Hyafil et al., 2015b]. Bruns and Eckhorn [2004] showed an example of such coupling between delta and gamma oscillations in the occipital cortex. In a few other studies, this type of coupling was reported between alpha and gamma rhythms in the human visual cortex, where the amplitude of alpha oscillations negatively modulated that of gamma fluctuations during a visual task [Jensen and Mazaheri, 2010; Spaak et al., 2012; Jensen et al., 2014]. Consistent with previous

Chapter 2: Literature review

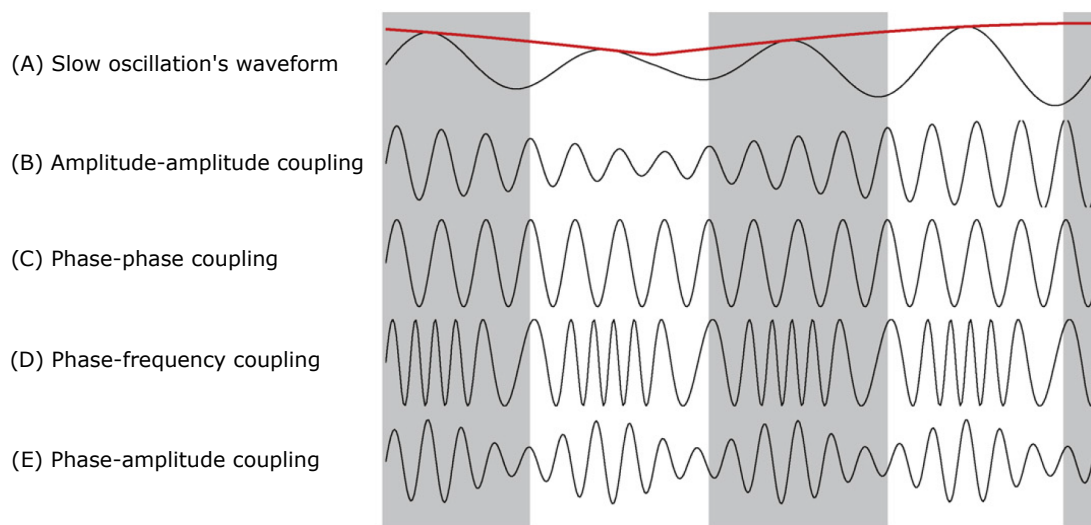


Figure 2.2: Cross frequency coupling types: A) A slow oscillatory signal (for example at 4 Hz): the frequency is fairly stable but the amplitude (red line) changes over time. This slow oscillation can be coupled to faster rhythms in different ways: B) amplitude-amplitude coupling: the amplitude of the fast rhythm is correlated with the amplitude of the slow oscillation. C) phase-phase coupling: there is a $n:m$ phase locking between the phase of fast and slow rhythms, here in each cycle of the slow rhythm there are four cycles of the fast oscillation (4:1). D) phase-frequency coupling: the frequency of fast oscillations is modulated by the phase of the slow rhythm. E) phase-amplitude coupling: the amplitude of fast oscillations changes with the phase of the slow oscillation in a rhythmic manner. These four types of coupling are not mutually exclusive. (Reproduced with permission from [Jensen and Colgin, 2007])

reports on AAC, such alpha-gamma AAC was accompanied by alpha-gamma PAC [Osipova et al., 2008; Roux et al., 2013], and the visual alpha rhythms evoked in this task are known to be asymmetric [Mazaheri and Jensen, 2008].

In phase-phase coupling, there is a $n:m$ phase locking between two oscillations at different frequencies (Fig. 2.2C). A fixed number (n) of fast oscillations' cycles occur over m cycles of the slower rhythm. Such type of coupling was observed between theta and gamma in the rat hippocampus during maze exploration [Belluscio et al., 2012], and in the human neocortex during a motor task [Darvas et al., 2009]. See also Schack et al. [2002]; Palva et al. [2005]; Fell and Axmacher [2011]; Zheng and Zhang [2013]; Scheffer-Teixeira and Tort [2016] for additional reports on this type of coupling.

Frequency-phase coupling is the modulation of the frequency of fast oscillations by the

Chapter 2: Literature review

phase of a slower rhythm (Fig. 2.2D). This is a type of CFC where a slow-rhythm network modulates the excitability of neural populations oscillating faster. Fontolan et al. [2013] and Onslow et al. [2014] proposed computational models and simulations of this type of coupling. To our knowledge however, it has not been reported in experimental data yet. One reason could be simply technical, due to difficulties in identifying instantaneous-frequency modulations in electrophysiological recordings [Hyafil et al., 2015b].

Phase-amplitude coupling is the modulation of the amplitude of fast oscillations by the phase of a slower rhythm (Fig. 2.2E). It is also referred to as "nested oscillations" in the literature. Empirical reports of PAC indicate observations in various frequency ranges and using a variety of recording and signal analysis techniques [Canolty and Knight, 2010; Schroeder and Lakatos, 2009b; van der Meij et al., 2012]. PAC between slow oscillations and gamma can be achieved via sparse-spiking Pyramidal Interneuron Gamma (PING) networks [Spaak et al., 2012; Hyafil et al., 2015a], but not occur in dense-spiking oscillations [Onslow et al., 2014]. Sparse-spiking gamma rhythms are prominent in sensory brain areas.

Phase-amplitude coupling (PAC) is a widely studied form of CFC [Canolty and Knight, 2010]. It has been suggested as a mechanistic component involved in spatial exploration [Jensen and Lisman, 1998], working memory [Lisman and Buzsáki, 2008] and visual perception [VanRullen and Koch, 2003; Palva and Palva, 2011]. Several other studies have shown that PAC measures reveal task-dependent neural responses in cognitive processes [Axmacher et al., 2010; Fell and Axmacher, 2011; Tort et al., 2008, 2009; Schutter and Knyazev, 2012]. It has been observed in several species (e.g., mice, rats, cats, monkeys, and humans) and in different brain regions including hippocampus, neocortex and basal ganglia [Canolty and Knight, 2010].

2.2.2 CFC functions

It has been suggested that CFC plays a functional role in neuronal local activation, inter-areal communication and neural plasticity [Tort et al., 2009; Canolty and Knight, 2010]. It is also

Chapter 2: Literature review

proposed that CFC may serve as a mechanism for information transfer from large-scale brain networks (operating at behavioral timescales) to the fast local cortical processing necessary for synaptic modification and effective computation [Canolty and Knight, 2010]. It is a candidate mechanism for the integration of multiple temporal and spatial scales in brain computation [Palva et al., 2005; Sauseng et al., 2008; Holz et al., 2010; Palva et al., 2010]. Possible functions of CFC can be categorized in three main groups: Multi-item and sequence encoding, synchronization of fast rhythms for long-distance communication, and temporal parsing of continuous stimuli [Hyafil et al., 2015b]. Each category and its putative architecture is detailed in the following.

Multi-item or sequence encoding

Neural systems need to maintain representations of distinct items without interference. Such items include visual objects or the motor commands to be performed in a successive order to enable a complex motor sequence, or multiple items to be retained and manipulated in working memory (Fig. 2.3A). Neural oscillations, and CFC in particular, provide an efficient mechanism to this aim by temporally clustering the spiking activities associated to each item in a distinct phase of an ongoing slow oscillation. This allows down-stream neural systems to retrieve a particular item as they tune to its associated phase [Jensen, 2001; Akam and Kullmann, 2010]. The original idea is based on a model proposed by Lisman and colleagues for hippocampal theta-gamma coupling [Lisman and Idiart, 1995; Jensen and Lisman, 2005]. Lisman and Idiart [1995] indeed suggested that humans can store up to 7 items in short-term memory through having them represented in a burst of gamma (~ 40 Hz) cycles nested in a slower oscillation (5-12 Hz). The memory patterns were shown to repeat at each cycle of the slow oscillation. Such a mechanism was also found in the alpha-gamma coupling over the occipito-parietal cortex in a visual working memory task [Roux and Uhlhaas, 2014], and multi-item representations in working [He et al., 2010; Fontolan et al., 2014] and spatial memory in the hippocampus [Lisman, 2005; Lisman and Buzsáki, 2008], and visual attention in visual cortex [Jensen et al.,

Chapter 2: Literature review

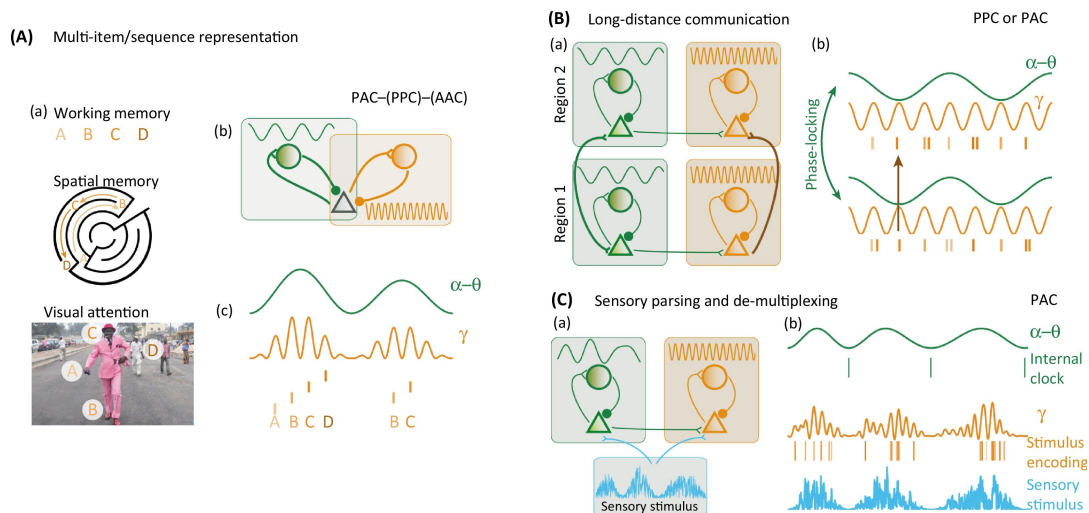


Figure 2.3: Cross frequency coupling functions. A) multi-item or sequence encoding: (a) Three examples of multi-item encoding in working memory, spatial memory and visual attention tasks, with (b) a possible associated architecture: an intermingled network with an excitatory sub-population shared between the inhibitory populations responsible for generating each of the slow and fast oscillations. This function can be computationally achieved by PAC, PPC and AAC. (c) Schematic of coupled slow and fast rhythms, and representation of each item in a separate cycle of the faster oscillation. B) Long-distance communication: (a) Potential architecture: four separate networks of excitatory-inhibitory neurons generating slow (green) and fast oscillations (orange), excitatory sub-networks of slow oscillations are connected making slow rhythms synchronized between Region 1 and Region 2. Local CFC in each of the two regions also facilitates the synchronization of faster rhythms. (b) Schematic of local PPC in each region and synchronized slow oscillations, resulting in phase-locked faster oscillations. C) Sensory parsing: (a) Potential architecture: a rhythmic sensory stimulus (blue) fed into both slow and fast oscillation networks. Direct connection from slow to fast oscillations controls and optimizes local sensory processing at fast oscillations with more power being assigned to more-informative stimulus periods. (b) Sensory decoding with fast oscillations nested in slower rhythms - main spiking occurs at a certain phase of the slow rhythm. (*Replicated with permission from [Hyafil et al., 2015b]*)

2014] and other instances of multi-item representations [VanRullen and Koch, 2003; Lisman and Buzsáki, 2008] (Fig. 2.3A-a). CFC enables a form of time compression for the neural representation of successive elements, and could be involved in binding mechanisms and neural plasticity [Fell and Axmacher, 2011].

This function of CFC can be expressed via an intermingled network consisting of two separate inhibitory sub-populations and a sharing pyramidal-cell sub-network [Tort et al., 2007],

Chapter 2: Literature review

or via a direct connection between two inhibitory sub-populations [Malerba and Kopell, 2013] (Fig. 2.3A-b). Phase-amplitude coupling, phase-phase coupling and amplitude-amplitude coupling can all implement a form of multi-item encoding [Hyafil et al., 2015b], although PAC is the most widely studied and observed in empirical data. With PAC, the number of items that can be stored depends on the number of cycles of fast oscillation that can fit in each cycle of the slow rhythm. Hence, the ratio between the typical theta and gamma frequency ranges would be compatible with the maximum number of items (7 ± 2) that can be stored in human short-term memory [Lisman and Idiart, 1995] (Fig. 2.3A-c). Interestingly, it is shown that even this capacity can be altered in high-load tasks, with modulations of the slow frequency (via decrease in slow oscillation's frequency to fit more gamma cycles in each period of it) [Axmacher et al., 2010].

Long-range communication

One of the main possible roles for neural oscillations is their capacity to enable selective communication between brain regions. One of the most studied hypotheses is that of coherent, phase-locked oscillations as markers of inter-regional communication between the nodes of brain networks [Fries, 2009]. The frequency range of these rhythmic fluctuations may depend on the spatial scale of the inter-node distances. For instance, faster oscillations at gamma frequency could channel a mechanism for communication at local scales, particularly for bottom-up processes [Fries et al., 2007; Fries, 2009; Von Stein and Sarnthein, 2000]. Alternatively, oscillations at lower frequencies (< 12 Hz) are hypothesized to channel longer-range functional connections [Von Stein and Sarnthein, 2000; Solomon et al., 2017]. Both local and long-range network communications could also benefit from a form of coupling between slow and fast rhythmic fluctuations [Buzsáki and Draguhn, 2004]. Indeed, synchronization of local gamma oscillations over distant regions could be accomplished by locking their occurrences to the same phase of slower rhythms of interconnected regions [Fell and Axmacher, 2011; Roux et al., 2013]. Fig. 2.3B, depicts how such mechanisms could yield synchronization of fast oscillations

Chapter 2: Literature review

at two distant regions (shown with a brown connecting line), subserved by the long-range connection of the networks generating the slow oscillations (shown in green) and local CFC in each region. This type of phenomenon has been shown in the hippocampus [Tort et al., 2007; Colgin et al., 2009] and visual cortex [Doesburg et al., 2009; Bosman et al., 2012; Saalmann et al., 2012; McGinn and Valiante, 2014]. The associated signalling principle of CFC could be either PPC or PAC [McGinn and Valiante, 2014; Hyafil et al., 2015b]. Fig. 2.3B-b shows how PPC would explain this phenomenon, with coherent fast oscillations locked to also-coherent slow rhythms via local PPC in each region. The raster plot shown under the faster oscillatory time series indicates how the firing pattern in Region 2 follows that of Region 1.

Temporal parsing of continuous stimuli

Many biological stimuli are temporally organised or composed of rhythmic patterns. For example, natural speech waveforms are modulated by the rhythmicity of prosody at different (syllable, phrase, sentence) rates [Rosen, 1992]. This extends to the vast majority of sensory inputs, especially in the conceptual framework of active sensing [Schroeder et al., 2010]: e.g., odors are best perceived with rhythmic sniffing patterns, visual scenes are explored with motifs of brief fixations separated by saccadic eye movements. We can posit that such active explorations of our sensory environment entrain slow rhythmic activity in primary sensory areas, with faster oscillations possibly signalling the actual processing of sensory inputs [Fries et al., 2007; Mazzoni et al., 2008; Pasley et al., 2012; Hyafil et al., 2015b,a]. The active sensing framework is aligned with the theory of predictive coding [Mehta, 2001]: the brain constantly predicts the sensory inputs based on the context; when this prediction does not match the sensory input, a prediction error is sent back to the higher-order circuits to update the biological representation of internal predictive model, which leads to behavioral adaptation and learning [Clark, 2013]. In this context, slow rhythms could support crucial timing processes involved in the prediction of sensory inputs, such as the parsing of time-varying stimuli (e.g., speech) and modulating the allocation of local computational resources (manifested e.g., via local gamma oscillations)

Chapter 2: Literature review

at the expected timing of sensory events [Schroeder and Lakatos, 2009a; Canolty and Knight, 2010; Gross et al., 2013b; Panzeri et al., 2014].

The notion of sensory entrainment is defined as the temporal alignment of neural activity in sensory systems with time-varying features of the environment [Sameiro-Barbosa and Geiser, 2016]. This entrainment results in local slow rhythms in sensory areas getting locked to some of the dynamical properties of sensory inputs [Luo and Poeppel, 2007; VanRullen and Macdonald, 2012]. For instance, the auditory cortex can be entrained by audio streams, from temporally-organised sequences of pure tones [Lakatos et al., 2013] to natural speech [Gross et al., 2013b]. Such entrainment is related to task performance in perception [Sameiro-Barbosa and Geiser, 2016], when the detection and registration of sensory cues are enhanced when occurring systematically at a preferred phase of intrinsic oscillations [Ng et al., 2012]. Faster oscillations coupled to slower entrained rhythms are hypothesized to be involved in the prediction and registration of predicted sensory events – a mechanisms which may extend beyond sensory perception to a generic communication process between brain networks.

Phase-amplitude coupling has been proposed as a possible mechanism to implement such functions [Hyafil et al., 2015b] (Fig. 2.3C). For example, MEG shows that beta-band (15-35 Hz) bursts issued by the motor system entrain a slower harmonic responses from auditory cortices to align their phase with the expected occurrence of incoming sounds [Morillon and Baillet, 2017]. There is further electrophysiological evidence that supports the idea that beta-band activity conveys temporal prediction signals in the context of sensory entrainment [Sameiro-Barbosa and Geiser, 2016]. One potential mechanism could be that beta-band activity in motor systems be a marker of predictive signaling for active sensing, resetting the phase, via PAC, of lower-order (e.g., sensory) systems.

Summary

In summary, CFC measures interdependencies between brain rhythmic fluctuations. The actual functional role of CFC is widely studied but remains to be clarified. The most researched manifestation of CFC is that of PAC, which has been observed in all three categories of investigated functions.

2.2.3 CFC in health and disease

Alterations of cross-frequency coupling, and of PAC in particular, have been reported in several neurological and mental disorders. In Parkinson's disease (PD), extensive beta to high-frequency oscillations (HFO) coupling was observed in LFP recordings from the subthalamic nucleus (STN) [López-Azcárate et al., 2010]. Such coupling decreased significantly when deep brain stimulation was applied to that structure. Hence, CFC could be signal marker of the pathophysiological mechanisms of the disease. Shimamoto and colleagues further showed exaggerated slow rhythms (theta–beta) to gamma PAC in the primary motor cortex (M1) synchronized to STN neural discharges in PD patients [Shimamoto et al., 2013]. High levels of PAC coupling strength between beta (13-30 Hz) phase and gamma (50-200 Hz) amplitude was also reported in the M1 arm region of PD patients by de Hemptinne et al. [2013]. Here too, the coupling strength was reduced after application of deep brain stimulation that alleviated PD symptoms [De Hemptinne et al., 2015].

Whether these observations generalize to other syndromes is being extensively studied. For instance, CFC reports are less clear in schizophrenia: Allen et al. [2011] compared CFC in an oddball task between large groups of schizophrenia patients vs. healthy controls. PAC was overall lower in patients, with exceptions over fronto-temporal scalp electrodes. There was also an association between genetic polymorphisms and CFC. Spencer et al. [2009] and White et al. [2010] also reported reduced coupling in the auditory cortex of schizophrenic patients, but between different bands (delta-to-gamma and alpha-and-gamma, respectively). Kirihara et al.

Chapter 2: Literature review

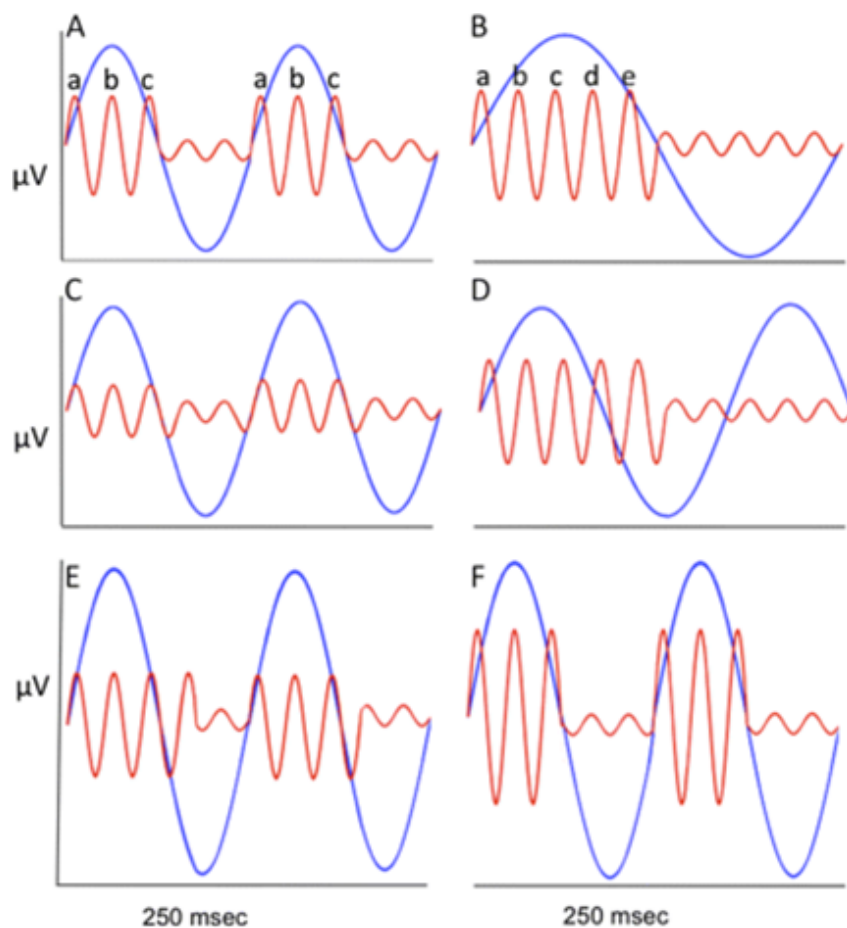


Figure 2.4: Hypothetical models of cross-frequency coupling in schizophrenia. A-B: possible forms of coupling in health; A) CFC during a memory task in which gamma amplitude (shown in red, 40 Hz) increases at the peak of the theta cycle (shown in blue, 8 Hz). B) Increased working memory load associated with the slowing of theta oscillations (from 8 to 4 Hz) while the amplitude of gamma signals remains constant: more items can therefore be registered within each theta cycle leading to increased working memory capacity. C-F: hypothetical CFC disease models ; C) gamma amplitude is altered while theta oscillations remains same as A. D) slowing of theta oscillations from 8 to 6Hz; hence, one theta cycle cannot cover all five cycles of gamma. E) increase of theta amplitude affects coupling by decreasing the relative salience of gamma amplitude at the peak of theta phase. F) increased theta amplitude leads to augmented gamma amplitude and enhances the strength of theta-gamma coupling. One negative consequence could be in decreasing the dynamic flexibility of network information processing (*replicated with permission from [Moran and Hong, 2011]*)

[2012] also tested a large group of schizophrenic patients and control subjects in a steady-state auditory stimulation study, but did not observe significant differences in CFC between the two groups. I emphasize that the experimental protocols and analysis methods were different from the other two studies, which may account for some of the discrepancy in their respective

Chapter 2: Literature review

findings. Moran and Hong [2011] suggested a model for CFC alteration in schizophrenia based on interactions between slow and fast oscillations in the form of phase-amplitude coupling (Fig. 2.4). Figure 2.4A-B depicts the possible dynamics of gamma-theta coupling in health, and Fig. 2.4C-F represents four hypothetical disease models of coupling.

Alzheimer's disease (AD) is another disorder currently investigated with CFC markers. In a transgenic mouse model of the disease, decreased theta-to-gamma coupling in hippocampal in vitro preparations were shown to precede $A\beta$ accumulation [Goutagny et al., 2013]. This suggests a possible role of PAC as signal marker of early AD pathogenesis. Such observations were replicated using in vivo LFP recordings in the same AD mouse model, with decreases of theta-to-gamma coupling in recordings from the hippocampus and parietal cortex, however not from prefrontal regions [Zhang et al., 2016].

In epilepsy, increased CFC was found in the seizure onset zone during ictal periods in children with medically-intractable epilepsy (secondary to focal cortical dysplasia) [Ibrahim et al., 2014] and during sleep in adult patients with pharmaco-resistant focal epilepsy [Amiri et al., 2016]. In social anxiety disorders, excessive resting-state delta-to-beta CFC coupling was decreased in response to behaviorally-efficient pharmacological interventions [Miskovic et al., 2011]. In obsessive-compulsive disorders (OCD) as well, effective deep brain stimulation decreased beta-to-gamma CFC in the mid-occipital cortex, to normal levels [Bahramisharif et al., 2016].

Summary

In summary, altered manifestations of CFC have been observed empirically in several disorders. The patterns of alterations with respect to normative variants are inconsistent between syndromes. This makes the picture more complex but may also points at CFC changes that may be disease specific. Overall, excessive expressions of CFC were more commonly reported in disorders so far. Further studies of the association of CFC parameters with specific pathophys-

iological changes are required.

2.2.4 Methods for PAC calculation

Cross-frequency coupling and PAC in particular have been receiving increasing interest in the last couple of decades. Several methods have been proposed, yet we need to emphasize several fundamental factors that negatively affect the performance of PAC measurements, leading to possible false detection and misinterpretations.

These factors originate from (see also Fig. 2.5A): (i) the biological dynamical system producing neural oscillations, (ii) the measurement of neural dynamics, or (iii) the mathematical approach for estimating PAC. For example, asymmetric slow oscillation cycles produce spurious PAC coupling in the absence of genuine cross-frequency interactions [Cole and Voytek, 2017]. Unavoidable filter distortions, instrument noise, or cross-talk between recorded signals can also lead to inaccurate CFC estimation. Finally, data non-stationarity, short data lengths and presence of signal discontinuities or artifacts in recordings also lead to inaccurate CFC estimates [Penny et al., 2008; Tort et al., 2010; Onslow et al., 2011]. Aru et al. [2015] suggested practical guidelines to minimize the influence of these nuisance factors.

There is presently no gold standard method for PAC estimation. Each published algorithm has its own advantages and limitations, depending on data length, signal-to-noise ratio (SNR), study design and required time resolution of PAC estimates (i.e. ongoing or event-related recordings), etc. All approaches typically proceed with completing the following three main steps: i) extraction of instantaneous narrow-band phase and amplitude from original recordings, ii) estimation of coupling between these two components and iii) evaluation of statistical significance of the resulting measure (Fig. 2.5). The first step mainly involves band-pass filtering of the signal and extracting the instantaneous phase and amplitude of the filtered data. Wavelet and Hilbert transforms are popular tools to this end. The different PAC algorithms are distinct mainly with respect to the second step.

Chapter 2: Literature review

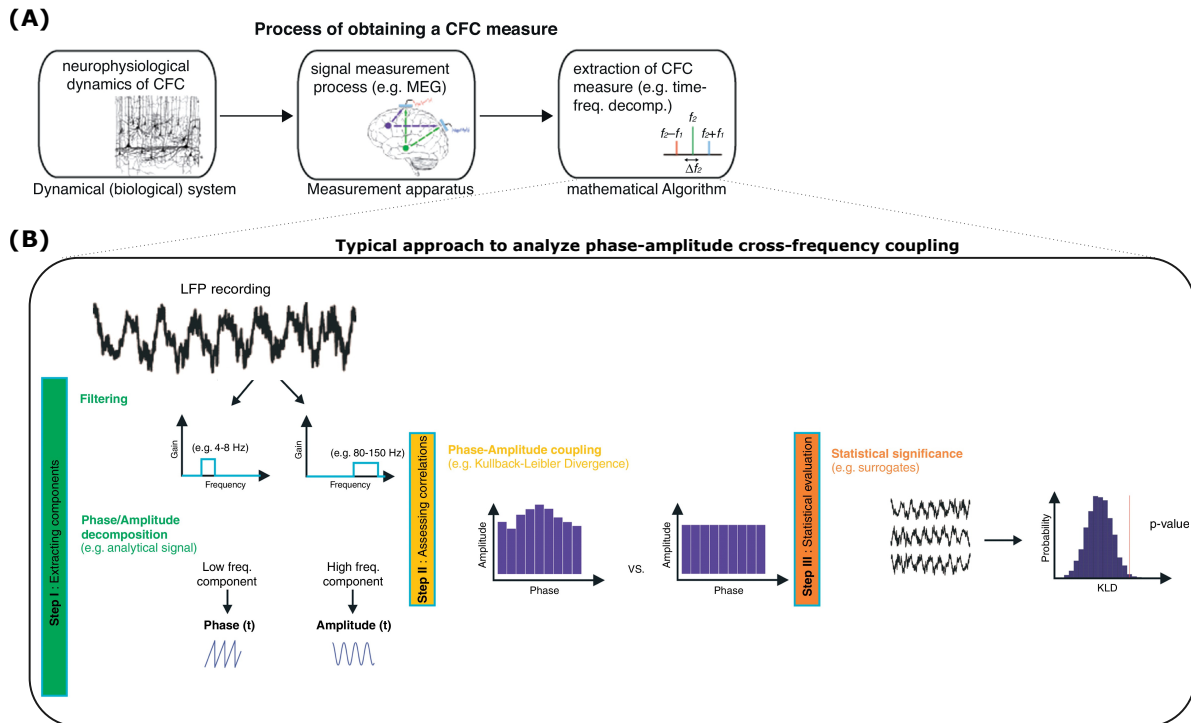


Figure 2.5: Estimation cross-frequency phase-amplitude coupling. A) Typical process for extracting CFC from time series: i) biological system producing observable dynamical changes, ii) recording of signal traces (e.g., LFP, EEG or MEG), and iii) CFC algorithmic estimation. B) Analytic pipeline for PAC estimation: i) Extraction of signal components: recordings are filtered within frequency bands of interest, instantaneous phase and amplitude are estimated, ii) Correlations between phase and amplitude statistics using a algorithm of interest (the schematic illustrates the modulation index method proposed by Tort et al. [2010]), iii) Statistical assessment: a parametric or non-parametric test is used to assess the statistical significance of the PAC estimate (*adapted from [Aru et al., 2015]*)

Canolty et al. [2006] suggested a method based on defining a complex signal consisting of the amplitude of the faster oscillations and the phase of slower rhythms at each time point. The temporal average of this signal provides estimates of the strength and the phase of the coupling. Two other algorithms were proposed and based on assessing the correlation between the instantaneous phase of the slow rhythms and the envelope of the fast oscillations using phase-coherence [Cohen et al., 2008], and phase-locking values [Penny et al., 2008]. Bruns and Eckhorn [2004] and Penny et al. [2008] investigated the correlation or the coherence between the amplitude of the slow rhythms – or original signal [Colgin et al., 2009] – and the envelope of the faster oscillations as a measure of phase-amplitude coupling. Later in 2010, Tort et al.

Chapter 2: Literature review

[2010] suggested an algorithm based on the Kullback-Leibler divergence between the uniform distribution and the distribution of faster oscillations' amplitude on the phase of slower rhythm. In absence of PAC, the amplitude of fast oscillations is expected to be randomly distributed over all phase angles of the slow-rhythm cycle, resulting in a uniform empirical distribution; therefore, the divergence from uniform distribution would be small and this outcome would reflect low coupling. Symmetrically, when faster oscillations occur preferentially at a certain phase angle of the slow cycle, the distribution (of fast oscillations' amplitude on the phase of slower rhythm) would peak at that phase angle, resulting in higher coupling strength values. Ozkurt [2012] proposed a method for PAC estimation based on a plain confidence limit formula, called normalized direct PAC (ndPAC), potentially improving the sensitivity and specificity of PAC estimation. Kramer and Eden [2013] suggested a PAC measure extracted from a general linear model (GLM) of the amplitude of fast oscillations depending on the phase of slower rhythms.

Most of these methods require relatively long data time series (several cycles of the slow rhythm) for meaningful estimation of PAC. However, one can expect that the strength of coupling changes dynamically with context, stimulus or brain states [Tort et al., 2008, 2009; Canolty and Knight, 2010]. Voytek et al. [2013] therefore proposed a method for deriving event-related estimations of PAC. With that approach, PAC coupling is measured over repeated trials rather than across time, yielding a time-resolved estimate of event-related PAC changes. This approach therefore cannot be used in studies of ongoing brain activity such as in sleep or the resting state. Dvorak and Fenton [2014] suggested an alternative approach using two different time scales: a global scale with longer time windows to detect coupled oscillations (i.e. the frequency of the coupled slow and fast rhythms), then a local time scale for time-resolved calculation of the coupling strength for this detected pair (from shorter time windows). Yet, transient expressions of PAC may not be detected after the first step is applied; hence, the method has poor sensitivity. Pittman-Polletta et al. [2014] used an adaptive decomposition approach to estimate PAC, and showed that their method was less sensitive to data non-stationarity with

Chapter 2: Literature review

optimum extraction of biological none narrow-band oscillations.

Assessment of the statistical significance of PAC estimates is the next key step. A common approach is to generate surrogate time series to derive an empirical distribution under the null hypothesis to be tested. Ideally, the surrogate dataset should only see its levels of CFC modified while keeping all other signal features (e.g., narrowband power) unchanged. This is challenging in practice with some approaches being more conservative than others [Aru et al., 2015; Florin and Baillet, 2018]. Phase-scrambling is a simple approach, but it alters the non-stationarity of the data (i.e., make it more stationary compared to real recordings) in addition to removing PAC [Nakamura et al., 2006]. An alternative is to select a few random time points (in the input) and shuffle the blocks defined between these points of either the instantaneous phase or amplitude time series [Canolty et al., 2006]. The smaller the number of points, the more conservative the outcome statistics will be [Aru et al., 2015]. van Wijk et al. [2015] also suggested a parametric approach for surrogate data generation based on a GLM of the epoched data, which is more computationally tractable.

In summary, several methods exist for PAC estimation, with respective assets and limitations. In the present thesis, I proposed a new method which alleviates most of the shortcomings of existing methods, which will be introduced and discussed in Chapter 3.

2.3 Epilepsy

2.3.1 Introduction and definitions

Epilepsy is a brain disorder which affects around 65 million people worldwide. It is one the most common chronic neurological syndromes [Thurman et al., 2011]. It is characterized by unpredictable and recurrent interruptions of brain's normal functions, called epileptic seizures [Fisher et al., 2005]. Epileptic seizures are defined as "a transient occurrence of signs and/or symptoms due to abnormal excessive or synchronous neuronal activity in the brain" [Fisher

Chapter 2: Literature review

et al., 2005].

The causes behind the disorder are diverse, which makes it a complex syndrome to capture generically. The International League Against Epilepsy (ILAE) defines epilepsy as a brain disorder presenting at least one of the following conditions: i) a minimum of two unprovoked (or reflex) seizures occurring more than 24 hours apart; (ii) one unprovoked (or reflex) seizure and a probability of further seizures (at least 60%) after two unprovoked seizures, occurring in next 10 years; (iii) diagnosis of an epilepsy syndrome [Fisher et al., 2014].

2.3.2 Treatment

The optimum goal of epilepsy treatment is seizure freedom without side effects. Unfortunately, this cannot be achieved in all patients. About 70% of patients keep their seizures under control with appropriate medication. The response rate and severity of side effects differ between variants of the epilepsy syndrome, its underlying causes, age and other factors [Duncan et al., 2006; Guerrini, 2006; Perucca, 2009; Perucca and Tomson, 2011]. Dietary changes can contribute to controlling seizure occurrences, in combination with drug treatment. The ketogenic diet is one of these interventions, with some efficacy in children with refractory (drug-resistant) epilepsy [Neal et al., 2008].

Despite a substantial increase of the number of anti-epileptic drugs over the past couple of decades [Moshé et al., 2015], one third of patients still do not respond to pharmacological interventions [Del Felice et al., 2010; Moshé et al., 2015]. Surgery is the only alternative option for cure in patients with focal epilepsy. The intervention involves the resection, destruction or disconnection of epileptic brain tissues, or neurostimulation implants [Moshé et al., 2015]. Surgical resection requires the clear identification of the seizure-onset zone [Jobst and Cascino, 2015]. Around half of the patients benefit from long-term seizure freedom after surgery [Petkar et al., 2012; De Tisi et al., 2011], with substantial improvement of their quality of life [Seiam et al., 2011; Hamid et al., 2014].

Chapter 2: Literature review

Therefore, improving the pre-surgical delineation of the seizure-onset zone would be key to the outcome for the other patients still affected by seizures [De Vos et al., 2007; Wang et al., 2013; Liu et al., 2016; Jacobs et al., 2016]. Magnetic resonance imaging (MRI) [Worrell et al., 2000], functional MRI (fMRI) [Seeck et al., 1998], positron emission tomography (PET) [Gok et al., 2013] and single photon emission computed tomography (SPECT) [Spencer, 1994; La Fougère et al., 2009] are all being used in the multidisciplinary assessment of complex cases. Beyond classical detection of spike and seizure onsets with scalp and intracranial EEG, neural oscillations have also raised a lot of interest in epilepsy research more recently. High-frequency oscillations (HFO) have been suggested as signal markers of the seizure-onset zone (SOZ) even during interictal periods [Urrestarazu et al., 2007; Jacobs et al., 2008; Dümpelmann et al., 2015]. The rate of HFO occurrences is higher in SOZ, and decreases with medication intake [Jacobs et al., 2008; Zijlmans et al., 2009].

2.3.3 Pathophysiology

Transient abnormal synchronization of neural assemblies is the electrographic signature of epileptic seizures. The phenomenon is thought to lead to the disruption of neuronal communication [Moshé et al., 2015]. Decreased inhibition or increased excitation are assumed to be physiological markers of the epileptic SOZ [Ackermann and Moshé, 2010; Galanopoulou, 2010; Liu et al., 2013]. Fig. 2.6 explains the mechanistic role of dis-inhibition in seizure generation. The extended seizure generation network (shown with an orange oval shape) consists of several excitatory and inhibitory neurons and interneurons at one or several brain regions. Under normal physiological conditions, the networks are controlled by inhibitory interneurons (shown in blue) (Fig. 2.6A). If the regulating inhibitory interneurons are further inhibited by other inputs, such exaggerated dis-inhibition can lead to over-excitation of the network, abnormal function and eventually a seizure (Fig. 2.6B). Therefore, multiple interacting aspects of inhibitory and excitatory cell types may contribute to pathological hyper-synchronization of neuronal networks into producing seizures (Fig. 2.6C) [Galanopoulou, 2010; Moshé et al., 2015].

Chapter 2: Literature review

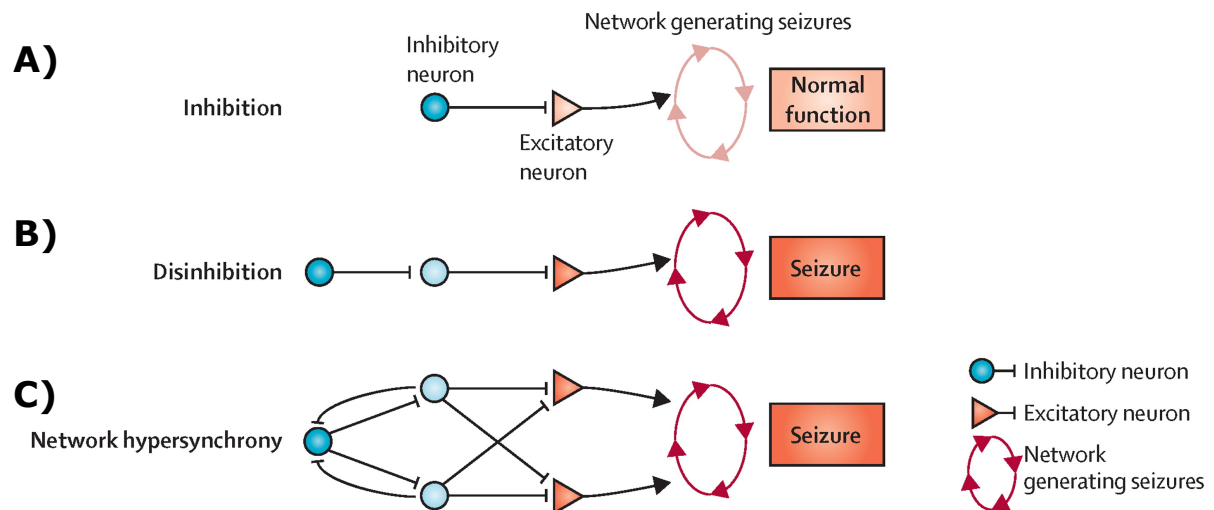


Figure 2.6: Role of dis-inhibition in seizure-generating neuronal networks. A) Normal function in a physiological condition: normal connection of inhibitory (small blue circle) and excitatory neurons (orange triangle) to the seizure generation network (orange oval shape) during normal brain function. The network that generates the seizures can be a complex network of several cell types located in one or expanding into several regions of the brain. B) Dis-inhibition leads to seizure: inhibition of inhibitory input can cause over-activation of the seizure generating network, which results in a seizure. C) Network hypersynchrony: interactions between inhibitory and excitatory neurons can also lead to pathological hypersynchrony of neurons and the initiation of seizures. (original figure from [Moshé et al., 2015])

Depending on the connectivity of the SOZ with other networks of the brain, a wide range of comorbidity disorders may affect epileptic patients, such as depression, attention-deficit hyperactivity disorders (ADHD), and other cognitive impairments [Beghi et al., 2006; Bertram, 2013]. Different networks can be involved at different stages of seizures: from their initiation to spreading and termination. The detection of the regions involved at each stage can be important to the diagnosis and intervention against seizures. The epileptic network may also change during development in the same individual [Galanopoulou, 2007]. Epigenetic factors (e.g., drug use, stress, inflammation) can also contribute to the plastic alterations of epileptic network dynamics [Galanopoulou and Moshé, 2014; Ono and Galanopoulou, 2012].

Several animal models of epilepsy have been contributed to better understand the factors of complexity of the syndrome [Coppola and Moshé, 2012]. Furthermore, advances in neuroimaging and neurophysiology have contributed to improve the localization of the SOZ and

Chapter 2: Literature review

the definition of propagation patterns in patients [Schevon et al., 2012; Toyoda et al., 2013]. These tools can be used to identify signal- and bio-markers of epilepsy development, progression, and to better identify the tissues that may be safely resected for treatment while preserving essential brain functions [Engel Jr et al., 2013].

2.3.4 Mesial temporal lobe epilepsy (MTLE)

Mesial temporal lobe epilepsy (MTLE) is the most common type of complex partial epilepsy in patients. MTLE seizures mainly arise from medial-temporal structures such as the hippocampus, amygdala, and entorhinal cortex [Spencer and Spencer, 1994; Salanova et al., 1994a; Engel Jr, 1996; Gloor, 1997; Chan et al., 1997; by Heinz-Gregor Wieser for the ILAE Commission on Neurosurgery of Epilepsy, 2004]. The syndrome is associated with cognitive impairments but do not affect attention and executive functions [Hermann et al., 1997]. MTLE patients do not usually respond well to anti-epileptic drug regimens; hence, surgery is the preferred option also because of the fairly localized seizure onset to medial temporal structures [Engel et al., 1997; Engel Jr, 2001]. In terms of pathophysiology, there is evidence of enhanced excitation in MTLE [Engel et al., 2001], or recurrent excitatory, inhibitory circuitry. More specifically, alterations of the expression of GABA_A receptor subunits can lead to decreased inhibition and hypersynchrony in MTLE. This alteration has been reported in both patients [Loup et al., 2000], and animal models of MTLE [Poulter et al., 1999; Peng et al., 2004]. GABA_A is one of the two types of principal inhibitory neurotransmitters in the brain (GABA: gamma amino butyric acid).

2.3.5 Summary

Epilepsy is one of the most common chronic neurological disorders, with great prevalence in development and adulthood. A possible cause is in the imbalance of inhibitory and excitatory mechanisms involving neural and brain networks. However, the syndrome is so diverse in its phenotypes that there is no single signal marker pertinent in all patients. Neuroimaging and

advanced electrophysiology are methods of choice for both the clinical and basic neuroscience of epilepsy, to better understand the mechanisms involved, improve detection and progression, and propose more efficient treatment alternatives to patients.

2.4 Pitch discrimination

Pitch discrimination is a basic capability of human perception used in our everyday life in auditory speech and music processing. Pitch is the fundamental frequency of a sound, which can be accurately measured with physical instruments, but can be perceived differently by each individual. Each person has a threshold for perceiving pitch differences beyond which stimulus discrimination becomes strikingly difficult [Albouy et al., 2013]. Individuals with severe forms of congenital amusia (tone deafness) are particularly challenged in perceiving tones at different pitches, which impairs their perception (and enjoyment) of music. The brain mechanisms for the perception of near-threshold stimulus changes are presently only partially understood.

Musical training contributes to improving pitch discrimination abilities [Micheyl et al., 2006] as found in trained musicians compared to the general population [Spiegel and Watson, 1984; Kishon-Rabin et al., 2001; Tervaniemi et al., 2005].

2.4.1 Anatomy of pitch perception

Functional brain imaging studies have mapped an extensive set of regions involved in pitch discrimination. They include the ventral auditory pathway with the superior temporal gyrus, inferior frontal lobule and some aspects of the prefrontal cortex [Zatorre et al., 1992; Gaab et al., 2003; Norman-Haignere et al., 2013; Albouy et al., 2013; Peretz, 2016; Hohmann et al., 2018]. Further anatomical evidence from diffusion-weighted MRI indicates that the connectivity of the arcuate fasciculus (AF), which connects the inferior frontal gyrus (IFG) to the auditory cortex, is also essential for the ability to detect small pitch changes [Loui et al., 2009]. AF connectivity is reduced in tone-deaf subjects, and superior AF connectivity strength is associated with indi-

vidual performances in pitch discrimination [Loui et al., 2009]. Furthermore, the motor cortex is involved in pitch discrimination, when temporal attention is required for the detection of pitch changes in a tone sequence [Chen et al., 2008; Zarate and Zatorre, 2008; Morillon and Baillet, 2017; Chang et al., 2018].

2.4.2 Brain dynamics of pitch discrimination

Empirical effects on brain oscillations have been reported during pitch discrimination [Albouy et al., 2013; Mazaheri et al., 2014; Florin et al., 2017]; however, the actual mechanisms involved remain elusive. Modulations of event-related potentials (ERP) – in terms of latency and amplitude – have been associated with individual performances in pitch discrimination [Sams et al., 1985; Tervaniemi et al., 1993; Brattico et al., 2001; Peretz et al., 2005; Tervaniemi et al., 2005]. Sams et al. [1985] reported on a mismatch negativity in the EEG around 170 ms after an unexpected deviant tone. The amplitude of this component is suggested to be associated with performance in pitch discrimination [Tervaniemi et al., 1993], and its latency is shorter in musicians vs. non-musicians [Brattico et al., 2001]. Albouy et al. [2013] performed the dynamical causal modeling of the N100m EEG component, which is salient in pitch processing. They showed in tone-deafness decreased intrinsic connectivity in both auditory cortices, increased lateral connectivity between auditory cortices, and decreased right fronto-temporal backward connectivity.

Florin et al. [2017] further showed that accuracy in a pitch discrimination task can be predicted from the amplitude of oscillatory activity before target-tone presentation. The power of theta oscillations (4-8 Hz) in the right inferior frontal cortex, and beta oscillations (12-30 Hz) in the right auditory cortex prior to the target tone presentation were found to be associated with correct detection of pitch changes [Florin et al., 2017].

More studies have reported effects in functional connectivity (based on neural oscillations) between brain regions during pitch processing. For example, Morillon and Baillet [2017]

Chapter 2: Literature review

showed that effective connectivity expressed in beta oscillations (18-24 Hz) from the left sensory-motor cortex directed to auditory regions, was associated with higher performances in the temporal anticipation of tones in a pitch discrimination task. Further effects in CFC interactions were also reported in auditory processing. [Fontolan et al. \[2014\]](#) showed that the phase of delta-beta activity in associative auditory cortex (AAC) modulated the gamma amplitude in A1 during speech processing, which suggests a possible role in information transfer between brain regions.

2.4.3 Congenital amusia

Congenital amusia or tone deafness is a disorder that mainly affects the perception and production of music [[Ayotte et al., 2002](#)]. It is not associated with any visible brain lesion, basic hearing impairment, cognitive deficit or lack of environmental stimulation [[Peretz et al., 2002](#)]. Around 4% of the general population is affected by the disorder [[Peretz et al., 2007](#)]. Amusia has a hereditary component: around 39% of first-degree relatives of amusics (i.e., individuals affected by amusia disorder) also suffer from amusia [[Peretz et al., 2007](#)]. The syndrome was discovered and characterized in 2002 by Dr. Isabelle Peretz [[Peretz et al., 2002](#); [Ayotte et al., 2002](#)], with whom I have collaborated during my thesis. The standard diagnosis approach for amusia is with the standardized tests from the Montreal battery of evaluation of amusia (MBEA) [[Peretz et al., 2003](#)].

Individuals with amusia have been increasingly studied because findings may reveal the brain structures and functions and genetic factors specifically related to music processing, which is considered a highlight of the human brain. The neurobiology of amusia is still not fully understood. Recurrent interactions between the right auditory and inferior frontal cortices are hypothesized to be key to pitch processing and were found to be affected in amusia [[Loui et al., 2009](#); [Albouy et al., 2013](#)]. Functional interactions between the auditory cortex and IFG develop with musical training, which is thought to be a protective factor against amusia [[Peretz, 2016](#)]. Further investigations are nevertheless necessary to understand the neural dynamics of

brain systems involved in pitch discrimination and how they are affected in amusia.

2.4.4 Summary

Pitch discrimination is a basic brain function involved in most aspects of auditory perception, including the prosody and intonations of spoken language. The brain dynamics between key regions involved in pitch processing remain essentially unknown. I have briefly introduced amusia as a specific disorder of pitch processing and discrimination, which does not affect other auditory abilities or cognitive functions. I propose to use this deficit as a model for advance our understanding of the brain dynamics subserving auditory pitch processing.

2.5 Conclusion

Neural oscillations reflect multiple dynamical aspects of brain activity. They interact with each other in a hierarchical manner, as a form of cross-frequency coupling. Such coupling is involved in perception, the temporal parsing of incoming stimuli, and mechanisms of communication between brain regions. Some brain disorders alter the typical local and inter-regional patterns of cross-frequency coupling.

Several approaches have been proposed to estimate this signal marker, but none so far is considered the gold standard. Improving on CFC methods would have major translational impact on studies of both (i) brain function in sensory and cognitive tasks, and (ii) dysfunction in disorders. This brief review highlights the necessity for further research on signal extraction and characterization from neurophysiological recordings, in relation to underlying physiological mechanisms and their role in brain functions and specific disorders.

3

Chapter 3: Time-resolved phase-amplitude coupling in neural oscillations

3.1 Preface

In this chapter, I contribute a new method for the estimation of phase-amplitude coupling from electrophysiological time series. The proposed algorithm, called tPAC, can be used to resolve in time the parameters of PAC, in both event-related and ongoing brain waveforms. Development and validation of tPAC was the object of my first study in the course of my thesis. I used the method thereafter to investigate (i) pathological activity in depth recordings from an animal model of epilepsy (Chapter 4), and (ii) the dynamics of brain networks for pitch discrimination in human participants (Chapter 5).

In the following chapter, I introduce the details of the tPAC method, provide algorithmic considerations and thorough evaluations with synthesized data. The performances of tPAC are then compared to other approaches in the field. Finally, I show empirical evidence that tPAC provides insight on dynamic physiological processes related to behavior using LFP recordings

Chapter 3: Time-resolved phase-amplitude coupling in neural oscillations

from the entorhinal cortex of a freely-moving rat. This chapter was published as:

Samiee, S. and Baillet, S. Time-resolved phase-amplitude coupling in neural oscillations. *NeuroImage*, 159:270–279, 2017

Contributions

SS introduced a new algorithm for time-resolved phase-amplitude coupling analysis that is presented in this manuscript. This involved identifying the problem, suggesting a solution with mathematical formulation, and software implementation. The method was evaluated with ground-truth simulated data and empirical local field potential (LFP) data. The initial draft and final version of the manuscript was written by SS, and she produced all figures of the paper. SB supervised all aspects of this work. He also reviewed and contributed to writing of the manuscript.

3.2 Abstract

Cross-frequency coupling between neural oscillations is a phenomenon observed across spatial scales in a wide range of preparations, including human non-invasive electrophysiology. Although the functional role and mechanisms involved are not entirely understood, the concept of interdependent neural oscillations drives an active field of research to comprehend the ubiquitous polyrhythmic activity of the brain, beyond empirical observations. Phase-amplitude coupling, a particular form of cross-frequency coupling between bursts of high-frequency oscillations and the phase of lower frequency rhythms, has recently received considerable attention. However, the measurement methods have relatively poor sensitivity and require long segments of experimental data. This obliterates the resolution of fast changes in coupling related to behavior, and more generally, to the non-stationary dynamics of brain electrophysiology.

We propose a new measure of phase-amplitude coupling that can resolve up to two cycles of the underlying slow frequency component. The method also provides a measure of the coupling strength, for augmented insight into the mechanisms involved. We demonstrate the technique with synthesized data and compare its performances with existing methods. We also show that the method reveals rapid changes in coupling parameters in data from the entorhinal cortex of a free-behaving rat. The time-resolved changes revealed are compatible with behavior and complement observed modulations of oscillatory power.

We anticipate that this new measure of dynamic phase-amplitude coupling will contribute to accelerate research into the dynamics of inter-dependent oscillatory components related to brain functions and dysfunctions.

Keywords:

Phase-amplitude coupling, cross-frequency coupling, neural oscillations, electrophysiology, brain dynamics.

3.3 Introduction

Classical studies of the role of neural oscillations in brain functions and behavior have reported on oscillatory rhythms within distinct, band-limited frequency ranges [Goldman et al., 2002; Klimesch, 1998; Tallon-Baudry and Bertrand, 1999] (see [Cohen, 2008] for a review). The oscillations that compose brain rhythms are known to be interdependent across frequency bands [Buzsáki and Draguhn, 2004]. This form of interaction known as *cross-frequency coupling* is a phenomenon readily observed in electrophysiology at multiple scales and with a range of experimental techniques [Buzsaki, 2006]. Phase-amplitude coupling (PAC) is one of the best-studied subtypes of cross-frequency coupling [Canolty and Knight, 2010], accounting for the more frequent occurrence of higher-frequency bursts at preferred phases of underlying low-frequency cycles. PAC has received tremendous attention recently, with several studies revealing modulations of such coupling depending on task and resting-state conditions in health and disease [Tort et al., 2008, 2009; Axmacher et al., 2010; Fell and Axmacher, 2011; Schutter and Knyazev, 2012; Florin and Baillet, 2015; De Hemptinne et al., 2015]. The physiological relevance for PAC is in the assumption that slow oscillations mark the cycles of relative net excitability of neural ensembles [Von Stein and Sarnthein, 2000; Fries, 2005; Haider et al., 2006; Lisman and Buzsáki, 2008], which in turn pace the occurrence of neural spiking and that of faster post-synaptic activity, marked by high-frequency and often broadband bursts [Canolty and Knight, 2010].

One can further hypothesize that such coupling is transient by nature, reflecting the elusive dynamics of polyrhythmic brain activity. Some early task-related evidence of this assumption was demonstrated in humans by Tort et al. [2008]. Ideally, measures of PAC need to provide the best possible frequency estimates of the oscillatory components related in phase and amplitude through this form of coupling. We would also need to assess the strength (intensity) of such coupling, to evaluate how it might be affected by behavior or physiopathological mechanisms. Finally and ideally, these measures would need to be accessible at the best possible

Chapter 3: Time-resolved phase-amplitude coupling in neural oscillations

temporal resolution, to detect and track such PAC changes at the natural “speed” of brain activity. This latter aspect has proven to be methodologically challenging, essentially because of the relatively poor signal-to-noise ratio affecting the higher-frequency portion of electrophysiological brain signals – in particular with non-invasive measures such as electro (EEG) and magnetoencephalography (MEG).

Event-related phase-amplitude coupling (ERPAC) was recently introduced in an attempt to bridge that methodological gap [Voytek et al., 2013]. The method indeed provides a PAC measure with high temporal resolution, however under the constraint that expected PAC changes are time-locked to a stimulus or event of interest across repeated trials. This aspect restricts the sensitivity and the range of applications of ERPAC to event-related experimental designs and analyses.

More recently, Dvorak and Fenton [2014] proposed to estimate PAC over two complementary *global* and *local* time scales. The global time scale – defined over 10 seconds or more, typically – is to identify the frequencies of the most coupled pair of oscillatory components: a slower oscillation (frequency for phase, f_P), which phase modulates the amplitude of faster bursts expressed at frequency f_A (frequency for amplitude). In turn, a local time scale – defined over the f_A cycles – is for detecting time variations in coupling strength. One identified issue with the approach though is that it assumes stationarity in coupled frequency pairs (a.k.a. modes) (f_A , f_P) over possibly long periods of observations: this is an unlikely eventuality in neurophysiology.

The strength of PAC is another measure of interest to obtain dynamically [Tort et al., 2008, 2009]. However, existing methods to assess PAC strength are also challenged by poor temporal resolution (see [Tort et al., 2010] for a review). We propose a new approach and practical method to address these issues in the widest range of experimental settings (task-related and spontaneous, ongoing electrophysiological data).

Chapter 3: Time-resolved phase-amplitude coupling in neural oscillations

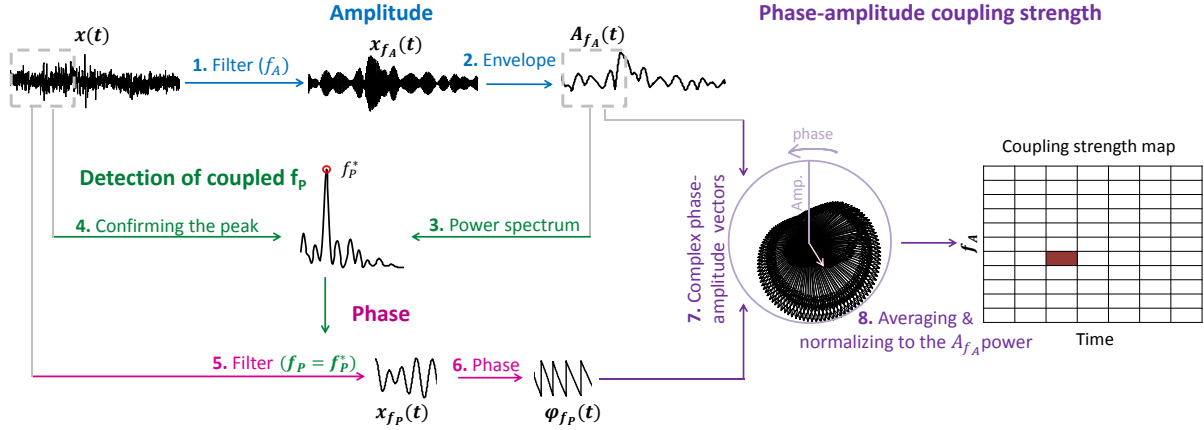


Figure 3.1: tPAC procedure: (1) The electrophysiological signal $x(t)$ is bandpass filtered around f_A , the tested frequency for amplitude modulations; (2) the envelope of the resulting bandpass filtered signal is extracted using standard Hilbert transform; A short temporal window slides on the resulting envelope: (3) the power spectrum of the windowed envelope (P_A) is estimated and its peaks are extracted; (4) the power spectrum of the original signal in the same time window is estimated, and is used for finding the highest peak in P_A that co-occurs with a peak in P_x . This determines the dominant frequency for phase f_P^* ; (5) windowed $x(t)$ (with a signal buffer on both sides) bandpass filtered around the selected frequency for phase f_P^* , (6) and its analytic phase is obtained via Hilbert transform; (7) for each time point, the amplitude of the fast-oscillation envelope and the instantaneous phase of the slow oscillation are reported using a polar vector; (8) the Euclidean norm of the summed vectors averaged over an integer multiply of f_P cycles is a measure of coupling strength within these time and frequency intervals. This value is further normalized with respect to the magnitude of $x_{f_A}(t)$, to minimize the influence of signal magnitude in the measurement of coupling strength. These steps are repeated for all predefined f_A frequency bins, and for all sliding time windows.

3.4 Material and Methods

3.4.1 Principles

Formally, let us define PAC as the modulation of the amplitude A_{f_A} of an oscillatory component of frequency f_A by the phase ϕ_{f_P} of a slower rhythm of frequency f_P , with $f_P < f_A$. Our approach to derive a time-resolved measure of PAC (tPAC) was inspired by Cohen [2008] and Canolty et al. [2006], which methods we combined and optimized to achieve the best possible temporal resolution and sensitivity to coupling strength. The methodological steps are detailed below and summarized in Fig. 3.1.

Chapter 3: Time-resolved phase-amplitude coupling in neural oscillations

The principle of the tPAC procedure is that it searches for the f_P oscillation with strongest PAC coupling with f_A bursts, over time windows that slide along the electrophysiological data signal $x(t)$. The user is first required to define a spectral range of interest for f_P and f_A – for instance, $[f_{P_{min}}, f_{P_{max}}]$ (e.g., [2, 12] Hz) for the f_P range. The range for f_A is then subdivided into twenty centre frequencies either linearly or logarithmically, determined by the user. The other parameter that should be defined by the user is the length of sliding time window. This window should be long enough to cover at least one full cycle of $f_{P_{min}}$.

For each f_A centre frequency tested, $x(t)$ is bandpass filtered around f_A with a zero-phase-shift, even-order, non-causal finite impulse response (FIR) filter. The bandwidth of each filter around each f_A centre frequency is defined as the maximum between i) the difference between consecutive f_A centre frequencies, and ii) the highest tested frequency for f_P . Thus, the filter bandwidth spans the interval between consecutive f_A frequency candidates and is inclusive of the range of interest for possible f_P oscillations. Note that to minimize the filter edge effects and increase frequency resolution, bandpass filtering needs to be performed on the full-length signal before extracting its components in the sliding time window.

The amplitude envelope $A_{f_A}(t)$ of the bandpass filtered signal around the f_A centre frequency, $x_{f_A}(t)$ is then extracted using the Hilbert transform before a sliding time window is applied to assess dynamic changes in PAC.

If in the current time-window, the amplitude of f_A oscillations is coupled to the phase of a slower rhythm oscillating at frequency f_P , then the power spectrum density (PSD) P_A of the windowed $A_{f_A}(t)$ is expected to feature a peak at f_P . Further, to avoid registering spurious manifestations of PAC, a peak around f_P shall also be expected in P_x , the PSD of the original data signal $x(t)$ limited to the same time window, as recommended by Aru et al. (2015). P_A and P_x are estimated using the Discrete Fourier Transform (DFT) magnitude coefficients. The best candidate for the frequency for phase (f_P^*) corresponds to the frequency of the highest peak of P_A coinciding with a peak of P_x . A tolerance threshold for the correspondence between peaks

Chapter 3: Time-resolved phase-amplitude coupling in neural oscillations

of P_A and P_x is set to the maximum between 1.5 the power spectrum's resolution (i.e. the inverse of the time window length) and 1.5 Hz. If no actual peak or peak coincidence is found, the coupling intensity is set to zero and an arbitrary value – outside the range of interest – is assigned to f_P . For robustness purposes, the peaks in P_x with an amplitude below 10% of that of the highest peak in the interval of interest for f_P are ignored. The reason for adding this step was that, as typical for the purpose of optimizing the FFT's computational time, the number of time points was set to the closest power of 2 (equal or larger than) of the data length, with zero-padding. This latter corresponds to signal windowing with an unknit boxcar in the time domain. Consequently, this produces spurious secondary peaks in the spectrum of the DFT magnitude coefficients. To avoid the detection of these side lobes as true signal peaks in P_x , we propose the aforementioned threshold applying procedure for the robust detection of the dominant slow oscillation in P_x . Furthermore, to prevent missing the peaks on the border of f_P range of interest, in peak detection from P_x and P_A , one extra point from both sides of the f_P interval were included. Note that decreasing the window length would potentially improve the temporal resolution of PAC estimation, but is detrimental to the detection of f_P^* , as it imposes a lower resolution to the f_P search.

Next, to extract the phase time-series of slow f_P^* oscillation, $x(t)$ in the time-window of interest is narrowband filtered around f_P^* (zero phase-shift, even-order, non-causal finite impulse response (FIR) filter, bandwidth = 3 Hz) to yield $x_{f_P}(t)$, which analytic phase $\phi_{f_P}(t)$ is extracted using the Hilbert transform. The FIR filters used in tPAC analysis have transient responses that should be discarded; a data buffer is a tool that is used for this purpose: 2 seconds of extra data from both sides are included analysis. This data buffer is neither used in the detection of f_P nor in the estimation of coupling strength. In the first and last few windows where extra data are not available, the signal was zero-padded.

To estimate the strength of coupling and the preferred phase of PAC occurrence along the f_P cycle, the modulation phase and amplitude at each time point are pooled into the complex signal

Chapter 3: Time-resolved phase-amplitude coupling in neural oscillations

$z(t) = A_{f_A}(t) \cdot e^{i\phi_{f_P}(t)}$ [Canolty et al., 2006]. A normalized estimation of coupling strength is obtained by computing the Euclidean norm of \bar{z} . \bar{z} is the vector sum of $z(t)$ across all time samples (in the current sliding time window), divided by the average amplitude $A_{f_A}(t)$ in the same time window (Eq. 3.1). Only full cycles of f_P oscillations are considered in the estimation of \bar{z} . The remaining part of the signal towards the end is cropped to avoid biasing the vector sum towards phase samples that would de facto repeat more often than others. To achieve this aim, we identified the phase angle at the start of each sliding time window, and used as effective signal length, that of the maximum number of cycles that would fit within the limits of the time window. In other words, while tracking the rotation of $z(t)$ vectors in the polar plane, we excluded the time vectors that came after the last occurrence of the phase measured at the onset of the time window. This was to prevent non-uniform sampling of f_P phase angles. The preferred coupling phase (ϕ_{tPAC}) was then estimated as the phase of the normalized vector \bar{z} .

$$\begin{cases} \bar{z} = \frac{\int_0^{t_p} A_{f_A}(t) \cdot e^{i\phi_{f_P}(t)} dt}{\sqrt{\frac{1}{t_p} \int_0^{t_p} A_{f_A}^2(t) dt}}, & tPAC = |\bar{z}|, \quad \phi_{tPAC} = \text{angle}(\bar{z}) \\ t_p = \frac{1}{f_P^*} \times \arg \max_{k: \text{integer} > 1} \{k \times 1/f_P^* \leq \Delta\} \end{cases} \quad (3.1)$$

t_p denotes the data length used in averaging (i.e. equal or shorter than sliding window length, Δ); and k is the number of f_P 's full cycles included in the sliding window.

The signal time window is then moved forward with an overlap that can be adjusted by the user. The procedure – from detecting the best f_P to estimating coupling intensity – is repeated for all successive time windows. This iterative process is subsequently repeated for all f_A centre frequency candidates. The resulting measures are pooled in a summary array, which can be conveniently represented as the map, as illustrated in Fig. 3.1.

In a real experimental context, the actual value of the driving frequency for phase (f_P^*) is unknown a priori. As previously mentioned, the minimum tested value for f_P is the most important factor for defining the temporal resolution of the PAC measure, as it imposes a minimum

Chapter 3: Time-resolved phase-amplitude coupling in neural oscillations

duration to the window length applied to the data. Indeed, at least one full cycle of the tested f_P is required to assess the possible interdependence of the f_P phase cycle with the amplitude of f_A bursts. And, the presence of a dominant slow oscillation at the frequency for phase is necessary for genuine PAC coupling [Aru et al., 2015]. Hence, peaks in the power spectrum of the data help identify potential frequency candidates for f_P . A relatively wide f_P range can help capture multiple, coexisting modes of coupling. If necessary and if the detected f_P^* s were notably faster than the minimum f_P of interest, a second pass of tPAC can be run with a narrower range of f_P of interest, around the previously identified f_P^* . This would also provide an opportunity to increase the temporal resolution of the tPAC analysis, with shorter time windows.

3.4.2 Sparse estimation of time-resolved PAC

The parameters of interest in PAC estimation span time, frequency for phase, and frequency for amplitude. Coupling strength can in principle be estimated at all points in this 3-D subspace of unknowns, however at a very high computational cost that is certainly not justified and necessary for all applications ($N_{f_P} \times N_{f_A} \times N_{time\ windows}$ PAC estimations, per data time series). We can also safely assume redundancy in the range of unknowns, for instance by considering that oscillatory bursts at frequency f_A are PAC modulated by one unique slow f_P oscillation within each sliding time window.

In practical terms, the method assumes that each f_A candidate is coupled to a single f_P frequency. Therefore, the resulting comodulogram – i.e. a 2-D map indicating the strength of coupling between different oscillations, with f_P values along the x-axis, and f_A values along the y-axis – over a sliding time window does not contain more than one peak in each f_A row across all possible f_P tested frequencies. Therefore, instead of testing several f_P frequencies for each f_A , tPAC detects the single most coupled f_P oscillation coupled to an f_A centre frequency candidate, and estimates the coupling strength for (f_P, f_A) . This yields a sparse representation of the comodulogram.

Chapter 3: Time-resolved phase-amplitude coupling in neural oscillations

For visualization purposes, the sparse comodulogram array can be projected on 2-dimensional hyperplanes, by averaging over the third dimension. The possible produces of such projections are: t vs. f_A , t vs. f_P , or f_P vs. f_A representations.

3.4.3 Statistical tests for tPAC

Statistical significance of tPAC parameter estimates is verified with a non-parametric resampling techniques. We followed the recommendations by Aru et al. (2015), suggesting to generate surrogate datasets using a block-resampling approach. A benefit is that phase distortion is minimized, which reduces the rate of false-positive detection. The envelope time-series of the f_A oscillation in each time-window were first split into five blocks. These blocks were then randomly permuted to yield a surrogate dataset that realizes the assumption of absence of PAC beyond chance levels. This approach were acknowledged to produce relatively conservative assessments of statistical significance of PAC measures [Aru et al., 2015].

In the experimental work reported below, $n = 500$ surrogate trials were produced per time-window and f_A centre frequency candidate. The coupling strengths within the 95th percentile of the surrogate distribution were considered statistically significant. Further, when assessing significance of PAC values reported in the time vs. f_A , and to compensate for multiple-comparison testing, the null distributions were that of the the maximum statistic across all time windows and tested f_A frequency candidates [Pantazis et al., 2005].

3.4.4 Experimental data

The comparison of tPAC against other methods was conducted with controlled, synthesized data. We then used electrophysiological recordings in animal preparations to relate observed tPAC effects to behavior. All electrophysiological data processing was performed using Brainstorm [Tadel et al., 2011], using default parameters, which distribution also contains the open Matlab source code of tPAC. We also share the Matlab scripts for reproducing and the synthe-

Chapter 3: Time-resolved phase-amplitude coupling in neural oscillations

size of more test data (<http://neuroimage.usc.edu/brainstorm/Tutorials/TutPac>).

Synthesized data

Data simulations were used to provide ground-truth signals, with controlled PAC parameters. It consisted of times series obtained from the sum of two sinusoids, with additive noise. The amplitude of the high-frequency component was modulated by the phase of the low frequency component according to Eq. 3.2.

$$x(t) = x_{f_P}(t) + x_{f_A}(t) + \epsilon(t), \quad (3.2)$$

where $\epsilon(t)$ is additive noise (see below), and each signal component is designed following Tort et al. [2010] model (Eq. 3.3).

$$\begin{cases} x_{f_P}(t) = K_{f_P} \sin(2\pi f_P t) \\ x_{f_A}(t) = A_{f_A}(t) \cdot \sin(2\pi f_A t), \\ \text{where: } A_{f_A}(t) = K_{f_A} \frac{(1-\chi)\sin(2\pi f_P t - \phi_c) + \chi + 1}{2} \end{cases} \quad (3.3)$$

K_{f_P} and K_{f_A} are fixed scalars that determine the peak amplitude of f_P and f_A sinusoidal components, respectively. ϕ_c indicates the phase of $x_{f_P}(t)$ where the magnitude of $x_{f_A}(t)$ bursts is maximum. $\chi \in [0, 1]$ determines the fraction of $x_{f_A}(t)$ that is not modulated by $x_{f_P}(t)$ and therefore controls for coupling strength, defined as $1 - \chi$. Fig. 3.2 shows two examples of synthesized signals, with different coupling strengths.

The additive noise $\epsilon(t)$ was generated from two components: random samples drawn from a power law, to mimic background brain activity, and white Gaussian realizations for simulating instrumental noise. The power of the Gaussian component was set to half that of the power-law samples'.

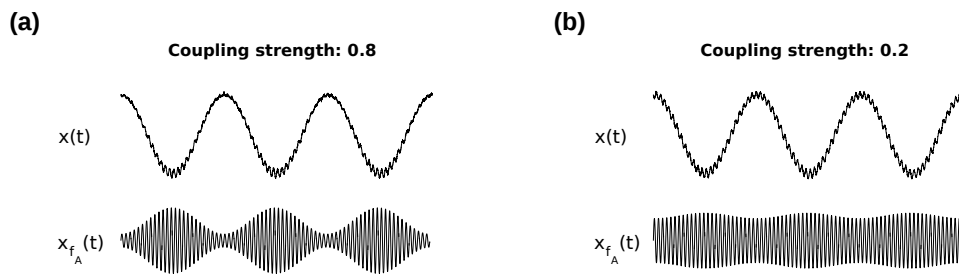


Figure 3.2: Illustrations of the effect of the coupling strength parameter on the power of modulated component ($x_{f_A}(t)$) in phase-amplitude coupling. Signals were synthesized from Eq. 3.3 (SNR=10): two different coupling strengths are illustrated: a) high ($1 - \chi = 0.8$), and b) low ($1 - \chi = 0.2$).

We provide more details in the Appendix for advanced simulations where the duty cycle of $x_{f_P}(t)$ is manipulated, to test whether asymmetrical cycles affect tPAC and other PAC measures [Belluscio et al., 2012].

Electrophysiological data

Local field potential (LFP) recordings from multiple mesio-temporal brain regions of Long-Evan rats were collected using eight-shank multi-site silicon probes (200 μm inter-shank distance). The freely-available data was published elsewhere [Mizuseki et al., 2009] and shared on the Collaborative Research in Computational Neuroscience website (<http://crcns.org>) by the Buzsaki laboratory. Recordings were carried out while the animals ran on a linear track (length: 250 cm), digitally sampled at 20 kHz (16-bit resolution, RC Electronics) and bandpass filtered (1 Hz – 5 kHz). The processed LFPs were downsampled to 1250 Hz (anti-aliasing filter applied). Two LEDs were connected to the animal's head. The position of the rat was extracted from the video file recorded during free behavior on the linear track, with a sampling rate of 39.06 Hz, and time aligned with the LFP recordings.

3.5 Results

3.5.1 Time-resolved estimation of PAC properties: frequency for phase, amplitude and coupling strength

The results of phase-amplitude coupling analysis of a synthesized data set using tPAC are illustrated in Fig. 3.3. This experiment covered two aspects of PAC analysis: the detection of coupling modes (Fig. 3.3a-c) and the estimation of coupling strength (Fig. 3.3d).

In the first part, the input signal was a synthesized data trace, generated using the model explained in section 3.4.4 (Fig. 3.3a). Multiple modes of coupling were present: during the first half of the signal (10 s duration), the phase of slow oscillation at $f_{P_1}^* = 9$ Hz was coupled to the amplitude of a faster rhythm at $f_{A_1}^* = 115$ Hz. In the second half, the first coupling mode was terminated and two other modes appeared simultaneously with $f_{P_2}^* = 13$ Hz, $f_{A_2}^* = 145$ Hz, $f_{P_3}^* = 5$ Hz, and $f_{A_3}^* = 87$ Hz, respectively. The signal-to-noise ratio was set to 6 dB, and the preferred coupling phase in the three modes are 270, 0, and 180 degrees, respectively. The coupling strength was kept constant and identical in all modes.

The bands of interest for f_P and f_A in tPAC analysis were defined as [3, 15] Hz and [20, 200] Hz, respectively. The duration of the sliding time window was set to 0.75 s, hence 2.25 cycles of minimum f_P of interest. Coupling strength was estimated for 20 centre frequencies distributed linearly along the f_A range of interest.

In Fig. 3.3b, the top panel depicts the initial outcome of tPAC algorithm, which shows time variations of coupling strength with f_A . This map reveals the time course of all three coupling modes expressed in the data. The time variations of coupling strength for each f_P estimated from the sparsely estimated coupling strengths (see Sec. 3.4.2). The resulting f_P vs. time map is shown in the bottom panel of Fig. 3.3b. The comodulogram was also reconstructed (Fig. 3.3c), as a typical, non time-resolved appreciation of PAC in signals.

Chapter 3: Time-resolved phase-amplitude coupling in neural oscillations

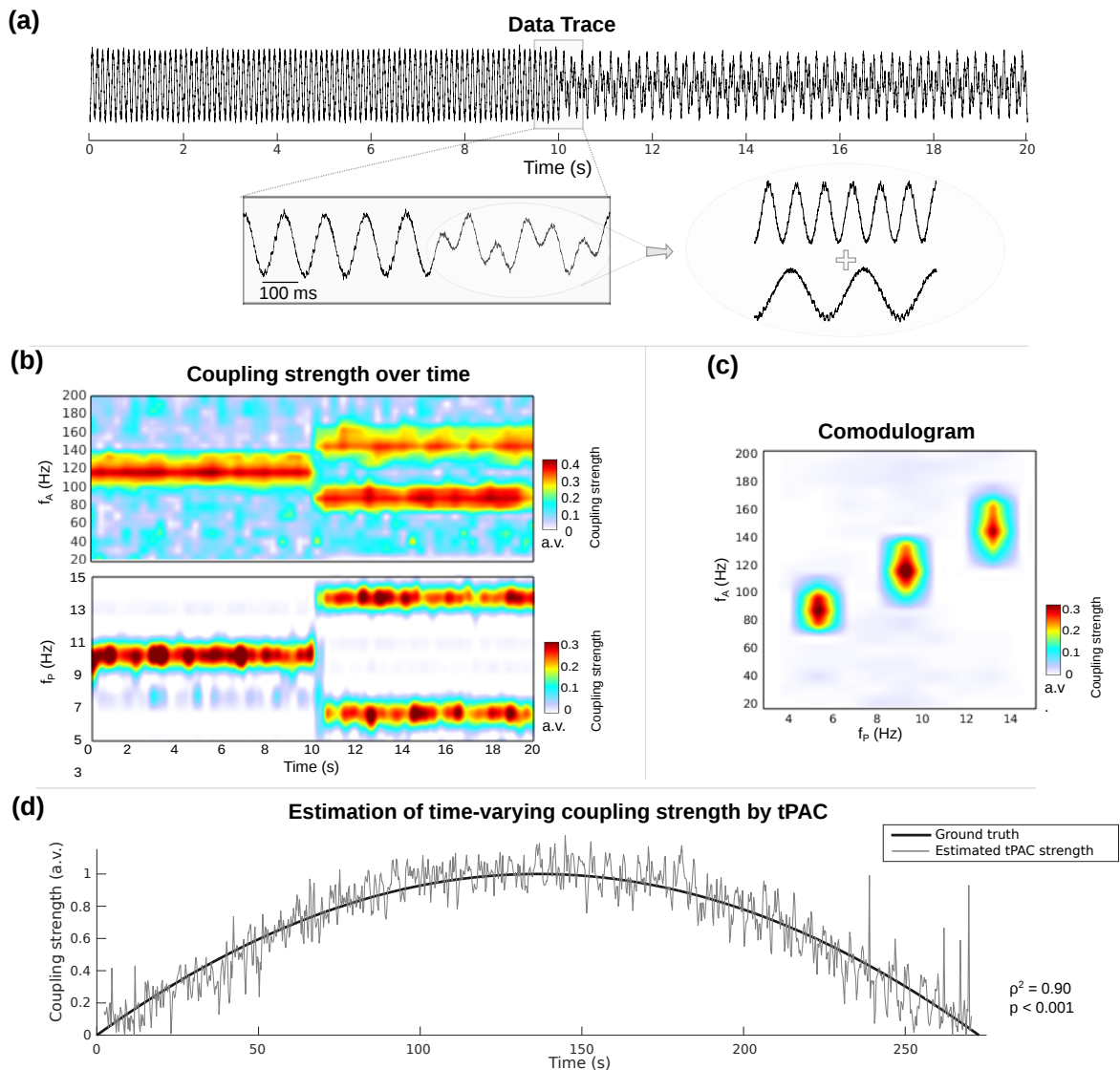


Figure 3.3: Illustration of tPAC analysis outcome on a synthesized data set. (a) A synthesized data trace, including three different coupling modes were generated. See text for details on the properties of simulated signals; (b) tPAC coupling strength maps for f_A and f_P vs. time extracted using tPAC from the signal depicted in panel (a); (c) tPAC comodulogram; (d) tPAC estimation of coupling strength: black trace shows the true coupling strength, the gray trace shows the estimated tPAC strength using a window length as short as 0.53 s – the estimated strength is normalized to its 98th percentile.

To further illustrate tPAC's ability to estimate phase-amplitude coupling strength, a synthesized data trace with continuously time-evolving coupling strength was generated: $f_P^* = 4\text{Hz}$, $f_A^* = 73\text{Hz}$, SNR = 5 dB, duty cycle = 0.35, sampling rate = 1000 Hz, 270 s signal duration. tPAC was applied to the data with f_P and f_A frequency ranges of interest, [2, 15] Hz and [50,

Chapter 3: Time-resolved phase-amplitude coupling in neural oscillations

140] Hz, respectively. The length of the sliding window was set to 0.53 s, which includes only 2 cycles of f_P^* , and at least one cycle of the minimum f_P of interest (i.e. 2 Hz as explained above). The normalized time-resolved tPAC strength is shown in Fig. 3.3d. The correlation between the estimated time-variation of tPAC coupling and ground truth was 0.95 ($p < 0.001$). Increasing the sliding window length from 2 cycles of f_P^* to 4 and 8 cycles led to similar results (correlation coefficient of 0.97 and 0.99, respectively).

3.5.2 Methods comparison study

The performances of tPAC on synthesized data were compared further to those of four published methods: phase-locking value (PLV) [Lachaux et al., 1999], Kullback-Leibler modulation index (KL-MI) [Tort et al., 2010], amplitude power spectral density (APSD) [Cohen, 2008], and mean vector length (MVL) [Canolty et al., 2006].

The dataset used consisted of 500 trials of short asymmetric (duty cycle = 0.35) synthesized time series, with $f_P^* = 4\text{Hz}$, $f_A^* = 73\text{Hz}$, SNR = 5 dB, and sampling rate of 1000 Hz. The ranges of interest for f_P and f_A were set to [2, 15] Hz and [50, 140] Hz, respectively. The signal duration was 1.07 cycles of minimum f_P of interest ($f_{P_{min}}$) – i.e. 0.53 s = 2.15 cycles of f_P^* . The signal length was a non-integer multiple of f_P cycles, to make the situation more challenging and realistic, when, with physiological data, the signal length is not expected to be a multiple of f_P cycles.

All tested methods (MVL, PLV, KL-MI, and APSD) were implemented in house, from the details provided in the respective publications. The methods parameters were identical to those used for tPAC. Zero-phase lagged FIR filters with 3-Hz and 15-Hz bandwidths were used for filtering in the f_P and f_A ranges of interest, respectively. Eighteen centre frequencies for f_A were selected linearly in the [50, 140] Hz range. For the methods that scan on f_P , fourteen centre frequency candidates were linearly distributed in the [2, 15] Hz range. The duration of filter transients (containing 99 percent of the energy from the filter’s transient effect) for all f_A

Chapter 3: Time-resolved phase-amplitude coupling in neural oscillations

filters was less than 75 ms (29-74 ms depending on the f_A center frequency – note that f_A filtering was performed on the full-length input signal, not on the shorter, sliding time windows). The transient effects for f_P filters were less than 1.03 seconds (289-1029 ms depending on f_P center frequency – a data buffer of 2 seconds was added prior to filtering).

Since MVL was originally introduced using a wavelet filter bank [Canolty et al., 2006], and wavelet filter banks are common in the PAC literature [Lakatos et al., 2005; Demiralp et al., 2007; Lakatos et al., 2008; Cohen et al., 2009; van der Meij et al., 2012], we also used an MVL implementation based on wavelet filtering. We used the actual code shared by Canolty et al. (2006) available in Brainstorm. Results from MVL-wavelet were obtained using a Morlet wavelet filter bank with 150 frequency candidates for f_A and f_P , that were distributed logarithmically within [2, 150] Hz.

In all tested methods, the frequency pairs (f_P, f_A) indicating the highest coupling strength was compared to the actual values used to generate the synthesized data. The relative errors in f_A and f_P were estimated (Eq.3.4). For each trial, the relative errors in f_P and f_A detection were averaged together, as a summarizing measure of accuracy.

$$\bar{E} = \left| \frac{f_{detected} - f}{f} \right| \times 100\% \quad (3.4)$$

Fig. 3.4 shows the performances of the tested methods in terms of identification of the coupled (f_P, f_A) pair, and quantification of coupling strength. Fig. 3.4a shows the relative errors in coupling detection for all algorithms. On these challenging short data segments, tPAC and APSD produced the smallest (< 5%) relative errors.

We performed a systematic examination of the sensitivity of data length on PAC estimation accuracy, Fig. 3.4b. The simulation procedure described above was repeated with signal lengths increasing from 2.15 to 10.15 f_P cycles. We found that for all tested methods, performances in coupling detection improved with increasing signal length, although at different rates. Overall, for signal duration longer than two f_P cycles, tPAC and APSD produced the best estimates of f_P

Chapter 3: Time-resolved phase-amplitude coupling in neural oscillations

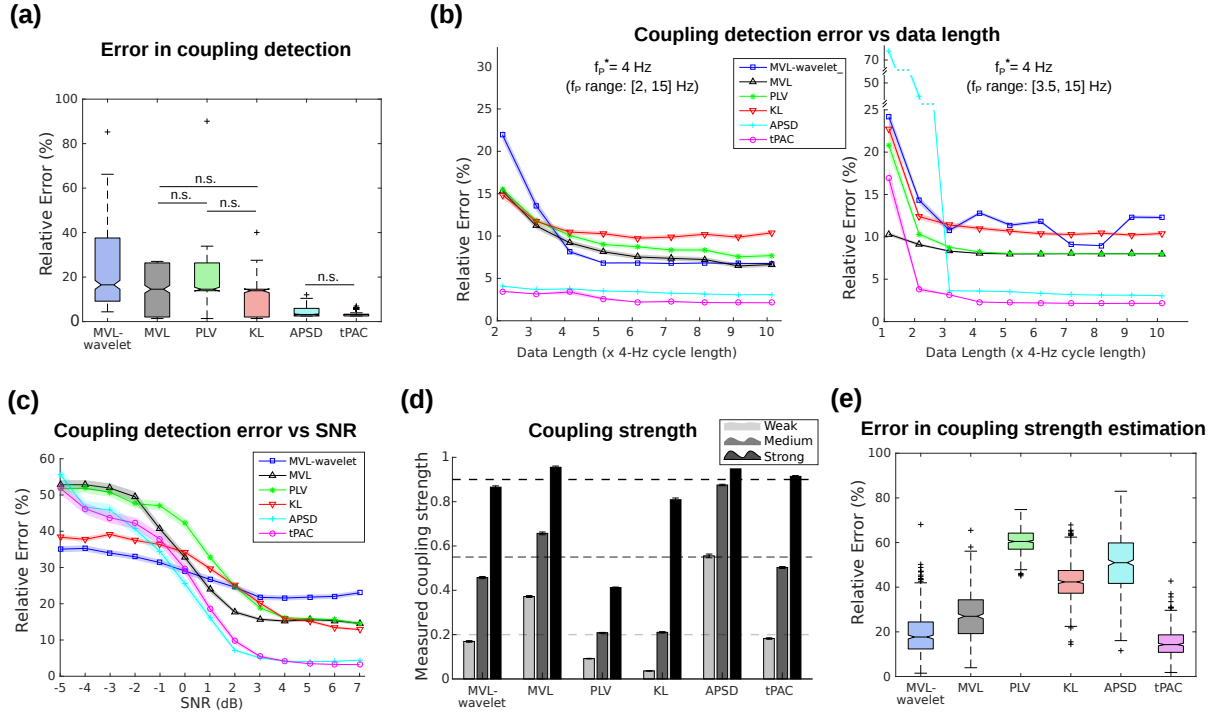


Figure 3.4: Performance comparisons of selected PAC methods against tPAC (synthesized data): estimation of f_P , f_A , and coupling strength. (a) Averaged relative error on coupled frequency pair (f_P , f_A) estimates obtained from a short ($2.15 f_P^*$ cycle duration) synthesized input signal. All methods show significantly different performances (Kruskal-Wallis rank test, Dunn’s test as post-hoc, $p_s < 0.001$), except where noted "n.s.". Coupled frequency pair estimates were tested depending on input data length (panel (b); SNR=5 dB - with two different bands of interest for f_P in left and right panels: [2,15] Hz and [3.5, 15] Hz, respectively.), and SNR (panel (c); signal length was identical as in panel (a)). (d) estimation of coupling strength (signal synthesis was identical as for panel (a)) with 3 tested coupling strengths: ($1 - \chi=0.2, 0.55$ and 0.9), shown with horizontal dashed lines. Average estimates of coupling strength and corresponding SEM over 500 trials. (e) relative error in estimated coupling strength averaged at three tested coupling strengths. All methods showed significantly different performances (Kruskal-Wallis rank test, Dunn’s test as post-hoc, $p_s < 0.001$). See text for details on synthesized signals.

and f_A . As explained in Sec. 3.4.1, at least one full cycle of the minimum tested f_P is required for PAC analysis. In this experiment, since the slowest tested f_P was 2 Hz (a 500-ms cycle) with data where the unknown true f_P^* was 4Hz (a 250-ms cycle), the shortest time window duration was $2 \cdot f_P^*$ cycles. Hence, we furthered the investigations concerning the temporal resolution of tPAC and other PAC estimators, by conducting another set of experiments where the smallest f_P of interest (3.5Hz) was brought closer to $f_P^*=4$ Hz (f_P range: [3.5, 15] Hz; see Fig. 4b-right panel). These experiments confirmed that the observation of too few f_P^* cycles affects the

Chapter 3: Time-resolved phase-amplitude coupling in neural oscillations

accuracy of PAC measures. They also indicate that the performances of methods such as APSD that rely on the detection of f_P peaks in the signal spectrum are negatively affected when the minimum tested f_P is too close to f_P^* . Although tPAC also relies on such peak detection, we have implemented several procedures that augment the robustness of the method, in that respect, as demonstrated in Fig. 3.4b. For example, if f_P^* is close to the minimum f_P of interest, APSD requires window lengths that cover at least 3 f_P^* -cycles, for best performances. Under the same conditions, coupling detection with MVL-wavelet became less stable with increasing time-window lengths. MVL, PLV, and KL were less sensitive to the proximity of f_P^* with minimum tested f_P , because these methods scan systematically and linearly the f_P range of interest for f_P^* and do not rely on spectral estimations. Interestingly, this new frequency range for f_P (narrower band, f_P^* closer to the bands lower bound) improved the performances of these algorithms slightly, for short signal duration of 2 f_P cycles.

We tested how signal-to-noise ratio (SNR) affected PAC estimation performances. The same simulation procedure as shown Fig. 3.4a's was repeated, with SNR increased from -5 to +7 dB (negative SNR values correspond to larger noise power compared to the signal's). Our results demonstrate that the performances of all tested methods go through the same three behaviors depending on SNR: i) a flat response segment for SNR levels below -3 dB; ii) a dramatic improvement in performances for SNR between -3 and 3 dB; and iii) an asymptotic plateau in performances for SNR above 3 dB (3 dB means that signal's power was twice of the noise's power).

MVL-wavelet was the most robust method against noise, however with relatively large errors in estimating coupling parameters ($> 20\%$), even in high SNR conditions. In positive SNR conditions, APSD and tPAC had the best performances compared to MVL, PLV, and KL (Fig. 3.4c).

The ability of PAC methods to recover the coupling strength was also tested quantitatively (see Fig. 3.4d-e). Again, the simulation scheme of Fig. 3.4a was reproduced, with three different

Chapter 3: Time-resolved phase-amplitude coupling in neural oscillations

coupling strengths ranging from low ($1 - \chi = 0.2$), to intermediate ($1 - \chi = 0.55$), then high ($1 - \chi = 0.9$). Fig 3.4d shows the coupling strengths recovered from the tested methods at the actual (f_P, f_A) mode. Bars indicate the SEM across trials. All PAC measures were normalized to their maximum possible value, as obtained in noiseless and maximum coupling strength ($1 - \chi = 1$) conditions.

The relative errors in coupling strength, on all trials with three coupling strength values, are depicted in Fig. 3.4e. The data demonstrate that MLV-wavelet and tPAC manifested the best ability to recover coupling strength quantitatively, while PLV was the most challenged method in that respect. Although tPAC uses an algorithm similar to MVL for coupling strength estimation, several optimized schemes in tPAC (namely the normalization to A_{f_A} power, window lengths reduced to multiple cycles of f_P , as described in section 3.4.1) resulted in significantly higher performances for tPAC (error: $14.88 \pm 0.27\%$) in coupling strength estimation, compared to MVL-wavelet (error: $19.33 \pm 0.43\%$) and MVL (error: $27.41 \pm 0.49\%$), with short input signals (All methods showed significantly different performances: Kruskal-Wallis rank test, Dunn's test as post-hoc, $p_s < 0.001$).

Taken together, tPAC demonstrated the best consolidated performances in estimating the frequency modes expressing PAC (f_P and f_A), and in recovering coupling strength. APSD showed high performances in detection of coupled frequency pair (f_P, f_A). However the APSD estimation of coupling strength was poor (error $> 40\%$). MVL performed well in estimating the coupling strength, but remained poorly accurate in recovering the coupled frequency pair, especially on short data lengths (error $> 15\%$). In MVL, using a wavelet filter bank produced mixed effects. More accurate coupling strength estimation, and less sensitivity to noise were the positive effects of using the wavelet filter bank. However, the wavelet version of MVL produced higher coupling detection error for short input ($< f_P^*$ -cycle), not stable results with f_P^* very close to the minimum f_P of interest.

These performances obtained with the shortest lengths of data input indicate that using

Chapter 3: Time-resolved phase-amplitude coupling in neural oscillations

tPAC, all phase-amplitude coupling parameters can be estimated in a time-resolved fashion, using short (length of two f_P cycles minimum) time windows. The next section details how we extended testing to electrophysiological data related to behavior.

3.5.3 Electrophysiological data

The time-resolved tPAC coupling strength in the third layer of entorhinal cortex (EC3) of a rat freely moving on a linear track was obtained, after setting the frequency of ranges of interest to [2, 15] Hz for f_P , and [35, 215] Hz for f_A . Coupling strength was calculated for 20 centre frequencies distributed linearly in the f_A range of interest. Data analysis was performed at two different temporal scales: one coarse assessment using 10-second overlapping windows; and a finer-grained investigation using sliding windows of 2.5-s duration. In both cases, the sliding windows were moved along the data time series with a 50% of overlap.

We show the tPAC coupling strengths both as comodulograms (f_P vs. f_A), and time-resolved maps (Fig. 3.5a and 3.6a, respectively - all maps were smoothed using 2-D interpolation, with details provided in the supplementary material). The overall strongest PAC mode of the coarse analysis was found between the phase of theta (7.5 Hz) and the amplitude of fast gamma ([90–130] Hz) oscillations (Fig. 3.5a). We verified the tPAC findings with the comodulogram obtained from MVL -wavelet [Canolty et al., 2006] (Fig. 3.5b): the results were consistent in terms of the principal (f_P, f_A) mode detected. Further, since tPAC detects the most coupled f_P to each time-window and f_A sub-band, only the dominant f_P modes were represented in the tPAC comodulograms. This, by construction, makes the resulting coupling maps look less smeared than the ones obtained by the other tested methods – see section 3.4.1 for more details). Also akin to [Canolty et al., 2006] and for visualization purposes, the spectrogram and the epoched LFP signal were averaged time locked to the troughs of the 7.5-Hz f_P cycle (Fig. 3.5c – spectrogram is depicted relative to the averaged power across time). This confirmed that the power of faster oscillations was indeed modulated by the phase of the slow rhythm, as detected by tPAC.

Chapter 3: Time-resolved phase-amplitude coupling in neural oscillations

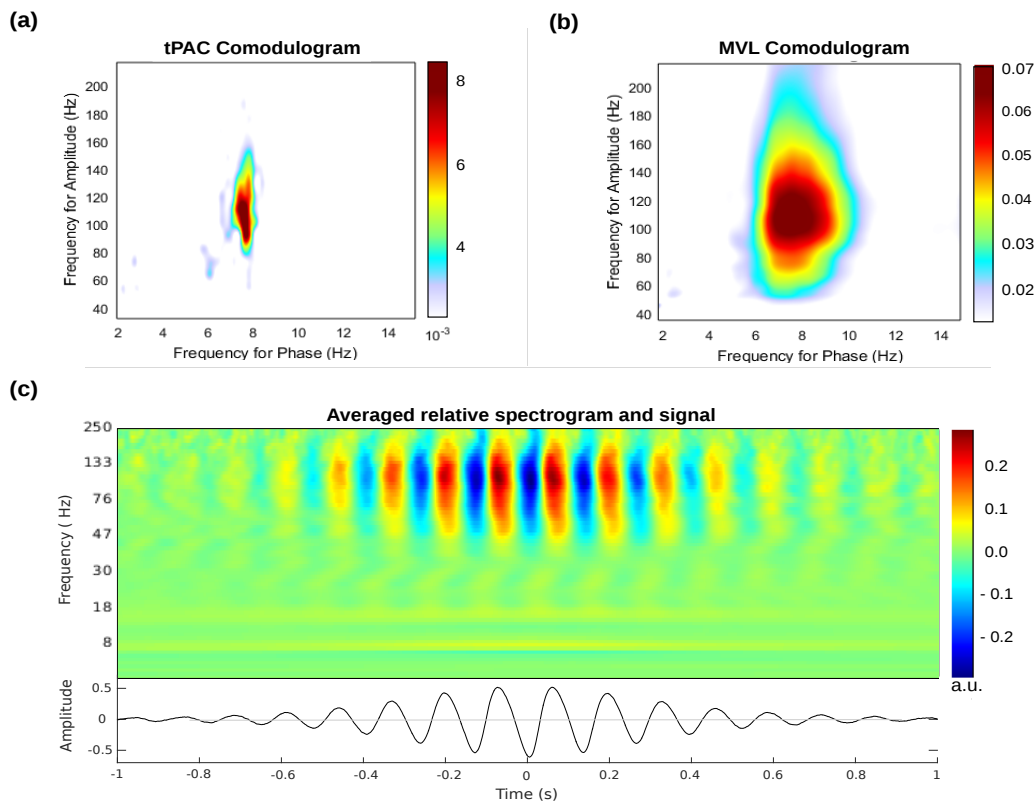


Figure 3.5: Phase-amplitude coupling from LFP data recorded in the third layer of a rat entorhinal cortex (EC3) – (a) tPAC sparse-estimated comodulogram map, indicating the principal (f_P, f_A) mode of PAC; (b) MVL-wavelet comodulogram from same recording ; (c) spectrogram (top) and ongoing LFP signal (bottom) averaged at the phase troughs of the low frequency oscillation with the highest PAC (7.5 Hz).

The dynamics of cross-frequency coupling related to behavior were investigated further, using time-resolved tPAC maps. Our results show that burst-like variations in coupling strength occurred in the recordings (Fig. 3.6a; displayed values are above 95th percentile of surrogate data distribution – corrected for multiple comparisons). The animal’s position on the track (showed with gray dashed lines in Fig. 3.6a) indicated that such bursts of higher coupling occurred when the animal was running.

We confirmed these observations by computing the PSD during respective periods of rest and running. The power spectra showed peaks in the theta band ([5, 10] Hz) in both cases, although at distinct frequencies (6 Hz and 7.5 Hz, respectively. Fig 3.6c). The time-frequency decomposition of the LFP signal also showed increase in fast-oscillation power during move-

Chapter 3: Time-resolved phase-amplitude coupling in neural oscillations

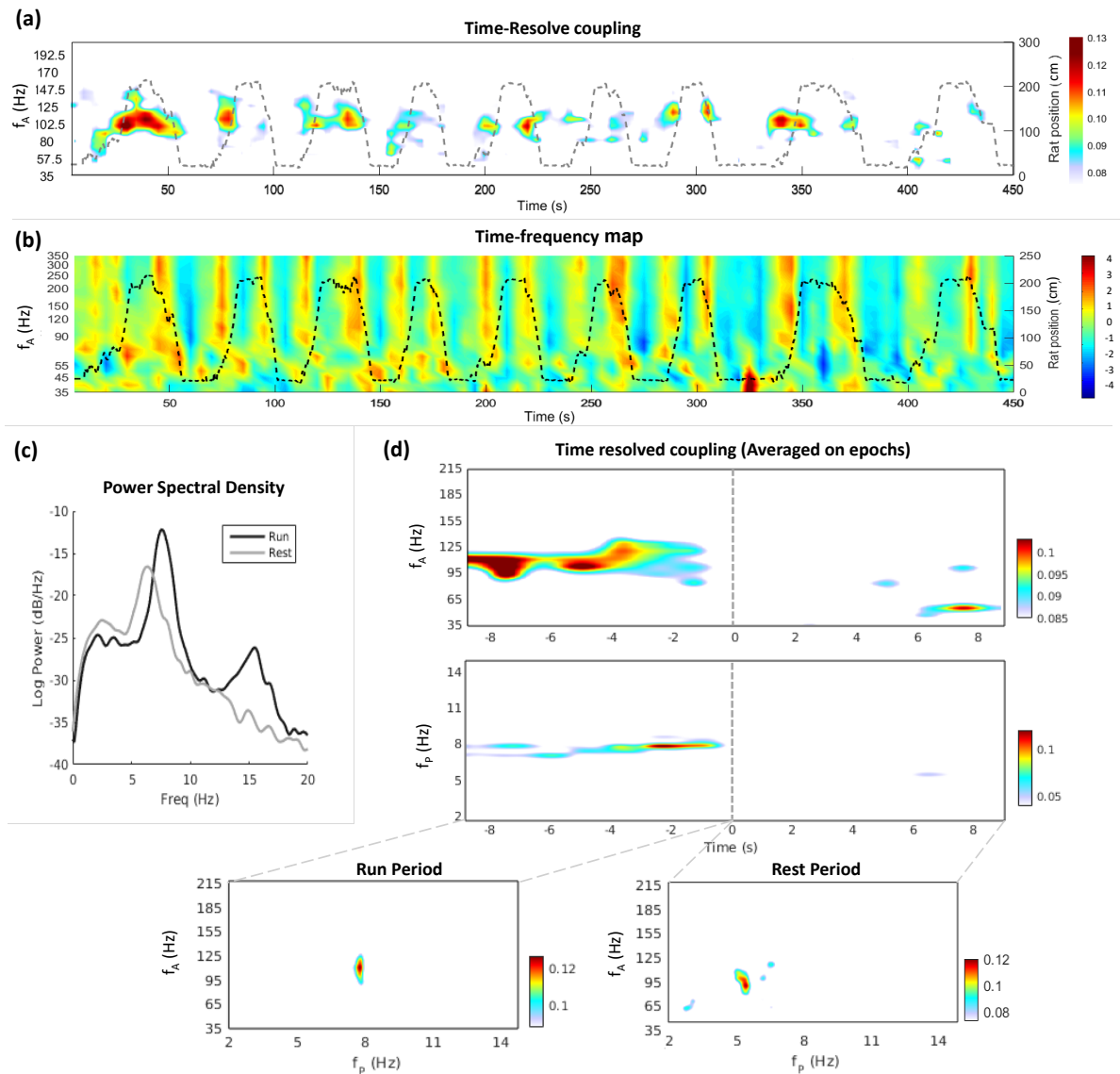


Figure 3.6: Time-resolved tPAC parameters related to behavior – a) Time-resolved tPAC coupling strength (sliding window length of 10 s); the dashed line indicates the animal’s position on the track; b) Time-frequency decomposition of the LFP signal with the animal’s position also superimposed (dashed line); c) Averaged power spectral density of the LFP signal in the running and resting behavior; d) tPAC comodulogram with window length of 2.5s, from epochs of data corresponding to the running and resting behavior. Comodulograms specific to the running and resting behavior are shown at the bottom of panel (e); e) tPAC coupling strength from epoched data. Time 0 s corresponds to when the animal stops running and rests at one end of the trace. Negative time stamps are for running – In all graphs, the minimum of the color bar is set based on threshold coming from statistical analysis (see sec. 3.4.3).

Chapter 3: Time-resolved phase-amplitude coupling in neural oscillations

ment (Fig. 3.6b). However, such increases spanned a wide frequency range ([80, 350] Hz), and were not specific of the f_A band we found was coupled to the phase of theta oscillations.

The PSD data further revealed that in addition to the dominant peaks in theta range, there was at least another smaller peak in the delta band (< 4 Hz) in both behavioral conditions (Fig. 3.6c). Previous studies reported on such slower rhythms in similar behavioral conditions, as possibly generated by the midline thalamic nucleus [Zhang et al., 2012].

All data segments consisting of at least 10 consecutive seconds of running followed by 10 seconds of resting at one end of the track were extracted. They were temporally aligned, with time 0 ms corresponding to when the animal stopped at the end of the track.

To detect possible event-related changes of cross-frequency coupling, tPAC was computed on 9 epochs of 20 seconds, collected on 8 channels in EC3, with a sliding window length of 2.5 s and 50% overlap, using the same ranges of interest for f_P and f_A as previous analysis. Our decision to set the minimum f_P of interest at 2Hz was guided by the available slow peaks in the power spectrum of the data, and behavioral aspects we wished to relate to dynamic PAC changes, namely the episodes of animal running vs. resting. These latter unfold over several seconds (about 10s each typically), hence the selection of a relatively slow minimum f_P , and therefore long tPAC window of 2.5s to sample these events in time. We also chose a larger time window because of its potential for revealing multiple, co-existing PAC modes, at slower f_P .

Fig. 3.6d illustrates the time-resolved fluctuations in coupling strength along the epoch duration. The figure also shows the respective comodulograms of the running and resting periods. Our findings confirmed that the dominant coupling mode during running was between theta (7.5 Hz) and fast gamma ([90,130] Hz), and that the strongest coupling was observed in the running behavior. Two other coupling modes were revealed: between delta and low gamma ([40, 60] Hz) – lower, but significant strength – and between lower theta and midrange gamma ([60,100] Hz) only during rest. These two modes were not clearly distinguishable from the non time resolved PAC analysis. The frequency of theta oscillations that drove fast gamma during

Chapter 3: Time-resolved phase-amplitude coupling in neural oscillations

running was close to the dominant global theta mode (7.5 Hz). The theta coupled with mid-gamma during rest was lower in frequency (about 6 Hz). This observation was consistent with the dominant peak of theta observed in the power spectrum of the full data. Our results also indicate that delta oscillations in EC3 were coupled to low-gamma rhythms, specifically during the resting behaviour. The frequency range of the three gamma components identified were consistent with the three modes of gamma in hippocampus reported previously by [Buzsáki and Schomburg \[2015\]](#).

These results illustrate the insight enabled by time-resolved PAC measures with tPAC. Further investigations would be required to actually comprehend the functional relevance of the distinct, behaviorally-dependent coupling modes observed.

3.6 Discussion

We introduced tPAC, a method to measure time-resolved parameters of phase-amplitude coupling in electrophysiological time series. tPAC performs comparatively better than existing methods for estimating at once the frequencies of coupled oscillations, the strength of such coupling, all using the shortest input signal length, with relative immunity to noise. One benefit of tPAC is therefore to resolve PAC measures in time, at best with the resolution of two cycles of the frequency for phase (f_P). This property alleviates the constraint of working previously with long data epochs, which was not compatible with the expected non stationarity of electrophysiological signals, for instance, in relation to behavior. Importantly, non stationarity may induce spurious spectral correlation between Fourier coefficients, and therefore yields artificial cross-frequency coupling [[Aru et al., 2015](#)]. This adds to the significance of time-resolved PAC methods.

tPAC was compared to selected published methods, with an emphasis on data length. The results using ground-truth synthesized data showed that tPAC is sensitive and accurate with at minimum a signal duration of two f_P cycles. Our data also showed that MVL-wavelet and

Chapter 3: Time-resolved phase-amplitude coupling in neural oscillations

KL-MI PAC methods performed relatively poorly on shorter input signals – especially when minimum f_P of interest is very close to f_P^* . This finding is consistent with claims by Tort et al. [2010], indicating that a minimum of 200 f_P cycles (about 30 s) are required for optimal performance of these methods. The necessity for long input signals for MVL was also discussed by Penny et al. [2008].

One practical solution to work against poor temporal resolutions was previously to concatenate short recording epochs. Although this indeed increases data length, the discontinuities induced by concatenation can lead to spurious high-frequency components, which may affect coupling estimation. For example, when epochs of identical lengths are concatenated, discontinuities induce an artifactual PAC regime that relates sharp variations (broadband high-frequency spectral contents) to the epoch edges, with an implicit oscillatory cycle corresponding to the epoch duration. Consequently, spurious PAC may occur [Kramer et al., 2008].

Further, the estimation of coupling strength is another asset of the tPAC method: most published methods do not properly recover this parameter [Tort et al., 2010]. Hence, tPAC provides higher temporal resolution to the analysis of phase-amplitude coupling of ongoing data (e.g., resting-state, epilepsy, sleep recordings, etc.), and time-resolved sensitivity to coupling strength. Note that in the context of event-related studies, with enough trial repetitions (above 150, typically), ERPAC (Voytek et al. [2013]) can provide the fastest possible temporal resolution, reaching up to the data's sampling rate.

3.7 Conclusion

We propose tPAC as a new time-resolved method for estimating cross-frequency phase-amplitude coupling in electrophysiological signals. tPAC combines the highest temporal resolution, the capacity of estimating coupling strength, and the lowest sensitivity to noise conditions, even for shorter data lengths. These properties are key to reveal transient coupling variations related to behavior, from continuous and event-related data collected with a range of electrophysiological

Chapter 3: Time-resolved phase-amplitude coupling in neural oscillations

techniques that are relevant to the neuroimaging community, including EEG and MEG sensor and source data series.

Acknowledgment

The authors thank Jean Gotman and Christine Cahaney for their insightful comments. S.S. acknowledges the support from McGill University Integrated Program in Neuroscience. S.B. was supported by the Killam Foundation, a Senior-Researcher grant from the Fonds de Recherche du Quebec-Sante, a Discovery Grant from the National Science and Engineering Research Council of Canada, the NIH (2R01EB009048-05) and a Platform Support Grant from the Brain Canada Foundation.

3.8 Supporting information

Appendix

3.8.1 Asymmetric synthesized data

In an asymmetric duty cycle model, the frequency of x_{f_P} signal changes linearly with time in each cycle ($f(t) = at + b$). This results in an asymmetric semi-sinusoidal signal (See Fig. 3.7).

Here, each cycle of this signal is defined as: $F(t) = \sin(2\pi(at + b)t)[U(t) - U(t - T_P)]$, where $U(t)$ is a step function. Thus, in the case of an asymmetric signal, x_{f_P} will be defined as Eq. A.1.

$$x_{f_P}(t) = \sum_{n=1}^N F(t - nT_P) \quad (\text{A.1})$$

The duty cycle (k) and the period of the signal ($T_P = 1/f_P$) are the main factors that constrain the parameters of the linear changes in frequency. After solving the equations, considering that the ascending phase of x_{f_P} should be faster than its descending phase [Belluscio

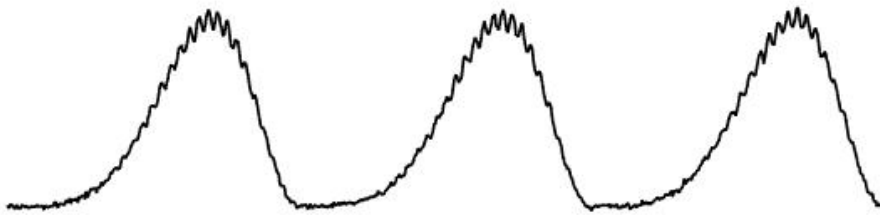


Figure 3.7: A sample of synthesized data with phase-amplitude coupling generated using asymmetric duty cycle model for frequency for phase.

Chapter 3: Time-resolved phase-amplitude coupling in neural oscillations

et al., 2012], the slope (a) and y-intercept (b) of the frequency are obtained as Eq. A.2.

$$\begin{cases} a &= \frac{1 - \frac{1-2k^2}{2k(1-k)}}{T^2} \\ b &= \frac{1-2k^2}{2kT(1-k)} \end{cases} \quad (\text{A.2})$$

x_{f_P} is then estimated with these parameters. Then, using a model similar to that of Eq. (3.3), asymmetric time series can be synthesized.

3.8.2 Interpolation of the coupling maps

All coupling maps (comodulograms, time vs. f_A , and time vs. f_P maps) shown in section 3.5.3 were interpolated in 2-D, for visualization purposes. The interpolation was performed on a 300x300 pixel grid with the two-dimensional spline interpolation featured in Matlab, with default parameters.

4

Chapter 4: Phase-amplitude coupling and epileptogenesis in an animal model of MTLE

4.1 Preface

In this chapter, I investigate how pathophysiological changes in epileptic tissues of an animal model of epilepsy affect phase-amplitude coupling, as a measure of interactions between oscillatory neural assemblies. We used tPAC, the method introduced in the previous chapter for the analyses presented. The Pilocarpine animal model of mesial temporal lobe epilepsy was provided by Prof Massimo Avoli's lab [Cavalheiro, 1995; Cavalheiro et al., 1996; Curia et al., 2008]. Pilocarpine induces hyperexcitability via imbalanced inhibitory-excitatory networks associated with GABA_A receptors alterations [Cossart et al., 2001; Stief et al., 2007; Zhan et al., 2010]. This imbalance is derived by decreased GABAergic inhibition in the network. Pilocarpine MTLE, as a relatively simple model of human temporal lobe epilepsy, can be used for investigating how such imbalance leads to alterations in cross-frequency coupling between neural oscillations. In this study, I did not directly analyze the relationship between imbalance in excitability and CFC, but investigated how CFC is affected in MTLE and corroborates seizure phenotypes.

Chapter 4: Phase-amplitude coupling and epileptogenesis in an animal model of MTLE

I extracted tPAC phase-amplitude coupling parameters from interictal NREM sleep recordings of several preparations of Pilocarpine MTLE rat model. The few previous studies on cross-frequency coupling in human epilepsy patients essentially reported from ictal (i.e., during seizures) recordings [Nariai et al., 2011; Ibrahim et al., 2014]. My core hypothesis was that the dynamical PAC expressions of epilepsy were latent in the epileptic brain, and could be detected using tPAC away from seizures (interictal periods).

Using interictal recordings to characterize epilepsy (e.g., to determine the location and extent of the seizure onset zone) in individual patients would have tremendous practical value, reducing the duration and risks of extensive EEG monitoring. Furthermore, we can extract NREM sleep recordings from interictal state, but it is almost impossible to get it from ictal state. Practically speaking, NREM sleep time series features clear slow oscillations (< 1.5 Hz), which are associated to the cycles of regional excitability. These observations are present in both control and epileptic animals. We therefore used this strong slow-frequency rhythm as a rhythmic candidate for coupling with faster oscillations, including High-frequency oscillations (HFO).

Previous studies also featured data from patients only, hence with no perspective on normative variants and with often complex cases of epilepsy and uncertain delineation of the SOZ, which required implantation of intracranial electrodes. Working with a well-controlled and stereotypical animal model of MTLE alleviated some of these limitations and is a first step before translating the findings to human data.

This chapter describes in details the experiment, analyses and findings from this study, which was published as: "Samiee, S., Lévesque, M., Avoli, M., and Baillet, S. Phase-amplitude coupling and epileptogenesis in an animal model of mesial temporal lobe epilepsy. *Neurobiology of disease*, 114:111–119, 2018"

Contributions

SS was responsible for designing the method, writing analysis scripts, performing data analyses, producing all figures and writing drafts and the final version of the manuscript. ML collected the data, marked the seizures and helped with interpreting the results and reviewed the manuscript. MA helped with results interpretation and reviewed the manuscript. SB supervised the project, provided funding, and contributed to the writing of the manuscript.

4.2 Abstract

Polyrhythmic coupling of oscillatory components in electrophysiological signals results from the interactions between neuronal sub-populations within and between cell assemblies. Since the mechanisms underlying epileptic disorders should affect such interactions, abnormal level of cross-frequency coupling is expected to provide a signal marker of epileptogenesis. We measured phase-amplitude coupling (PAC), a form of cross-frequency coupling between neural oscillations, in a rodent model of mesial temporal lobe epilepsy. Sprague-Dawley rats ($n = 4$, 250-300 g) were injected with pilocarpine (380 mg/kg, i.p) to induce a status epilepticus (SE) that was stopped after 1 h with diazepam (5 mg/kg, s.c.) and ketamine (50 mg/kg, s.c.). Control animals ($n = 6$) did not receive any injection or treatment. Three days after SE, all animals were implanted with bipolar electrodes in the hippocampal CA3 subfield, entorhinal cortex, dentate gyrus and subiculum. Continuous video/EEG recordings were performed 24/7 at a sampling rate of 2 kHz, over 15 consecutive days.

Pilocarpine-treated animals showed interictal spikes ($5.25 (\pm 2.5)$ per minute) and seizures ($n=32$) that appeared $7 (\pm 0.8)$ days after SE. We found that CA3 was the seizure onset zone in most epileptic animals, with stronger ongoing PAC coupling between seizures than in controls (Kruskal-Wallis test: $\chi^2(1,36) = 46.3$, Bonferroni corrected, $p < 0.001$). Strong PAC in CA3 occurred between the phase of slow-wave oscillations (< 1 Hz) and the amplitude of faster rhythms (50-180 Hz), with the strongest bouts of high-frequency activity occurring preferentially on the ascending phase of the slow wave. We also identified that cross-frequency coupling in CA3 ($\rho = 0.44$, $p < 0.001$) and subiculum ($\rho = 0.41$, $p < 0.001$) was positively correlated with the daily number of seizures. Overall, our study demonstrates that cross-frequency coupling may represent a signal marker in epilepsy and suggests that this methodology could be transferred to clinical scalp MEG and EEG recordings.

Keywords:

Chapter 4: Phase-amplitude coupling and epileptogenesis in an animal model of MTLE

Temporal lobe epilepsy; Pilocarpine; Cross-frequency coupling; Phase-amplitude coupling; Neural oscillations; CA3; Seizures.

4.3 Introduction

Mesial temporal lobe epilepsy (MTLE) is a focal epileptic disorder characterized by recurrent seizures arising from limbic structures such as the hippocampus, the amygdala or entorhinal cortex [Spencer and Spencer, 1994; Salanova et al., 1994b; Engel Jr, 1996; Gloor, 1997]. Seizures occur following a latent period of several years after an initial brain insult such as status epilepticus (SE), traumatic brain injury, encephalitis or febrile convulsions [Cendes et al., 1993; French et al., 1993]. Approximately one-third of MTLE patients are unresponsive to antiepileptic drugs [Jallon, 1997; Wiebe et al., 2001; Engel et al., 2012]: MTLE is one of the most refractory forms of focal epilepsy. Surgical resection of the epileptic tissue remains the only therapeutic alternative [Salanova et al., 1994b; Wiebe, 2004; Blume and Parrent, 2006; Engel et al., 2012], provided that the seizure onset zones (SOZ) are correctly localized. The identification of the SOZ is challenging, in particular since it is mainly obtained from inter-ictal electrophysiological data. Therefore, the present study emphasizes the possible role of cross-frequency coupling between oscillatory components of neural signal as a signal marker of epilepsy. Cross-frequency coupling is a phenomenon of inter-dependence between brain rhythms of different frequencies. It has been observed in multiple preparations in rodents and humans, using a variety of electrophysiology techniques, from invasive recordings to scalp magnetoencephalography and source imaging [Canolty and Knight, 2010; Florin and Baillet, 2015; Baillet, 2017]. Phase-amplitude coupling (PAC) is a type of cross-frequency coupling where the phase of slow oscillations modulates the amplitude of faster rhythms [Tort et al., 2010]. Invasive recordings in rodent models and epileptic patients revealed that PAC was stronger in the seizure onset zones [Amiri et al., 2016; Nariai et al., 2011; Weiss et al., 2013; Ibrahim et al., 2014; Guirgis et al., 2015; Weiss et al., 2016], and during the pre-ictal and ictal phases [Colic et al., 2013; Alvarado-Rojas et al., 2014; Zhang et al., 2017]. We used here the pilocarpine animal model of MTLE [Curia et al., 2008] to investigate the possible association between expressions of PAC and ictogenesis in temporal lobe regions. We measured PAC be-

Chapter 4: Phase-amplitude coupling and epileptogenesis in an animal model of MTLE

tween the phase of slow oscillations (slow-wave in the delta band: 0.184 Hz) and the amplitude of faster rhythms (beta to ripple band: 20250 Hz) in controls and in pilocarpine-treated rats. Our results indicate a strong association between PAC signal markers (coupling strength and phase) and seizure activity in temporal lobe regions in this rodent model of MTLE.

4.4 Material and methods

4.4.1 Animal Preparations

The methods for animal preparation have been described in detail previously [Behr et al., 2015, 2017; Lévesque et al., 2011, 2012; Salami et al., 2014]. All procedures were approved by the Canadian Council on Animal Care and the Institutional Animal Care Committee of McGill University. Every effort was made to minimize the number of animals used and their suffering. Male Sprague-Dawley rats (250-300 g; Charles-River (St-Constant, QC, Canada)) were let habituate for 72 h before pilocarpine treatment. Animals were housed at 22 (\pm 2) °C under 12 h light/12 h dark cycle with food and water ad libitum. Scopolamine methylnitrate (1 mg/kg i.p.; Sigma-Aldrich, Canada) was administered 30 min before pilocarpine hydrochloride (380 mg/kg, i.p.; Sigma-Aldrich, Canada) to induce a status epilepticus (SE). SE was terminated after 1 h using diazepam (5 mg/kg, s.c.; CDMV, Canada) and ketamine (50 mg/kg, s.c.; CDMV, Canada) (Martin and Kapur, 2008). Three days after SE, rats underwent surgery for the implantation of bipolar depth electrodes. Rats were anesthetized with isoflurane (3%) in 100% O₂. Four bipolar electrodes (20-30 k; 4-10 mm length; distance between exposed tips: 500 μ m, MS303/2-B/spc, Plastics One, VA, USA) were implanted in the CA3 subfield of the ventral hippocampus (AP: -4.4, ML:-4, DV: -7.8), the medial entorhinal cortex (EC) (AP: -6.6, ML: -5.2, DV: -6.8); the ventral subiculum (Sub) (AP: -6.8, ML: +4, DV: -6), and the dentate gyrus (DG) (AP: -4.4, ML: +2.4, DV: -3.4) (Paxinos and Watson, 1998). The CA3 region and the EC were implanted on the right side, the subiculum and the dentate gyrus were implanted on the left side. Four stainless steel screws (2.4 mm length) were fixed to the skull bone and electrodes

Chapter 4: Phase-amplitude coupling and epileptogenesis in an animal model of MTLE

were fastened to the skull with dental cement. A fifth electrode was used as reference, after removal of insulating material, and placed under the frontal bone. Ketoprofen (5 mg/kg, s.c. Merail, Canada), buprenorphine (0.01-0.05 mg/kg, s.c. repeated every 12 h; CDMV, Canada) and 2 ml of 0.9% saline. After surgery, continuous EEG-video recordings were performed 24h/day. EEG signals were amplified via an interface kit (Mobile 36ch LTM ProAmp, Stellate, Montreal, QC, Canada), and sampled at 2 kHz. Infrared cameras were used to record day/night video files that were time-stamped for integration with the electrophysiological data using monitoring software (Harmonie, Stellate, Montreal, QC, Canada). Throughout the recordings, animals were placed under controlled conditions (22 ± 2 C, 12-hour light/dark schedule) and provided with food and water ad libitum.

4.4.2 Analysis of seizures and seizure onset zones

Seizures were identified with the ICTA-D seizure detector (Harmonie; Stellate) and seizure onset zones were identified according to Lévesque et al. [2012]. Briefly, the first region showing fast activity (5-20 Hz) was considered as the seizure onset zone. The seizure onset zone was defined according to previous published reports of animal models of MTLE [Lévesque et al., 2012, 2015; Behr et al., 2017; Toyoda et al., 2015; Karunakaran et al., 2016] and clinical studies [Wendling et al., 2010, 2013]. Seizures were categorized into four types: (1) CA3 seizures initiated in CA3; (2) CA3+ seizures originated from CA3 and another region simultaneously; (3) multi seizures originated simultaneously at all recording sites; and (4) CA3- seizures did not involve CA3.

4.4.3 Extraction of NREM sleep epochs

Periods of sleep characterized by non-rapid eye movement (NREM) were defined by muscular hypotonia (curled body position) and prominent delta activity (1-6 Hz). NREM segments were selected from the video recordings at least 1 h from the last/next seizure episode [Lévesque et al., 2011; Salami et al., 2014]. One 10-min artefact-free epoch of NREM sleep was selected

Chapter 4: Phase-amplitude coupling and epileptogenesis in an animal model of MTLE

in each animal for each day of recording. The data selected consisted of 137 epochs from 6 controls and 4 epileptic animals. These epochs were exported to Matlab (The Mathworks, Natick, MA) and analyzed off-line. Power line contamination (main and harmonics) was reduced using notch filters with default settings available from Brainstorm, a free open-source application for electrophysiology signal analysis [Tadel et al., 2011]. Fig. 4.1A shows samples of wide-band recordings from all recorded regions, in a control and in an epileptic animal. Power spectrum density analysis revealed that slow oscillations were recorded in all four regions (Fig. 4.1B). The frequency peak of the slow oscillation was extracted in each animal, after compensation of the 1/f decrease of the power spectral density, using Brainstorm. We call here slow-wave oscillations, oscillatory signals below 1 Hz. No substantial differences in slow oscillatory power were found between the control and epileptic groups, except in the dentate gyrus, where slow oscillatory power was higher in controls (Kruskal-Wallis test: $p < 0.001$ Fig. 4.1C).

We standardized the definition of peaks and troughs of the observed slow oscillations across animals and recording sites. The rationale is that the polarity of the oscillatory cycles collected from the bipolar recordings depends on uncontrolled factors, such as the electrode location with respect to the current flow of neural generators, which varies across sites and animals. We followed the recommendations from Ellenrieder et al. [2016], whereby the peaks of slow oscillations are defined as the extrema of the half oscillatory cycles concomitant with stronger beta-gamma band activity. We therefore extracted the instantaneous amplitude of the recordings in the 20-80 Hz band using the Hilbert transform also available in Brainstorm. We then identified the half cycle of the dominant slow oscillation with strongest beta-gamma amplitude. In each animal and at each recording site, the polarity of the signal was flipped if the peak of beta-gamma activity did not correspond to a positive half-cycle of the slow oscillation. Therefore, the peak of the slow oscillation marks a dynamical state similar to the on state from sleep surface EEG [Nir et al., 2011].

Chapter 4: Phase-amplitude coupling and epileptogenesis in an animal model of MTL

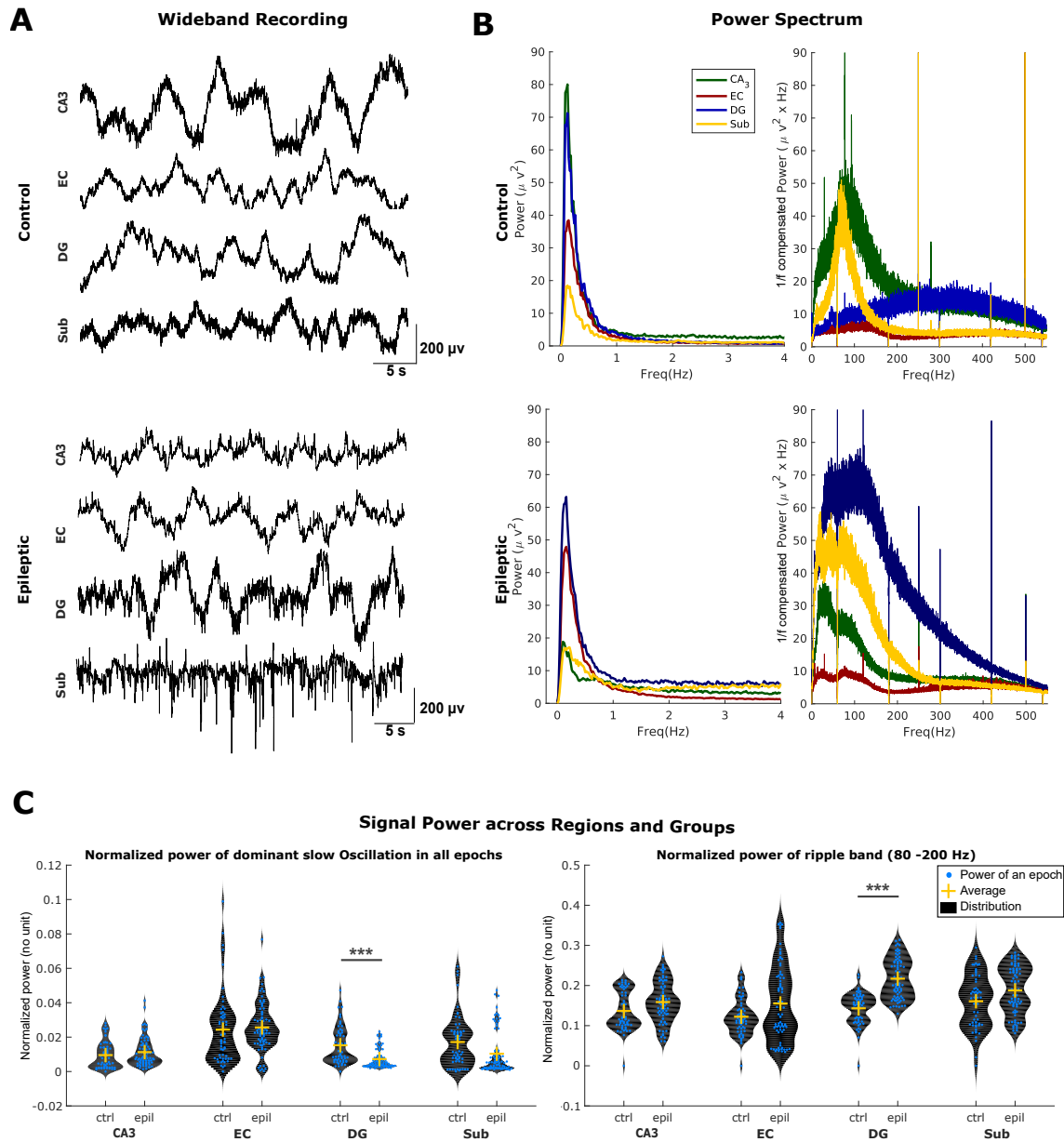


Figure 4.1: Typical recordings from control and epileptic animals. A: Wideband sample recordings from a control (top) and from an epileptic animal (bottom). B: Power spectral density plots extracted from the same animals shown in A, after compensation of $1/f$ decrease: note a strong peak below 1 Hz at all recording sites in both animals. C: Regional distribution of normalized signal power of dominant slow oscillation (left), and of the ripple band: 80-200 Hz (right) across epochs. No differences were found between groups, except in DG, where slow activity was weaker and ripple-band activity was stronger in the epileptic group (Kruskal-Wallis test, d.o.f: 136, $p < 0.001$, Bonferroni corrected for multiple comparisons). Comparisons between regions for each group are reported in section 4.5.2.

4.4.4 Phase-amplitude coupling analysis

PAC is the modulation of the amplitude of an oscillation at frequency f_A (frequency for amplitude) along the phase of a slower rhythm of frequency f_P (frequency for phase), with $f_P < f_A$. The frequencies f_A and f_P of the dominant PAC mode need to be identified in each animal and at each recording site, together with their coupling strength. The frequency ranges of interest for identifying f_A and f_P were set to 0.18 – 4 Hz for the slow oscillation, and 20 – 250 Hz for the faster components. We used a recent time-resolved PAC measure (tPAC) with sliding time windows length of 18 s, also available in Brainstorm [Samiee and Baillet, 2017]. Briefly (see Samiee and Baillet [2017] for methodological details), the tPAC method proceeds as follows: at each recording site, the instantaneous amplitude $A_{f_A}(t)$ of fast oscillatory activity is extracted over sliding time windows (18 s long) using the Hilbert transform in multiple sub-bands of the 20 – 250 Hz frequency range of interest. The periodogram of $A_{f_A}(t)$ and of the original signal are then obtained and the frequency for phase f_P is identified as the common peak of maximum amplitude in both power spectra, if any. If no common peak frequency is found, the conclusion is the absence of PAC in the time series. The electrode signal is then bandpass filtered around f_P , and its instantaneous phase ($\phi_{f_P}(t)$) is extracted, also using the Hilbert transform. PAC coupling strength is measured via Euclidean averaging of the complex signal vectors of amplitude $A_{f_A}(t)$ and phase $\phi_{f_P}(t)$ across time, divided by the average signal power at frequency f_A . This procedure was repeated for all time-windows and all high-frequency sub-bands. Large-band spiking signal waveforms can bias PAC estimates. For this reason, interictal spikes were identified in all recordings using a custom detection process: for all 10-min trials, spike events were marked when electrode signals crossed an amplitude threshold of 4 standard deviations above the signal average. All detected events were visually inspected, and events possibly produced by movement artefacts were excluded. We quantified the density of interictal spike occurrences along the phase of slow-wave oscillations, as a preferred phase concentration of spiking activity would bias PAC scores. The phase of slow oscillations was extracted from the Hilbert

Chapter 4: Phase-amplitude coupling and epileptogenesis in an animal model of MTLE

transform of data signals filtered in the band of interest. As detailed in the Results section, we found that spike occurrences were uniformly distributed (see Fig. 4.2) along the phase of the f_P oscillation, and concluded they did not produce spurious PAC activity. For this reason, data epochs containing interictal spike events were not discarded from the data presented below. Another possible confound in PAC measures is their sensitivity to the harmonics of non-sinusoidal waveforms of the f_P oscillations [Gerber et al., 2016; Lozano-Soldevilla et al., 2016; Cole and Voytek, 2017]. We followed the guidelines suggested by Jensen et al. [2016] and verified there was no correlation between the respective time variations of the amplitude of f_P oscillations and of the PAC coupling strength.

4.4.5 Statistical analysis

We used inferential statistics to assess the significance of differential effects in power, PAC coupling strength, and preferred PAC phase patterns in all 4 recorded regions, between control and epileptic animals. We used non-parametric Kruskal-Wallis tests for assessing the main effect, and Dunns tests as post-hoc. We used parametric Watson-Williams multi-sample tests with equal means, the circular equivalent of one-way ANOVA, for the analysis of phase effects. We determined whether the distribution of phase angles of the f_P oscillations when interictal spikes occurred departed from uniformity using Rayleigh's test. A larger z -value of Rayleigh statistics would have been indicative of interictal spikes occurring at a preferred phase of the slow-wave oscillations. Phase angles were computed between 0° and 360° , where 0° (respectively 180°) corresponded to the peak (respectively the trough) of the oscillatory signal, as defined above. For correlation between measures we used Pearson correlation. Bonferroni corrections for multiple comparisons were applied in all tests.

4.5 Results

4.5.1 Seizures and interictal spikes

Pilocarpine-treated animals showed recurrent spontaneous seizures, on average $7 (\pm 0.8)$ days after SE. As previously reported [Lévesque et al., 2012], CA3 was involved as a seizure onset zone in most cases across all epileptic animals ($n = 32$ seizures) (CA3 = 7, CA3+ = 7, CA3- = 3, widespread = 15, Fig. 4.2A). Interictal spikes were observed in all recorded regions. Control animals did not show interictal spikes or seizures.

We recorded an average of $5.25 (\pm 2.5)$ interictal spikes per minute in all epileptic animals. The number of interictal spikes was significantly different between regions (Kruskal-Wallis test: $\chi^2(3, 308) = 128.24$, $p < 0.001$). As previously reported [Behr et al., 2015; Lévesque et al., 2015] interictal spikes occurred at higher rates in CA3 and subiculum, than in EC or DG (post-hoc: Dunns tests, $p < 0.001$, Fig. 4.2B). CA3 and subiculum interictal spike rates were not significantly different ($p = 0.37$).

Bandpass filtering of interictal spikes produce fast oscillatory artefacts, which may bias PAC measures if spiking activity occurs at a preferred phase of background slow-wave oscillations. We verified this was not the case in our data: the distribution of interictal spikes occurrences did not show clustering at a preferred phase of the slow oscillations (Fig. 4.2C). This verification was derived considering two low-frequency ranges for phase-driving slow oscillations: 1) the band of interest for f_P (0.184 Hz), and 2) all frequencies below 2 Hz where PAC was strongest in all regions (see Fig. 4.3C). No spike clustering was found with either of the low-pass settings (Rayleigh's test for non-uniformity, $p > 0.10$). We therefore proceeded with performing PAC analysis over the entire 10-min time-period, without excluding interictal spikes.

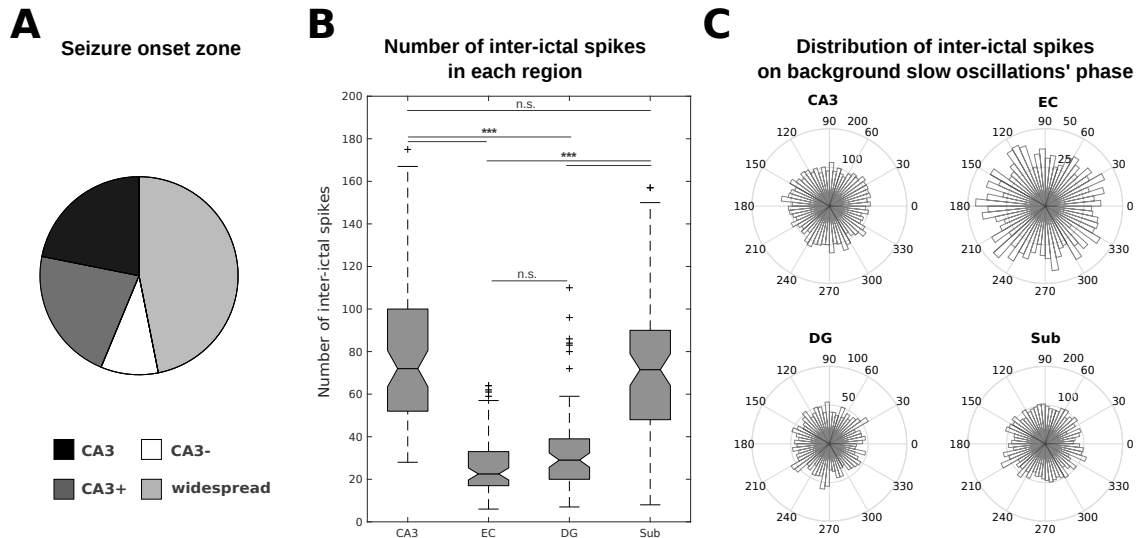


Figure 4.2: **Seizure onset zone and interictal spikes in epileptic animals.** A: Pie chart showing the distribution of seizure onset zones in epileptic animals. CA3 was mostly involved as a seizure onset zone. B: Number of interictal spikes at each recording site (***: $p < 0.001$). CA3 and subiculum showed the highest rate of interictal spikes compared to EC and DG. C: Polar plots showing the distribution of interictal spikes relatively to the phase of background slow-wave oscillations: the phase distribution of the data was not significantly different from a uniform distribution (Rayleigh's test for non-uniformity, $p > 0.10$).

4.5.2 Power effect: slow-wave oscillations and ripple band

The presence of a dominant slow oscillation in the band of interest for f_P is a safeguard condition for valid (not spurious) PAC detection (Aru et al., 2015). Dominant slow oscillations (< 1 Hz) were observed in all epochs in all recorded regions, both in controls and in epileptic animals (Fig. 4.1). To investigate possible influence of slow-oscillatory signal power on the estimation of PAC coupling strength, we measured the relative power of the dominant slow oscillations with respect to the total power spectrum of the signal at each recording site and in each epoch. In comparison of groups, difference in relative signal power was only found in DG (Kruskal-Wallis test, Bonferroni corrected for multiple comparison, $p < 0.001$), where power in epochs from epileptic group was lower than controls. There was no significant correlation between this power and number of seizures per day in this region (Pearson correlation, $p > 0.3$). In comparison of this power for different regions, in control animals the only significant difference was

Chapter 4: Phase-amplitude coupling and epileptogenesis in an animal model of MTLE

found between power of CA3 and EC, where EC was stronger than CA3 (Kruskal-Wallis test, Dens post hoc, $p < 0.001$). In epileptic animals, we had higher power in EC compared to all other regions (Kruskal-Wallis test, Dens post hoc, $p < 0.001$). We also checked the power in ripple band. Again, DG was the only region with significantly different power between groups, but this time higher in epileptic (Kruskal-Wallis test, Bonferroni corrected for multiple comparison, $p < 0.001$). In comparison of this power for different regions, in control animals only subiculum was stronger than EC (Kruskal-Wallis test, Dens post hoc, $p < 0.01$), and in epileptic animals, power in DG was stronger than CA3 and EC (Kruskal-Wallis test, Dens post hoc, $p < 0.001$).

4.5.3 Phase-amplitude coupling

As already mentioned, all PAC analysis was derived from data epochs of non-REM sleep, during interictal periods at least 1 hour apart from seizures. Our objective was to research new signal markers of epileptogenicity away from seizures. Sleep was a period of particular interest because of signal quality (no movement) and the presence of dominant slow oscillations, as frequency-for-phase candidates.

Figure 4.3A shows the EEG recorded from an epileptic animal that included ripple-band oscillations (80 – 200 Hz). The amplitude of oscillations in the ripple band was coupled to the phase of background slow-wave oscillations. Figure 4.3B reveals phase amplitude coupling in the time-frequency domain of this sample trace. Akin to [Canolty et al. \[2006\]](#), we obtained the time-frequency decompositions of raw EEG epoch (10 min). It was then averaged time-locked to each trough of the dominant slow oscillation (here 0.7 Hz). The top panel shows the normalized average time-frequency map (using logarithmic scale for frequency), and the bottom panel indicates the raw EEG epoch averaged about the trough of the 0.7 Hz cycle. This confirmed that the power of faster oscillations was indeed modulated by the phase of the slow rhythm. As shown in figure 4.3C, our PAC analyses covered high-frequency candidates in 20 – 250 Hz range. Systematic investigation of slow-to-fast PAC coupling over the frequency

Chapter 4: Phase-amplitude coupling and epileptogenesis in an animal model of MTLLE

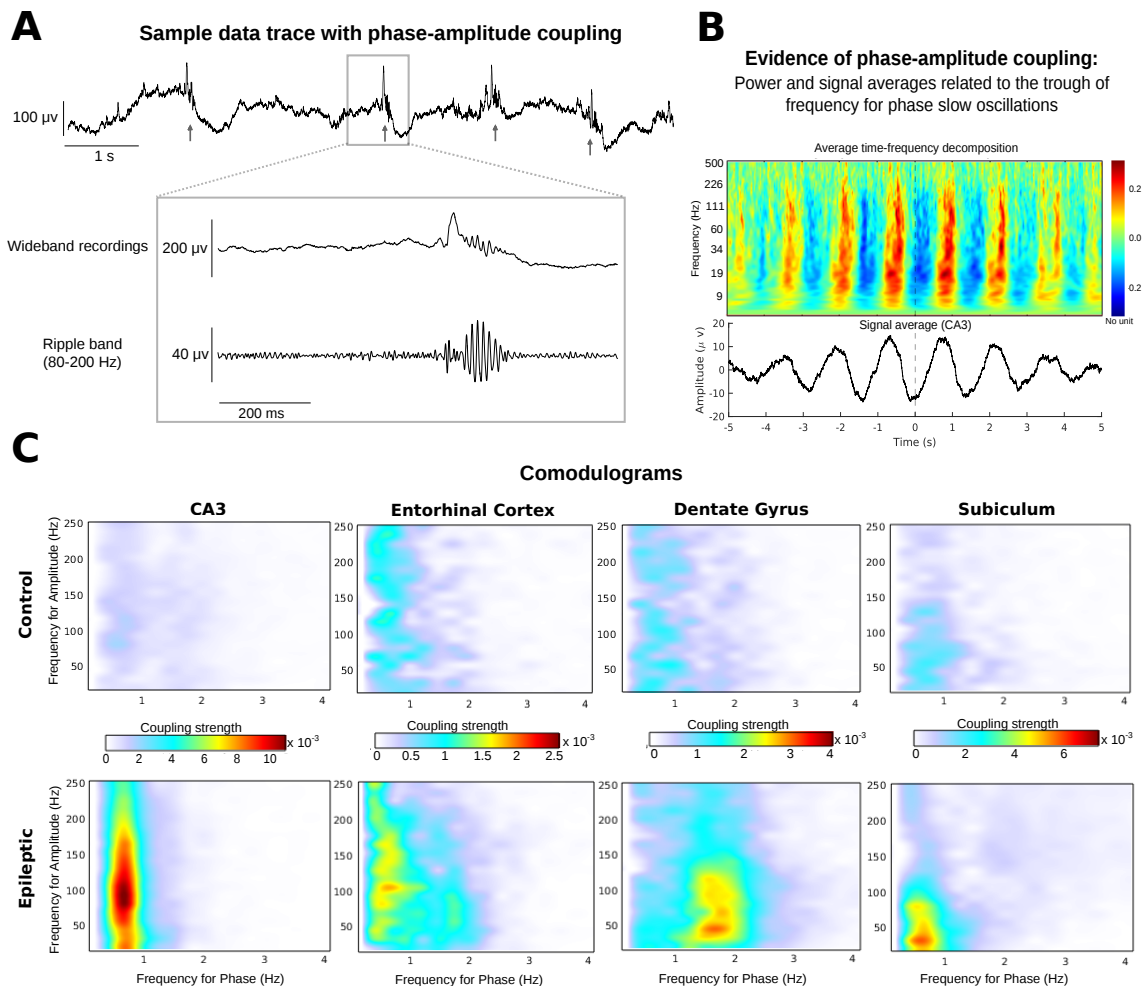


Figure 4.3: Phase-amplitude coupling in EEG recordings. A: Sample EEG trace from CA3 of an epileptic animal showing that oscillations in the ripple frequency band (80 – 200 Hz) are modulated by the phase of slow-wave fluctuations (signal polarity is negative up). B: Visualization of phase-amplitude coupling in the sample data trace shown in panel A: top panel plots the normalized time-frequency decompositions of EEG signal epoch time-locked averaged with respect to the troughs of the dominant slow oscillation (here 0.7 Hz); the bottom panel plots the corresponding averaged EEG signal (CA3). C: Average comodulogram representations of phase-amplitude coupling between slow (0.18 – 4 Hz) and fast (20 – 250 Hz) oscillations, in the control (top row) and epileptic (bottom row) groups. A comodulogram is a two-dimensional representation of the strength of PAC coupling between pairs of oscillatory signal components: frequency for phase f_P values is along the x-axis, and frequency for amplitude f_A values is along the y-axis. The strength of PAC coupling for each (f_P, f_A) pair is color-coded.

ranges of interest revealed that coupling strength was overall stronger in specific frequency bands in the epileptic group compared to controls (Fig. 4.3C). The plots illustrated in panels B and C of figure 4.3 indicate that PAC in the analyzed data was not caused by wide-band

Chapter 4: Phase-amplitude coupling and epileptogenesis in an animal model of MTLE

non-oscillatory activity, but presumably by band-limited ripple oscillations.

The maximum PAC coupling strength across all (f_P, f_A) tested frequency pairs was identified for each epoch and recording site, and compared between groups (Fig. 4.4A). We found that cross-frequency coupling in CA3 was stronger in epileptic animals compared to controls (Kruskal-Wallis test: $\chi^2(1,36) = 46.3$, Bonferroni corrected, $p < 0.001$). In the epileptic group, PAC was also stronger in CA3 compared to other regions (Kruskal-Wallis test: $\chi^2(3, 308) = 81.35$, post-hoc Dunns test for pairwise comparison: $p < 0.001$ compared to EC and DG, $p = 0.017$ compared to subiculum). The subiculum was the region with the second strongest PAC coupling values (post-hoc Dunns test, $p < 0.001$). In the control group, PAC was weaker in CA3 and DG than in EC and subiculum (post-hoc Dunns test for pairwise comparison: $p < 0.01$). We also found that the PAC coupling strength in CA3 and subiculum was positively correlated with the number of seizures per day, across all data epochs from the epileptic group (Pearson correlation, CA3: $\rho = 0.44$, number of epochs = 78, $p < 0.001$; Sub: $\rho = 0.41$, number of epochs = 78, $p < 0.001$, Fig. 4.4B). There was no relationship between daily seizure count and coupling strength in the other recorded regions ($p > 0.10$).

We did not find a monotonic positive relation between the power of slow oscillations and PAC strength measures (Pearson correlation: $\rho < 0$, $|\rho|s < 0.06$, $p > 0.49$). Therefore, we can safely assume that the PAC effects reported were not spuriously produced by harmonics in the electrophysiological waveforms [Jensen et al., 2016].

We also investigated whether the fast oscillatory bouts were generated at consistently preferred phase angles of the underlying slow-wave oscillations across all animals tested. Figure 4.5A shows the circular histograms of the PAC coupling phases, at each recording site and in both groups. We found preferred phase angles for PAC coupling, except in EC in controls (Rayleigh's test for non-uniformity, Bonferroni-corrected, $p < 0.01$). CA3 was the only recording site where both 1) PAC coupling was stronger in epileptic animals than in controls, and 2) fast oscillations occurred around one preferred phase angle of the underlying slow waves.

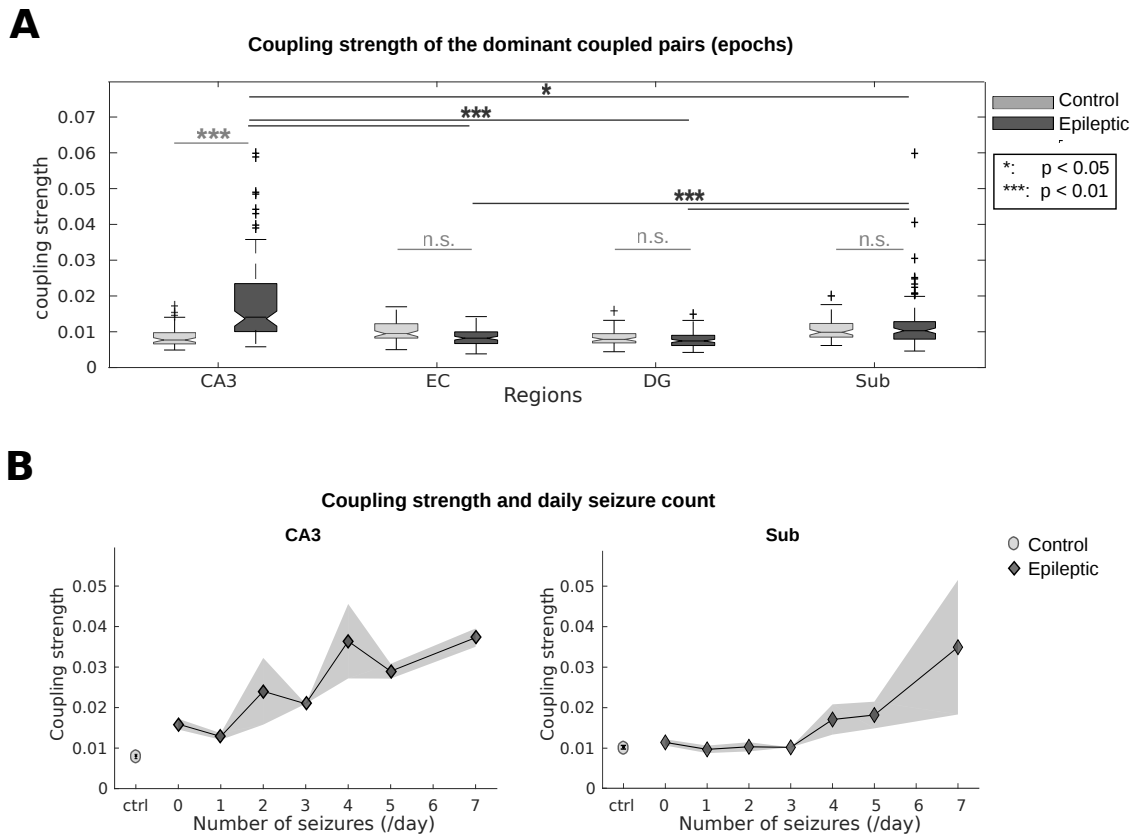


Figure 4.4: **PAC coupling strength.** A: Strength of PAC coupling in each group and at each recording site. In epileptic animals, PAC was stronger in CA3, followed by the subiculum (Kruskal-Wallis test: $\chi^2(1,36) = 46.3$, post-hoc Dunn’s test for pairwise comparison: $p < 0.05$). PAC coupling only in CA3 was stronger in epileptic animals than in controls (Kruskal-Wallis test: $\chi^2(3, 308) = 81.35$, Bonferroni corrected, $p < 0.001$). B: PAC coupling strengths across all data epochs from epileptic group were positively correlated with the number of seizures per day in CA3 (left, Pearson’s correlation, $\rho=0.44$, number of epochs = 78, $p < 0.001$) and Sub (right, Pearson’s correlation, $\rho = 0.41$, number of epochs = 78, $p < 0.001$).

Therefore, we performed detailed analyses of PAC phase angles in CA3, and found that in both control and epileptic animals, fast oscillations occurred preferentially over the ascending phase of the slow-wave oscillation (mean phase angle in controls: -0.53 rad, in epileptic animals: -0.60 rad). The observed mean phase angle was not significantly different between the two groups (Watson-Williams multi-sample test for equal means, $F(1,136)=0.08$, $p = 0.77$). In epileptic animals however, we found that the distribution of preferred phases of PAC coupling was unimodal and substantially more present over the ascending phase of the slow oscillation than in controls (Fig. 4.5B). Overall, the fast oscillatory PAC events occurred preferentially

Chapter 4: Phase-amplitude coupling and epileptogenesis in an animal model of MTLE

at the transition phase between the trough and peak of the slow oscillations associated with NREM sleep (Fig. 4.5C). The preferred phase concentration of fast oscillations towards the end of the transition between the trough and peak of concurrent slow oscillations, are consistent with previous reports in which different signal analysis methods were used to analyze human EEG data [Frauscher et al., 2015; Amiri et al., 2016; Song et al., 2017].

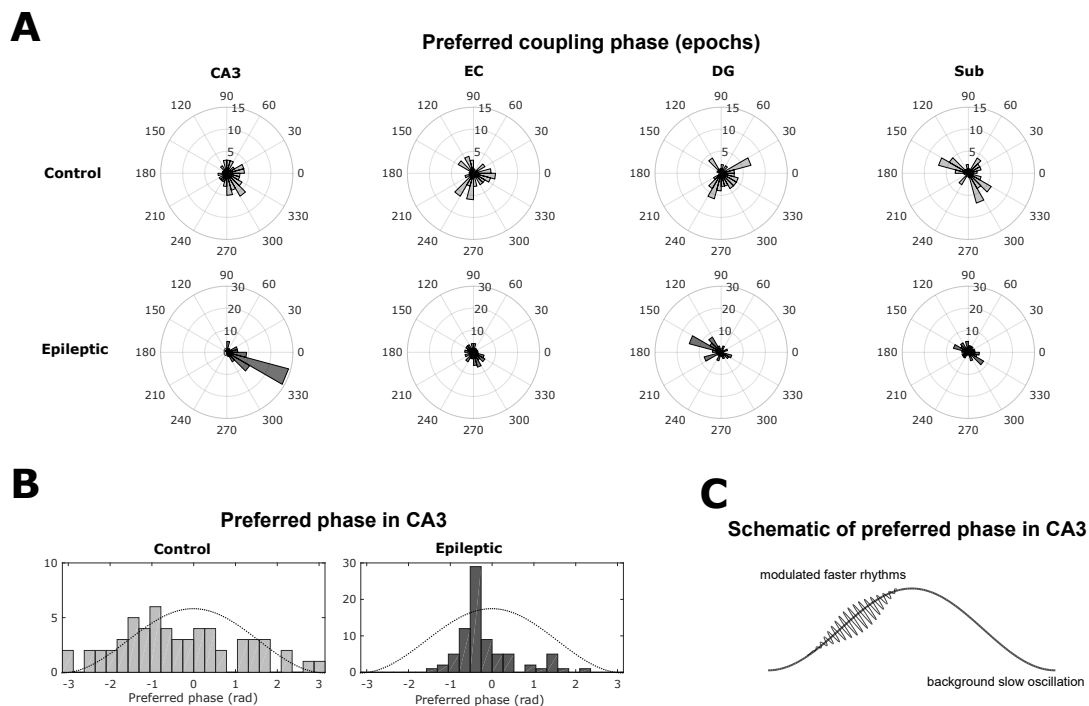


Figure 4.5: Distributions of the phase of fast oscillatory activity coupled to slow-wave oscillations. A: Polar plots show the preferred phase of fast oscillatory activity along the cycle of slow oscillations, across all epochs, for all recording sites and both groups (in degrees angle). Note that in all regions except EC in control animals, the distribution of PAC phase angles was not uniform (Rayleigh's test for non-uniformity, Bonferroni-corrected, $p < 0.01$) B: Histogram of observed coupling phase angles in CA3 along the cycle of the slow oscillatory signal, for control and epileptic animals (in radian). The distribution was more expressed towards the end of the ascending phase of the slow oscillatory cycle in epileptic animals. C: Schematic illustration of the observed phase and amplitude PAC effects: stronger bouts of fast rhythmic activity occurred consistently and preferentially towards the end of the ascending phase of the underlying slow-wave oscillations in CA3 of the epilepsy group. Akin to sleep surface EEG, the polarity of the slow oscillation was adjusted so that positive peaks mark the on state.

4.6 Discussion

Our study emphasizes multiple aspects of NREM sleep polyrhythmic activity in the seizure onset zone, in the pilocarpine animal model of MTLE: 1) at all recording sites, we confirmed the expression of PAC: the amplitude of fast oscillations above 20 Hz was modulated by the phase of an underlying slow wave below 4Hz ; 2) this coupling was stronger in the CA3 region of epileptic animals compared to controls; 3) PAC strength in CA3 was positively correlated with the number of seizures per day; and 4) in CA3, high-frequency (50 – 180 Hz) oscillations occurred preferentially towards the end of the transition between the trough and peak of the underlying slow cycles (< 1 Hz). Our results confirm that PAC is a ubiquitous phenomenon in electrophysiology [Canolty and Knight, 2010; Buzsáki et al., 2012; Baillet, 2017]. However, they also reveal that PAC signal parameters, such as coupling strength and phase, are relevant to understand the properties of epileptic networks in MTLE. Our findings also emphasize that stronger PAC coupling in the seizure onset zone is related to seizure occurrence.

By extension of the communication through coherence hypothesis [Fries, 2015], it has been proposed that phase-amplitude coupling may be a signal marker of information transfer from large-scale cellular networks to small-scale fast processing networks engaged in effective synaptic modification [Canolty and Knight, 2010]. Rodent studies of the mesial temporal regions engaged in working memory processes have shown how PAC may enable multiplexed signal communication between sub-regions of the hippocampus and adjacent structures [Colgin, 2016]. Recent imaging work of the electrophysiology of the human resting state also points at the possible role of PAC as a mechanism for large-scale network communication [Florin and Baillet, 2015]. PAC parameters are related to the dynamics of network excitability in neural assemblies [Buzsáki and Wang, 2012]. For this reason, they are pertinent measures of electrophysiological manifestations of neurological diseases and syndromes that primarily or secondarily affect neural excitability. For instance, early, pre-symptomatic reductions of PAC coupling were observed in vivo in the temporal regions of a mouse model of Alzheimer's disease [Goutagny

Chapter 4: Phase-amplitude coupling and epileptogenesis in an animal model of MTLE

et al., 2013]. Alternatively, strong PAC coupling was found in the motor cortex of Parkinsons patients [van Wijk et al., 2016].

We showed here that fast oscillations, essentially in the gamma-ripple band (50-180 Hz), were modulated in amplitude by the phase of slow-wave oscillations (< 1 Hz) in all regions, both in controls and epileptic animals. Our data are in line with previous studies showing strong PAC coupling between the gamma band and slow-wave oscillations in rodents [Andino-Pavlovsky et al., 2017; López-Azcárate et al., 2013], primates [Steriade et al., 1996; Isomura et al., 2006; Takeuchi et al., 2015] and humans [Monto et al., 2008].

To the best of our knowledge, our study is the first to measure phase-amplitude coupling in the temporal lobe after a pilocarpine-induced SE, between the gamma-ripple band and slow-wave oscillations. Epileptic animals showed stronger PAC coupling in the CA3 area, which is often identified as a seizure onset zone in the pilocarpine model of MTLE [Lévesque et al., 2012; Behr et al., 2017; Toyoda et al., 2013]. Therefore, our observations are in agreement with previous reports showing strong PAC in the seizure onset zone of epileptic patients [Amiri et al., 2016; Nariai et al., 2011; Weiss et al., 2013; Ibrahim et al., 2014; Guirgis et al., 2015; Weiss et al., 2016]. Taken together, these results are consistent with the idea that large networks of neurons fire in synchrony, and produce local-field oscillatory signals in the gamma ripple band that are triggered by slow-wave oscillations. Such fast signals were previously found in the seizure onset zone of epileptic patients [Medvedev et al., 2011; Urrestarazu et al., 2007], with slow-wave oscillations (< 1 Hz) modulating these faster oscillatory signal components [Frauscher et al., 2015]. Widespread high-amplitude slow waves are prominent during sleep and could facilitate the expression of such high-frequency activity [Nazer and Dickson, 2009; Frauscher et al., 2015]. The mechanisms of generation of high-frequency activity facilitated by slow-wave oscillations remain unclear. Partial evidence suggests that slow-wave oscillations enhance synaptic excitability and hyper-excitability, which would in turn facilitate the development of pathological hyper-synchrony, and eventually epileptiform activity [Nazer and

Chapter 4: Phase-amplitude coupling and epileptogenesis in an animal model of MTLE

Dickson, 2009; Schall et al., 2008; Wolansky et al., 2006].

We also found that PAC coupling strength in CA3 and subiculum was positively related to seizure occurrence, with stronger PAC coupling associated to high seizure rates. This is presumably the first report of such association between seizures occurring after SE and PAC coupling strength in temporal regions. These findings are in line with the hypothesis that episodes of enhanced excitability - marked in the EEG by stronger coupling between gamma-ripple band activity and slow-wave oscillations - are associated with a higher probability of seizure occurrence. Our data are also in agreement with previous evidence showing that interictal spikes are coupled to high-frequency activity in CA3 during episodes of high seizure activity in the pilocarpine model of MTLE [Behr et al., 2015; Lévesque et al., 2011]. The subiculum was also previously described as the onset zone of spontaneous seizures in some cases of the pilocarpine model of MTLE [Lévesque et al., 2012; Toyoda et al., 2013]. We may therefore assume that changes in PAC in the seizure onset zone reflect time-windows during which neuronal networks undergo substantial changes in neuronal network excitability.

Furthermore, we found that high-frequency oscillations in CA3 occurred preferentially towards the end of the phase transition between troughs and peaks of slow-wave oscillations. Several previous reports pointed at the influence of the coupling phase in the registration of perceptual items by brain systems [Jensen and Colgin, 2007; Gips et al., 2016]. In epilepsy, a recent study suggested that the phase of occurrence of high-frequency oscillations may be used to distinguish physiological from pathological events [Song et al., 2017]. Our findings are concordant with this relatively scarce literature published so far. However, one limitation of our study is that we did not use a surface reference electrode, which would have facilitated the registration of the slow-wave peaks and troughs we observed with the actual up and down states of NREM sleep. Nevertheless, we followed the guidelines published by Ellenrieder et al. [2016] for slow-wave signal interpretation under similar circumstances. Moreover, our data showing a preferred coupling phase towards the end of the transition from slow-wave troughs to peaks are

Chapter 4: Phase-amplitude coupling and epileptogenesis in an animal model of MTLE

concordant with previous reports on epileptic PAC in human recordings [Frauscher et al., 2015; Amiri et al., 2016; Song et al., 2017].

In this study, we report on data epochs exclusively from NREM sleep. The rationale is twofold: 1) Contrarily to our data from other sleep stages and wakefulness, NREM sleep data showed a dominant slow oscillation throughout epochs, which we considered a conservative requisite for measuring PAC; 2) interictal NREM sleep produced the lowest rate of movement artefacts, compared to active wakefulness, which was a factor of data quality in support of our findings. Subsequent research would be required to investigate whether similar PAC signal markers of epileptogenicity would be present during wakefulness and other sleep stages. We also look forward to further PAC studies of the transition between interictal and ictal status. Such research may clarify the physiological mechanisms and circuits involved in seizure activity.

Taken together, our results indicate that measures of phase-amplitude coupling between the phase of slow-wave oscillations and the amplitude of local gamma-ripple band oscillations, are indicative of pathological network activity in the seizure onset zone of pilocarpine-treated epileptic animals. These findings emphasize the potential role of PAC measures as a signal marker of epilepsy. We also anticipate that PAC measures will contribute to improve our understanding of how polyrhythmic brain activity structures the neural dynamics of communication within and between brain systems, and how it is impaired during epileptogenesis and around seizure occurrence. Future studies should consider producing histological analyses in addition to electrophysiological recordings, to further relate the observed PAC signal markers with anticipated structural and morphological changes in tissues.

Conflict of interest

None of the authors has any conflict of interest to disclose.

Chapter 4: Phase-amplitude coupling and epileptogenesis in an animal model of MTLE

Acknowledgments

The authors thank Dr. Charles Behr for his help in surgical preparation of the animals used in this study that was supported by the Canadian Institutes of Health Research (CIHR grants 8109 and 74609 to M.A.). S.S. acknowledges the support from McGill University Integrated Program in Neuroscience. S.B. was supported by a Discovery Grant from the National Science and Engineering Research Council of Canada (436355-13), the NIH (2R01EB009048-05) and a Platform Support Grant from the Brain Canada Foundation (PSG15-3755).

5

Chapter 5: Neurophysiological network dynamics for pitch discrimination

5.1 Preface

This chapter is dedicated to the analysis of phase-amplitude coupling as a marker of neural activation and network dynamics for pitch discrimination. The study used magnetoencephalography recordings from both healthy controls and individuals with amusia. I investigated how this congenital disorder affects the oscillatory mechanisms (via CFC) and associated functional connections found in healthy individuals. The details of study design, analyses and results are provided in this chapter.

This chapter is submitted for publication in a journal as: "Samiee, S., Florin, E., Vivan, D., Albouy, P., Peretz, I., and Baillet, S. Oscillatory network dynamics for pitch discrimination. *Submitted*"

Contributions

SS was responsible for designing the analysis method, wrote the codes, performed data analyses, produced all figures and wrote drafts and the final version of the manuscript. EF and DV were involved in data collection and study design. PA contributed to the approach and reviewed the final version of the manuscript. IP was responsible for the study design, co-funding, and reviewed the final version of the manuscript. SB was responsible for supervising the project, co-funding, as well as editing drafts and the final version of the manuscript.

5.2 Abstract

Pitch discrimination is crucially involved in music and speech auditory processing. It is compromised in several chronic and developmental neurological conditions and mental-health disorders. Yet, the brain mechanisms involved at the systems level remain poorly understood. Here we used neurophysiological brain imaging to identify the hierarchy of oscillatory neural dynamics expressed in a pitch-discrimination task requiring the detection of pitch changes in a sequence of pure tones. We sought to clarify the cross- and poly-frequency network dynamics within and between auditory and downstream brain regions associated with task performance. To this end, we recruited normal-hearing and congenital amusic participants and used magnetoencephalography time-resolved source imaging. Amusics have difficulties in discriminating pitch variations in auditory sequences. Their data were used to identify the components of local and network brain dynamics essential for correct task performance.

We found that in the auditory cortex, delta-to-beta band cross-frequency coupling increased dynamically at the onset of the tone sequence and culminated at the occurrence of the target tone. We also found hierarchical and frequency-specific expressions of directed connectivity between the auditory, inferior frontal and motor cortices during tone-sequence presentation. Our data show bottom-up signaling directed from auditory regions to the inferior frontal and motor cortices, which were entrained at the rate of the tone sequence presentation. Symmetrically, we also found that beta-band activity was directed, in a top-down fashion, from motor cortex towards both inferior frontal and auditory regions. Top-down beta coupling was also expressed during baseline resting state but became time-locked to tone occurrences during the presentation of the auditory sequence.

Overall, our results emphasize the dynamical and anatomically-distributed nature of cross- and poly-frequency interactions between bottom-up stimulus-driven signalling, and top-down motor signals of predictive timing in auditory perception. Functional impairment in amusics

Chapter 5: Neurophysiological network dynamics for pitch discrimination

was associated with both chronically elevated levels of delta-to-beta phase-amplitude coupling during rest and task performance, and depressed bottom-up connectivity between auditory cortex and downstream regions.

Keywords:

Pitch discrimination, Neural oscillations, Audition, Active inferences, Predictive coding, Predictive timing, Phase-amplitude coupling, Phase transfer entropy, Amusia, Directed connectivity, Magnetoencephalography, Brain network dynamics.

5.3 Introduction

Pitch discrimination is essential to the identification and registration of complex auditory stimuli as in music and speech [Ahmed et al., 2018]. A wide body of functional brain imaging studies have reported on the anatomically-distributed nature of the brain processes involved. At the cortical level, the superior temporal gyrus, inferior frontal lobule and prefrontal cortex are regions along the ventral auditory pathway recruited by pitch discrimination [Zatorre et al., 1992; Gaab et al., 2003; Albouy et al., 2013; Peretz, 2016; Hohmann et al., 2018]. The strength of structural connections between the inferior frontal gyrus and the superior temporal auditory cortex along the arcuate fasciculus is associated with pitch discrimination abilities [Loui et al., 2009]. Further, when temporal attention is required to discriminate between tones presented in temporally-organized sequences, the brain network involved also includes the lateral motor cortices [Morillon and Baillet, 2017; Chang et al., 2018], highlighting the functional interactions between endogenous predictive timing and the registration of incoming sensory events [Chen et al., 2008; Zarate and Zatorre, 2008; Fujioka et al., 2012; Arnal and Giraud, 2012].

Beyond mapping, the dynamic, neurophysiological aspects of pitch discrimination remain elusive. To approach this question, we adopted the mechanistic view that hierarchically coupled, poly-frequency neural oscillations contribute to brain sensory registration and processing [Schroeder and Lakatos, 2009b]. Such cross-frequency interactions between the typical frequency bands of electrophysiology are actively studied as possible vehicles for inter-regional brain network integration [Engel et al., 2001; Engel and Fries, 2010; Florin and Baillet, 2015]. Fontolan et al. [2014] for instance reported on cross-frequency interactions between brain oscillations in the delta ([1-4] Hz), beta ([15-35] Hz) and gamma ([40-80] Hz) bands in auditory cortex during speech listening. Phase-amplitude coupling (PAC) is one of the most studied forms of cross-frequency coupling in neurophysiology. Changes in PAC characteristics – in terms of slow frequency for phase or fast frequency for amplitude, coupling strength and preferred phase of fast-frequency bursts occurrences along the slow-frequency cycle – have been related

Chapter 5: Neurophysiological network dynamics for pitch discrimination

to sensory, motor and cognitive events [Canolty and Knight, 2010] and in the dynamics of inter-regional connectivity in resting-state brain networks [Florin and Baillet, 2015]. Although PAC emerges from interconnected cell-assemblies and networks in normal healthy functions, there is growing evidence from patient and preclinical data in Parkinson's disease [de Hemptinne et al., 2013; van Wijk et al., 2016], epilepsy [Amiri et al., 2016; Samiee et al., 2018] and autism spectrum disorder [Berman et al., 2015] that excessive levels of PAC are associated with brain dysfunctions. The actual pathophysiological mechanisms could be related to the notion that PAC is related to the dynamical fluctuations of net excitability in cell assemblies – a mechanism primarily or secondarily impaired in multiple brain conditions.

In the present study, we aimed to identify the local and inter-regional cross-frequency cortical dynamics involved in pitch discrimination. We sought to establish which of these components are essential to the realization of the task, by contrasting the neurophysiological activity of healthy participants with that of subjects affected by congenital amusia. Amusia, or tone deafness, is a disorder that affects the perception and production of music [Ayotte et al., 2002]. In particular, amusics have difficulties in detecting variations of auditory pitch in tone sequences [Peretz, 2016].

We restricted our investigations to a set of regions of interest along the ventral auditory pathway and to their functional interactions with the motor cortex. Indeed, pitch discrimination from a sequence of tones engages predictive processes in terms of timing and encoding of the target auditory input. Based on Morillon and Baillet [2017], we expected that these processes of active inference would manifest in the coupling between the phase of low-frequency cortical rhythms entrained at the rate of presentation of the tone sequence, and the amplitude of beta oscillations associated with the predictive timing of the occurrence of the target tone [Arnal and Giraud, 2012]. Also following Morillon and Baillet [2017], we expected neurophysiological activity to be entrained downstream along the auditory ventral pathway at the rate of the tone presentation. We also anticipated to observe top-down inter-regional influences from the

Chapter 5: Neurophysiological network dynamics for pitch discrimination

motor cortex on auditory regions, expressed in the beta range [Michalareas et al., 2016]. We sought to identify differences along these measures between the two groups of participants to further characterize the mechanistic aspects in brain neurophysiology that are essential to pitch discrimination. We also tested whether these latter would be expressed by default, in the brain resting-state of the amusic brain vs. normal-hearing controls.

5.4 Material and Methods

5.4.1 Participants

Sixteen participants with no musical education were recruited in the study (age: 62.6 ± 6 y, 4 male). Eight were affected by the amusia disorder, according to the Montreal Battery of Evaluation of Amusia (MBEA) [Peretz et al., 2003]. The other eight participants were controls with no musical impairment, matched in age, gender and years of education. The experimental paradigm was reviewed and approved by the ethics review procedures of McGill University Health Centre (Protocol: NEU-12-023). All participants gave written informed consent to take part in the study.

5.4.2 Experimental design

The paradigm was adapted from Hyde and Peretz [2004] and Peretz et al. [2005]. Each trial consisted of a sequence of five pure tones: Tones 1, 2, 3 and 5 were identical and played at the pitch level of C6 (1047 Hz; standard pitch). Tone 4 was the target tone played at 5 different pitch levels across trials. In half of the trials, the target tone was played at the standard C6 (1047 Hz) pitch ("standard" trials). In the other half of the trials ("deviant" trials), the target tone was played with a deviation of 25, 50, 100, or 200 cents (100 cents corresponds to 1 semitone) from the standard tone. Each tone was presented for 100 ms, and the time interval between two consecutive tone onsets in a sequence (inter-tone interval, ITI) was 350 ms. The total duration

Chapter 5: Neurophysiological network dynamics for pitch discrimination

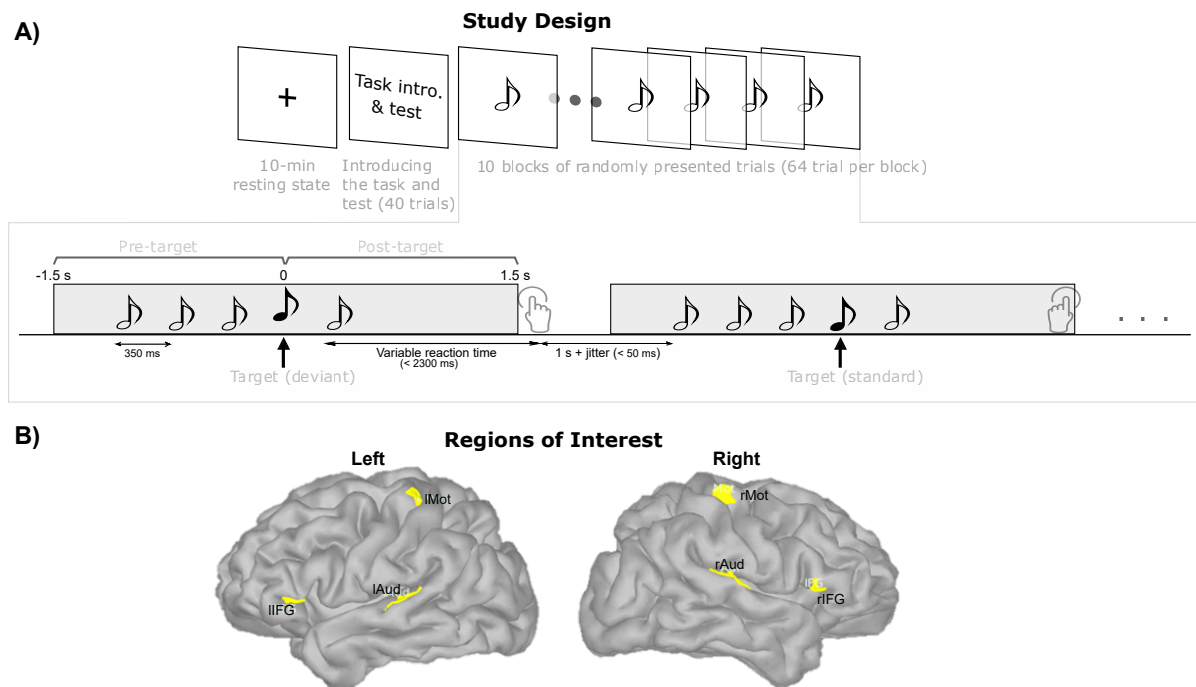


Figure 5.1: A) Experimental design. B) Anatomical regions of interest in a representative subject.

of a sequence was 1.4s (Fig. 5.1A).

Ten minutes of resting-state were recorded from all participants (eyes open) at the beginning of the session. Task instructions were then given to the participants: they were asked to listen to tone sequences and to press a button with either of their index fingers, to indicate whether the presented sequence comprised a standard or a deviant target sound. They were instructed to keep their gaze fixed on a crosshair displayed on a back projection screen positioned at a comfortable distance. Responses with the right or left hand to standard vs. deviant trials were intermixed between participants. All subjects received 40 training trials prior to data collection with magnetoencephalography (MEG). Following training, no feedback was provided to participants about whether their detection of pitch deviation was correct.

A total of 640 tone sequences were presented to every participant, in 10 blocks of 64 trials. There were a total of 320 standard tone sequences and 80 deviant trials per pitch deviance level. Trials started in succession, 1 second ($\pm < 50\text{ ms}$ jitter) following the subject's response to the

previous trial.

5.4.3 Data acquisition

MEG data was collected during resting-state and task performance in seated position using a 275-channel CTF MEG system, with a sampling rate of 2400 Hz. Simultaneous EEG data was recorded from four standard electrode positions: FZ, FCZ, PZ, and CZ. The audio presentations, subject button presses, heartbeat and eye movement electrophysiological signals (ECG and EOG, respectively) were also collected in synchronization with MEG. Head position was monitored and controlled using three coils attached to the subject's nasion and both pre-auricular points. The headcoil locations and 100 scalp points were digitized prior to MEG recordings in each individual, using a Polhemus 3-D digitizer system. We performed T1-weighted MRI in each participant (1.5-T Siemens Sonata, 240×240 mm field of view, 1 mm isotropic, sagittal orientation) for cortically-constrained MEG source imaging [Baillet, 2017].

5.4.4 Data preprocessing and source modeling

Contamination from system and environmental noise was first attenuated using CTF's 3rd-order gradient compensation. All further data preprocessing and modeling was performed with Brainstorm [Tadel et al., 2011] following good-practice guidelines [Gross et al., 2013a]. The recordings were visually inspected, with segments contaminated by excessive muscle artifacts, head movements or remaining environmental noise marked as bad and discarded from further analysis. Powerline artifacts at 60 Hz and harmonics were reduced using notch filters. Signal-space projectors (SSP) were designed using Brainstorm's default settings to attenuate the electrophysiological contamination from heartbeats and eye blinks.

The MRI data was segmented using the default FreeSurfer pipeline. For distributed source imaging, we used Brainstorm to downsample the cortical surface tessellation produced to 15,000 vertices. We derived a forward MEG head model for each individual using the overlapping-

Chapter 5: Neurophysiological network dynamics for pitch discrimination

sphere analytical approach (with Brainstorm default settings). We then obtained a weighted minimum-norm estimate (wMNE; Brainstorm with default settings) to project sensor-level pre-processed data onto the 15,000 vertices of the individual cortical surface, in each individual. The empirical covariance of sensor noise, required for wMNE modeling, was estimated from a 2-min empty-room MEG recording collected at the beginning of each session.

5.4.5 Event-related responses

The event-related brain responses were extracted from the time-locked average of correctly-detected trials in all experimental conditions (standard and various degrees of pitch deviance). Electrophysiological signals were bandpass filtered between [0.5, 50] Hz, and baseline corrected using the 150 ms before the presentation of the target tone ([-150, 0] ms).

5.4.6 Regions of interest

We defined six anatomical regions of interest in each individual using a MEG functional localizer. The right and left auditory cortices (rAud and lAud) were identified as the regions presenting the strongest M100 (100 - 120 ms) event-related average response to all tones. The surface area was restricted to $\sim 3 \text{ cm}^2$ per region. We defined rIFG and lIFG as portions of Brodmann BA45, identified in each individual from the Brodmann cortical atlas provided by Freesurfer. rIFG and lIFG were the regions where maximum differential activity was observed between deviant and standard tones, around 100 ms after target tone presentation. Their surface area was restricted to $\sim 1.3 \text{ cm}^2$. Left and right cortical motor regions (lMot and rMot, respectively) were defined with a surface area of $\sim 3 \text{ cm}^2$ at the pre-central locations with the largest M50 50-ms latency responses evoked after right-hand and left-hand button presses in all trials, respectively (Fig. 5.1B).

5.4.7 Monitoring of vigilance: posterior alpha-band activity

We selected a cluster of five posterior MEG channels presenting the highest levels of pre-target alpha-band activity ([8, 12] Hz) across subjects (MZP01, MLP31, MRP31, MLP32, MRP32). We computed the power of MEG signals at these sensor locations over the pre-target period ([-1.5, 0] s) of each trial. We used the even-order linear-phase FIR filters in Brainstorm (band-pass: [8, 12] Hz, stop-band attenuation: 40 dB, 99% energy transient: 0.402 s) and computed the root-mean-square signal strength across the sensor cluster for each trial. We used the same approach for EEG, restricted to electrode PZ.

5.4.8 Phase-amplitude coupling

We used a time-resolved measure of phase-amplitude coupling (tPAC) between co-localized slow and fast cortical signal components [Samiee and Baillet, 2017]. tPAC measures the temporal fluctuations of the coupling between the phase of slower activity (at frequency f_P) and the amplitude of faster signal components (at frequency f_A). Briefly, the instantaneous amplitude of faster signals ($A_{f_A}(t)$) in a sub-band of the f_A band of interest was extracted using Hilbert transform. Power spectral analysis was used to identify the frequency of strongest oscillation in $A_{f_A}(t)$ (in the f_P band of interest), coinciding with an oscillation in the original time series. This frequency was then labelled as the f_P frequency coupled to the current fast f_A frequency. The coupling strength between $A_{f_A}(t)$ and the instantaneous phase of the signal filtered around f_P was then calculated. All methodological details for tPAC were published elsewhere [Samiee and Baillet, 2017] and we used the implementation openly available in Brainstorm.

We extracted comodulograms to identify the strongest modes of (f_P, f_A) coupling over time windows of 1.5 s that contained the entire tone sequence at every trial, testing 20 different f_A centre frequencies in the [15, 250] Hz band. The f_P band of interest was [2, 12] Hz. When resolving PAC in time, we tracked the temporal variations of the strongest mode of coupling observed in the comodulograms extracted in the previous step. tPAC was derived from 700-ms

Chapter 5: Neurophysiological network dynamics for pitch discrimination

time windows with 50% overlap, and with [2, 4] Hz as the f_P band and [15, 35] Hz as the f_A band.

5.4.9 Stimulus-brain response coupling

We assessed whether the auditory stimulus tone sequence induced modulations of beta activity in the auditory cortex. We therefore generated a reference sinusoidal signal at 2.85 Hz (the rate of the tone presentations every 350 ms), with its peak at the onset of each tone presentation. We then estimated the tPAC cross-frequency coupling between the phase of this reference signal and the amplitude of beta oscillations in the auditory regions of interest. We tracked the variations in time of this coupling using tPAC with a sliding window length of two cycles of the tone presentation rate (700 ms), with 50% of overlap. We identified the preferred phase of tPAC coupling along the frequency cycle of reference. We transformed the corresponding phase angle to a time latency over the 350-ms cycle of the stimulus reference signal.

5.4.10 Effective connectivity estimation with directed phase-transfer entropy

We evaluated the directed functional connectivity between the regions of interest (ROIs) using directed phase-transfer entropy (dPTE) [Lobier et al., 2014]. Akin to Wiener-Granger causality, dPTE measures effective connectivity based on the respective instantaneous phases of pairs of narrow-band neurophysiological signals. The frequency bands of interest for the source signals extracted from each ROI were in the delta [2, 4] Hz and beta [15, 35] Hz ranges. The delta band contains the tone-sequence presentation rate (2.85 Hz). The beta band was expected to mark top-down inter-regional communications between motor and auditory cortices [Morillon and Baillet, 2017]. dPTE is a signed measure, which is indicative of the estimated direction for effective connectivity. For example, considering two regions A and B, positive (respectively negative) dPTE values indicate information transfer from cortical node A (resp. B) to cortical

note B (resp. A). We used the dPTE code openly shared by Hillebrand et al. [2016] and available in Brainstorm.

5.4.11 Statistical analyses

Parametric tests (e.g., t-tests against zero-mean, paired t-tests, repeated measure ANOVAs) were employed. Tukey’s tests were used for post-hoc analyses and corrections against multiple comparisons. tPAC values were assessed for statistical significance using a non-parametric resampling approach: for each trial, we generated 500 surrogates using block-resampling [Samiee and Baillet, 2017]. Each surrogate was produced from selecting five time points randomly in the trial epoch to subdivide the instantaneous phase signal into five blocks. These blocks were then randomly shuffled. tPAC was estimated from the resulting block-shuffled phase signal and from the original instantaneous amplitude time series. This resampling technique provides reference surrogate signals with no phase-amplitude coupling beyond chance levels and with minimum phase distortion. The tPAC values obtained from the surrogate data were normally distributed (Shapiro-Wilk test, $p > 0.8$). tPAC values from each original trial was z-scored with respect to the empirical distribution of tPAC values obtained from the surrogate data generated from the same trial (Eq. 5.1):

$$tPAC_z(\text{trial } i) = \frac{tPAC(\text{trial } i) - \text{average}(tPAC_{\text{Surrogate}}(\text{trial } i))}{\text{std}(tPAC_{\text{Surrogate}}(\text{trial } i))}. \quad (5.1)$$

5.5 Results

5.5.1 Behavior

We call hit-rate the ratio of correctly detected trials for all five deviance levels (Fig. 5.2A). A two-factor (group \times deviance level) between-subject ANOVA on observed hit rates revealed a significant interaction between groups and deviance levels, $F(1, 4) = 19.1$, $p < 0.001$. There

Chapter 5: Neurophysiological network dynamics for pitch discrimination

was no difference in accuracy between deviance levels of 25 and 50 cents (post-hoc Tukey test, $t(70) < 1.1$, $p_{Tukey} > 0.98$), and between deviance levels of 100 and 200 cents ($t(70) \leq 0.28$, $p_{Tukey} = 1$). For this reason, we combined the trials with deviance levels of 25 and 50 under one condition called *low deviance*, and all trials with deviance levels of 100 and 200 cents under another condition labelled *high deviance*.

Fig. 5.2B shows the behavioral performances expressed as the differences in hit rates versus false detection rates in both conditions. In both deviant conditions, the hit rate was the percentage of correctly detected deviant trials; false detection was for trials when standard target tones were detected as deviants. In the standard condition (deviance = 0 cent), the hit rate was the percentage of correctly detected standard trials; the false detection rate was the percentage of deviant tones mistakenly reported as standards.

There was a significant interaction $F(1, 2) = 39.6$, $p < 0.001$ between groups and deviance level. Controls performed better than amusics in the standard ($t(74) = 4.53$, $p_{Tukey} < 0.001$) and low deviance conditions ($t(74) = 12.70$, $p_{Tukey} < 0.001$). There was no significant difference in performances of controls between the high and low deviance conditions ($t(74) \leq 2.58$, $p_{Tukey} \geq 0.11$). Amusics did perform significantly better in the high deviance condition and significantly worse in the low deviance condition (standard vs low deviance: $t(74) = 6.19$, $p_{Tukey} < 0.001$, standard vs. high deviance: $t(74) = -6.19$, $p_{Tukey} < 0.001$, low vs. high deviance: $t(74) = -15.16$, $p_{Tukey} < 0.001$).

We used d' as a measure of sensitivity in behavioral performances of each participant in the low and high deviance conditions (Fig. 5.2C). We found a significant interaction between the level of target pitch deviance and groups ($F(1,1)=20.3$, $p < 0.001$). Both controls and amusics showed significantly higher sensitivity to high deviance compared to low (controls: $t(60) = 4.07$, $p_{tukey} < 0.001$, amusics: $t(60) = 10.45$, $p_{tukey} < 0.001$). Controls were more sensitive than amusics in the low-deviance condition ($t(60) = 7.53$, $p_{tukey} < 0.001$) but not in high-deviance trials ($t(60) = 1.15$, $p_{tukey} = 0.66$).

Chapter 5: Neurophysiological network dynamics for pitch discrimination

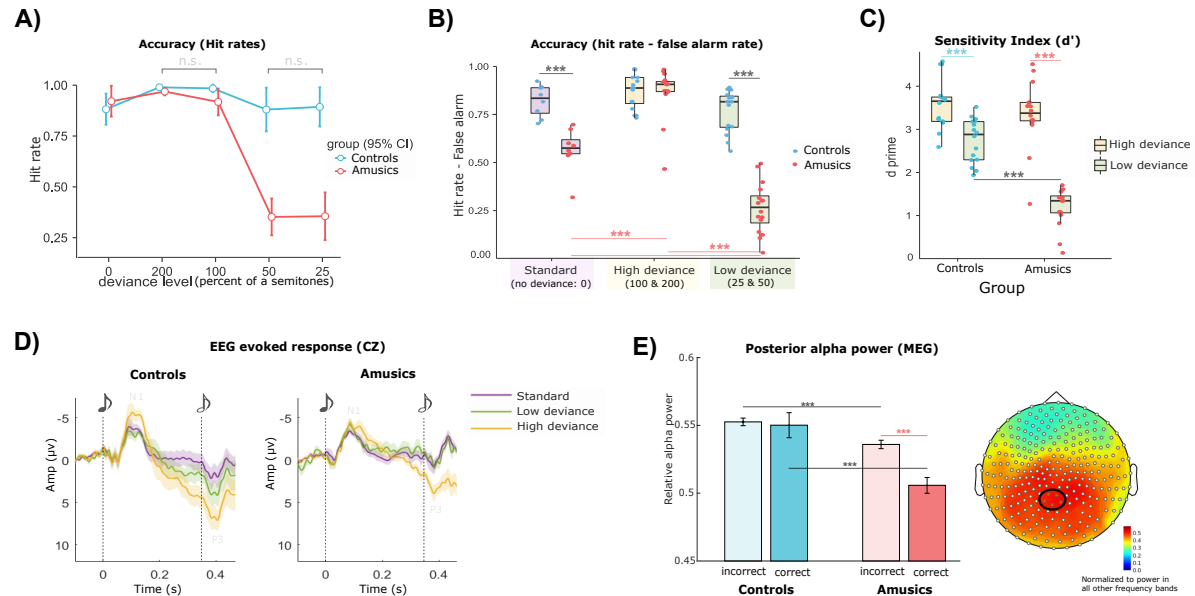


Figure 5.2: Behavioral performances, vigilance and event-related EEG responses. A-C) Behavioural performances: A) hit rate for 5 different deviance levels of target tone (with respect to the first three tones in each trial): 0 deviance reflects the condition with all tones having the same pitch frequency (standard trials). In all other four conditions there was a deviant pitch tone presented as target. There were no significant interactions between groups and pitch deviance levels of 25 and 50 cents, and 100 and 200 cents, respectively. The trials from each of these two trial subgroup were combined under "low" and "high" deviance conditions in all subsequent analyses. B) The difference between hit rates and false detection rates are presented for the two resulting grouped conditions. C) Sensitivity index (d') for amusics and controls in the high and low deviance conditions. D) EEG event-related responses in the standard, low and high deviance conditions in both groups. E) Posterior alpha power averaged over trial baselines (pre-target period) across a cluster of posterior MEG sensors as a measure of vigilance.

5.5.2 Event-related responses

Group average event-related responses to target tone presentations are shown for electrode CZ in Fig. 5.2D. There was a clear N1 component around 110 ms following the onset of the target tone in both groups and all three conditions. In line with previous reports [Peretz et al., 2005], both amusics and controls produced a P3 component in the high-deviance condition (yellow trace). The P3 response was weaker for standard tones in both groups. In the low-deviance condition, amusics showed similar responses than to standards, with controls producing a P3 which amplitude was intermediate between those in standard and high-deviance conditions.

5.5.3 Posterior alpha power

We measured the posterior normalized alpha power as a proxy for vigilance [Valentino et al., 1993], attention [Aftanas and Golocheikine, 2001] and the cognitive demand of the task [Gevins and Smith, 2000; Ciesielski et al., 2007]. Higher alpha levels could indeed account for lower task performances between groups and confound the interpretation of the data. There was a main effect for group and task performance (Fig. 5.2E). Amusics produced lower levels of posterior alpha activity ($F(1)=28.37, p < 0.001$), which could be indicative of the task requiring higher attentional demands for this group [Gevins et al., 1979; Smith et al., 1999]. Posterior alpha activity was reduced in correct trials ($F(1)=8.1, p = 0.004$), which is consistent with its negative relationship with attention and vigilance. Interactions between response accuracy and groups were significant (accuracy \times group interaction: $F(1)=5.86, p = 0.01$), with a post-hoc Tukey's test showing lower alpha power in correct trials in amusics ($t(9262)=-4.46, p_{Tukey} < 0.001$) and significantly lower posterior alpha levels in amusics compared to controls in both correct and incorrect trials (correct: $t(9262)=3.98, p_{Tukey} < 0.001$, incorrect: $t(9262)=4.16, p_{Tukey} < 0.001$). We produced similar observations from the simultaneous EEG recordings at electrode Pz (not shown).

5.5.4 Phase-amplitude coupling

We set the search frequency range for f_P to [2, 12] Hz and [15, 250] Hz for f_A , for the detection of local phase-amplitude coupling in the right-hemisphere ROIs using tPAC. Previous studies reported on right-hemisphere dominance in similar pitch discrimination tasks [Peretz, 2016; Zatorre et al., 1992]. Across participants and for both groups, we found that PAC was the strongest between the phase of delta-band activity at [2,4] Hz and the amplitude of neurophysiological signals in the beta frequency range at [15,35] Hz (Fig. 5.3A).

Time-resolved analysis of PAC variations along the tone sequence in rAud is shown in Fig. 5.3B. We found in both groups and across all tested time windows that the strength of

Chapter 5: Neurophysiological network dynamics for pitch discrimination

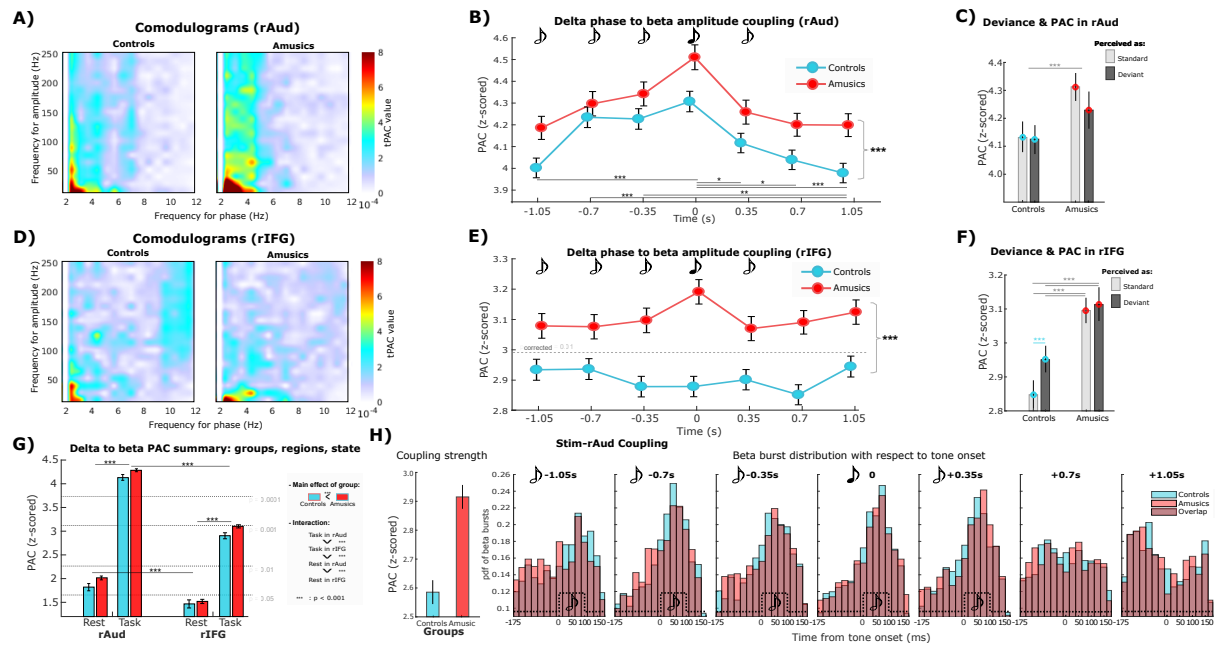


Figure 5.3: Phase-amplitude coupling analyses. A) The comodulograms extracted from source signal in the rAud ROI are shown for controls and amusics. In both groups, the strongest mode of phase-amplitude coupling was between the phase of delta activity at [2,4] Hz and the amplitude of neurophysiological signals in the beta range at [15,35] Hz. B) Time-resolved analysis of phase-amplitude coupling between these frequency ranges in rAud, z-scored with respect to surrogate data ($z = 3.63$ was above chance levels with corrected $p = 0.001$ across time windows). C) Interaction between accuracy of perceived pitch deviance and group, for delta-to-beta PAC in rAud. D) PAC comodulograms of MEG source signals from rIFG ROI in both groups. E) Time-resolved local delta-to-beta PAC in rIFG, z-scored with respect to surrogate data. F) Interaction between accuracy of perceived pitch deviance and group, for delta-to-beta PAC in rIFG. G) Delta-to-beta coupling in rAud and rIFG in both groups, during baseline resting-state and during task performance. H) Time-resolved stimulus (pure 2.85-Hz sinusoidal signal) to brain (beta activity in rAud) phase-amplitude coupling, left panel: coupling strength z-scored with respect to surrogate data ($z = 2.44$ is above chance levels with corrected $p = 0.05$ across time windows); right panel: Distribution of the preferred phase angles for coupling between the auditory tone presentations and the peak of beta amplitude, across trials and for each time window along the tone sequence (translated in relative latencies with respect to each tone onset time). Vertical dashed lines indicate when each tone was presented in the sequence (for a duration of 100 ms). The bars indicate the 95% confidence interval and the shaded traces report the standard error on the mean.

phase-amplitude coupling was above chance levels ($z > 3.4$, $p_{corrected} < 0.01$). Overall, coupling was stronger in amusics than in controls ($F(1)=11.1$, $p < 0.001$), with no effect of response accuracy ($F(1)=0.02$, $p = 0.88$) or pitch deviance ($F(1)=0.94$, $p = 0.33$; Fig. 5.3C).

There was also a main effect of time ($F(6)=6.53$, $p < 0.001$): in both groups, a post-hoc

Chapter 5: Neurophysiological network dynamics for pitch discrimination

analysis showed that PAC increased after the onset of the tone sequence ($p = 0.0006$) and decreased after the occurrence of the target tone (over the three subsequent time windows: $p = 0.0187$, $p = 0.0126$, and $p < 0.0001$, respectively).

In the right inferior frontal cortex (rIFG), phase-amplitude coupling was also the strongest between the phase of regional delta activity and the amplitude of beta-range activity (Fig. 5.3D). Time-resolved tPAC analysis in that region revealed a main effect for groups ($F(1)=43.95$, $p < 0.0001$; Fig. 5.3E): as in rAud, amusics showed overall stronger PAC levels than controls ($p < 0.001$, Fig. 5.3E & F). We also observed a main effect of deviance level ($F(1)=5.84$, $p = 0.0157$) and an interaction between deviance and accuracy of pitch change detection ($F(1)=13.09$, $p < 0.001$). Indeed in controls, phase-amplitude coupling was stronger in rIFG when target tones were correctly or incorrectly perceived as deviants, compared to PAC when the target tone was correctly or incorrectly reported as standard ($p_{corrected} = 0.007$; Fig. 5.3F).

We performed a two-factor ANOVA (group x perceived deviance) of phase-amplitude coupling in rIFG, which confirmed a main effect of group ($F(1)=43$, $p < 0.0001$) and of perceived deviance ($F(1)=13.71$, $p = 0.0002$). In the right auditory cortex, there was only a main effect of group ($F(1)=21.35$, $p < 0.0001$) and no effect of perceived deviance ($F(1)=2.25$, $p = 0.13$).

These observations point at a neurophysiological marker in the inferior frontal cortex of the actual perception of the target tone as deviant, regardless of accuracy. There was no such effect in the right auditory region, and it was absent in amusics.

We also derived phase-amplitude coupling statistics in the baseline resting state prior to the auditory-testing session, to evaluate a possible predictive relation with the values observed during task performance (Fig. 5.3G). Resting-state PAC between delta and beta was above chance level in rAud for both groups ($p < 0.05$), but only marginally in rIFG ($p > 0.07$). We found a main effect of group ($F(1)=13.93$, $p = 0.0002$), region ($F(1)=411.44$, $p < 0.0001$), and behavior (i.e. resting-state vs. task performance, $F(1)=2241.1$, $p < 0.0001$), with a significant interaction between group and state ($F(1)=93.97$, $p < 0.0001$). Post-hoc analysis of the inter-

Chapter 5: Neurophysiological network dynamics for pitch discrimination

action showed that overall and in both groups, PAC in the baseline resting state was lower than during task performance in the tested regions ($p < 0.0001$), with lower coupling in rIFG than in rAud in both states ($p < 0.0001$).

We derived measures of phase-amplitude stimulus-to-brain coupling in right auditory cortex. The goal was to replicate previous observations of stimulus-induced beta-amplitude modulations in auditory cortex in similar conditions [Fujioka et al., 2012; Cirelli et al., 2014; Chang et al., 2018]. We observed stronger coupling between the different phases of the tone sequence and auditory beta amplitude modulations in amusics than in controls ($F(1)=60.5$, $p < 0.001$; Fig. 5.1H:left). There was no significant effect of time ($F(6)=1.16$, $p = 0.32$), accuracy ($F(1)=2.08$, $p = 0.14$) or pitch deviance ($F(1)=0.41$, $p = 0.53$). Overall, neurophysiological delta-to-beta phase-amplitude coupling was stronger than stimulus-to-beta coupling in the tested region ($t(119985)=69.45$, $p < 0.001$).

For each trial, we also extracted the latency of maximum beta amplitude after each tone onset in the sequence. The right panel of Fig. 5.1H shows the empirical distributions of these latencies for both groups. The dashed vertical lines show the onset and offset of each tone presentation in the sequence. We found that in both groups beta-range activity peaked at the temporally-expected presentation of the tone (~ 50 ms after tone onset), starting immediately after at the first tone in the sequence.

In summary, we observed significant cross-frequency coupling between the phase of delta activity and the amplitude of beta-range signals in the right auditory (rAud) and the inferior frontal cortices (rIFG), with overall stronger coupling in rAud, where it was also stronger than stimulus-to-beta coupling. Beta activity was the strongest at the actual occurrence of the tones in the sequence. Neurophysiological delta-to-beta coupling was related to behavior, with higher levels during task performance than over baseline resting state. The amplitude of beta oscillations was maximum at the expected latencies of the tones in the sequence. Phase-amplitude coupling increased dynamically after the onset of the tone sequence and culminated at the oc-

Chapter 5: Neurophysiological network dynamics for pitch discrimination

currence of the target tone. Overall PAC was chronically stronger in amusics than in controls in auditory and inferior frontal regions. We found only in controls a neurophysiological marker of perceived deviance of the target tone, regardless of accuracy, with increased phase-amplitude coupling in the right inferior frontal region (rIFG).

5.5.5 Directed functional connectivity

From the frequency ranges identified by the phase-amplitude coupling analyses above, we derived dPTE directed connectivity measurements between the regions of interest in both hemispheres in the delta ([2,4] Hz) and beta ([15,30] Hz) frequency bands, over the baseline resting-state period, the [-1500,0] ms pre-target and the post-target [0,1500] ms time segments of the tone sequence presentation.

We tested the observed dPTE values against zero in each group and behavioral state (baseline resting state, pre- and post-target) with statistical corrections for the 18 comparisons performed (3 pairs \times 2 frequency bands \times 3 states).

In controls during the resting state, we found a directed connectivity transfer in the beta range from motor cortex to Aud ($t(15) = -6.48, p < 0.001$) and to IFG ($t(15) = -6.31, p < 0.001$; Fig. 5.4A: left panel). We found the same directed connectivity pattern during task performance in both pre- (Aud: $T(15) = -12.42, p < 0.001$, IFG: $T(15) = -8.42, p < 0.001$) and post-target segments (Aud: $T(15) = -7.33, p < 0.001$, IFG: $T(15) = -4.6, p = 0.006$). We observed a reversed directed connectivity transfer in the delta range from the auditory cortex to IFG and motor regions in pre- (IFG: $T(15) = 4.06, p = 0.018$, Mot: $T(15) = 4.07, p = 0.017$) and post-target (IFG: $T(15) = 3.71, p = 0.038$, Mot: $T(15) = 4.66, p = 0.006$) segments, but not in the resting state.

In controls, a three-factor ANOVA (pairs of ROIs \times state \times frequency bands) of directed connectivity measures (dPTE) confirmed a significant main effect of the frequency band ($F(1) = 4.57, p < 0.001$) with opposite directions of connectivity transfer for delta- vs. beta-band activ-

Chapter 5: Neurophysiological network dynamics for pitch discrimination

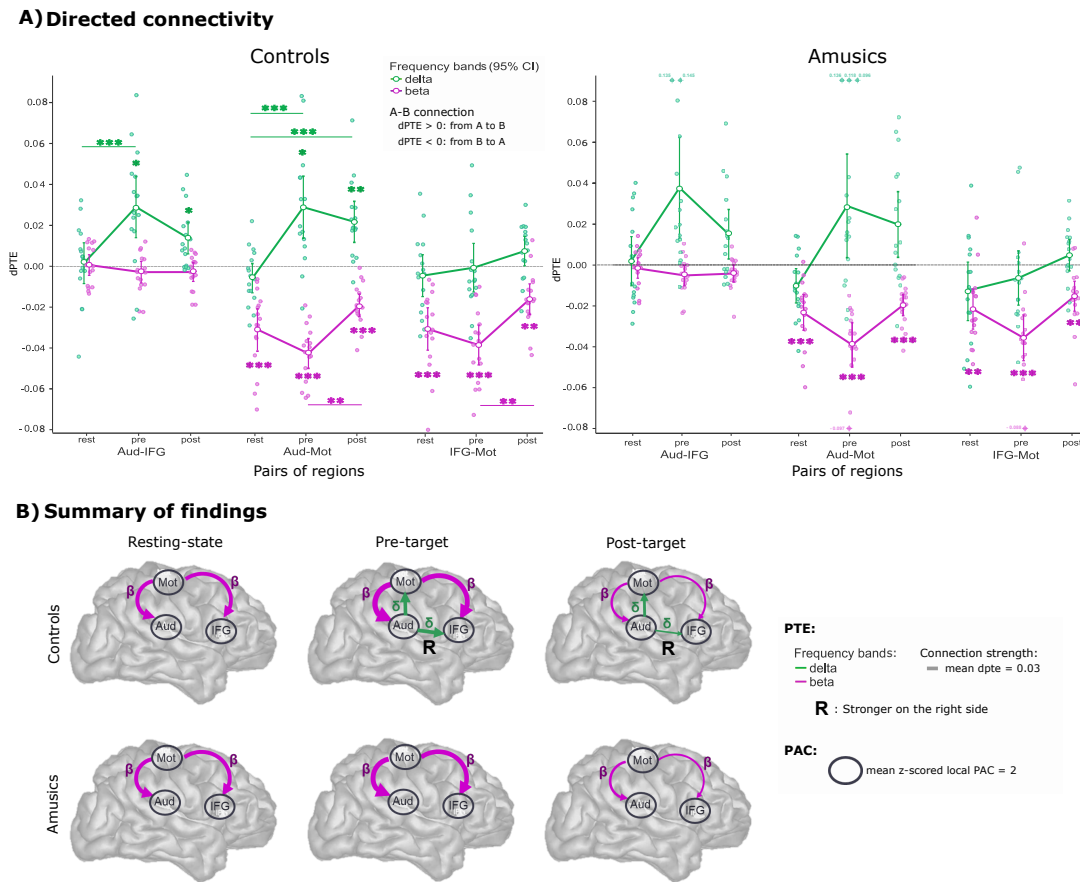


Figure 5.4: Directed functional connectivity analyses: A) Measures of directed phase-transfer entropy for each pair of left and right ROIs, frequency band, and stage of the experiment, for controls (left) and amusics (right). The distributions of dPTE values are shown for each inter-regional connection and over the baseline resting state, the pre- and the post-target segments of the tone sequences. The green and pink traces are for beta- and delta- band dPTE, respectively. The circles show the group average, with bars indicating 95 – % confidence intervals. All statistics were corrected for multiple comparisons (*: $p < 0.05$, **: $p < 0.01$, ***: $p < 0.001$). B) Summary of findings plotted on a template cortical surface: the arrows are schematics for significant dPTE directed connections. Line thickness indicates the strength of the dPTE group average. Similar patterns were found in both hemispheres (not shown), with stronger delta-band bottom-up transfers from Aud to IFG on the right side in controls ($t(84) = -2.7$, $p_{Tukey} = 0.04$). The thickness of the circles around the auditory (Aud) and inferior frontal (IFG) cortices recalls the strength of local cross-frequency phase-amplitude coupling between the phase of delta-band activity and the amplitude of beta-band activity.

ity. Interactions showed that directed connectivity transfer of delta-band activity from auditory regions (rAud and lAud) to inferior frontal cortices (rIFG and lIFG) was increased during pre-target tone presentations, compared to baseline resting state ($t(90) = 4.73$, $p < 0.001$). Delta-

Chapter 5: Neurophysiological network dynamics for pitch discrimination

band transfer was also stronger from auditory to motor regions (rMot and lMot) over the entire tone sequence (pre- and post-target) compared to the baseline resting state (pre: $F(90) = 5.39$, $p < 0.001$, post: $F(90) = 4.27$, $p < 0.001$). Reversed directed connectivity transfers were observed in the beta band from motor to auditory regions, and from motor to inferior frontal cortices. There were stronger dPTE scores over the pre-target segment compared to post-target (from motor to auditory regions: $F(90) = 3.65$, $p = 0.006$; from motor to inferior frontal cortices: $F(90) = 3.52$, $p = 0.009$).

All these observations were identical for both hemispheres, with the exception of delta transfer from auditory to inferior frontal cortex, which was stronger on the right side (post-hoc: hemisphere \times frequency band interaction: $t(84) = -2.7$, $p_{corrected} = 0.04$).

Qualitatively, the variations of dPTE measures were strikingly similar between controls and amusics (Fig. 5.4A). There was no significant main effect of the group or interaction of the group with other factors. Yet in amusics, the strength of dPTE of bottom-up delta-band connectivity from the auditory to the inferior frontal cortices, and from the auditory to the motor cortices was not significantly different from zero during tone sequence presentation (both during pre- and post-target segments, $p > 0.099$).

Akin to controls, top-down beta-range directed transfer was significant from motor to auditory cortices (resting-state: $t(15) = -6.49$, $p < 0.001$, pre: $t(15) = -7.67$, $p < 0.001$, post: $t(15) = -8.11$, $p < 0.001$), and from motor to inferior frontal cortices (resting-state: $t(15) = -6.31$, $p = 0.005$, pre: $t(15) = -6.80$, $p < 0.001$, post: $t(15) = -4.44$, $p = 0.009$). There was no difference between right and left hemispheres in amusics ($F < 1.33$, $p > 0.25$).

In summary, the presentation of an auditory tone sequence induced delta-band effective connectivity bilaterally, emerging from the auditory cortices and directed to the inferior frontal and motor cortices. This bottom-up transfer was significant only in controls and was not present during baseline resting state. In both groups, directed connectivity in the opposite direction (top-down) was observed in the beta band from motor to auditory and to inferior frontal cortices, by

Chapter 5: Neurophysiological network dynamics for pitch discrimination

default during resting-state baseline, and was emphasized during the pre-target segment of the tone-sequence presentation (Fig. 5.4B).

5.6 Discussion

We used non-invasive neurophysiological measures of local and inter-regional brain dynamics to reveal some of the basic mechanisms of sensory integration during a simple pitch discrimination task. These analyses were performed in controls with normal hearing and in congenital amusia participants, to resolve the mechanistic elements that are essential to pitch perception, which is deficient in amusia. Our behavioral results confirmed that amusics had more difficulty than controls in detecting small pitch variations of up to 50 cents. Their lower accuracy was not due to a lack of vigilance in performing a task that was difficult and possibly frustrating to them [Ciesielski et al., 2007]. This observation was derived from electrophysiological measurements of posterior alpha-band activity, which was actually lower in amusics than controls [Valentino et al., 1993; Aftanas and Golocheikine, 2001].

We performed in-depth analyses within and between brain regions of interest that had been highlighted consistently in previous pitch-discrimination studies with a variety of functional exploration techniques [Zatorre et al., 1992; Albouy et al., 2013; Peretz, 2016; Morillon and Baillet, 2017]. They comprised, bilaterally, the Heschl/superior temporal gyrus in auditory cortices, the posterior aspect of the inferior frontal gyrus and the pre-central motor cortices. These ROIs were identified with a functional-localizer strategy on the individual anatomy of every participant.

During the presentation of tone sequences, we found in both groups local expressions of cross-frequency coupling between the phase of delta-band activity and the amplitude of beta-band signal components in the right auditory and inferior frontal cortices. The frequency of delta-band activity was close to the rate of the tone sequence (2.85 Hz), which is typical of cortical entrainment at the dominant rate of auditory signals [Doelling and Poeppel, 2015;

Chapter 5: Neurophysiological network dynamics for pitch discrimination

Morillon and Baillet, 2017]. By boosting neural signals in response to rhythmic sensory inputs, cortical entrainment increases signal-to-noise ratio and improves the detection of genuine phase-amplitude coupling effects [Aru et al., 2015; Samiee and Baillet, 2017]. There was no delta-to-beta coupling in the absence of tone-sequence presentation, namely during the baseline resting state in IFG (Fig. 5.3G). The fact that we observed delta-band entrainment in IFG with the task (Fig. 5.3B-C) is compatible with this region being a downstream node of the ventral auditory pathway [Zatorre et al., 1992; Gaab et al., 2003]. Expressions of beta-band activity during pitch processing have been previously reported in auditory regions [Cirelli et al., 2014; Fujioka et al., 2012], including in the pre-target time period [Florin et al., 2017].

In both groups, phase-amplitude-coupling was elevated in auditory and inferior frontal cortices during task performance compared to baseline resting state (Fig. 5.3G). This observation is in line with published reports of higher transient PAC levels during task performance, such as with working memory [Axmacher et al., 2010], associative learning [Tort et al., 2009; van Wingerden et al., 2014] and visual attention [Szczepanski et al., 2014].

A striking overall effect between groups was that delta-to-beta coupling in the auditory and inferior frontal cortices was higher in amusics than in controls, both during tone-sequence presentations and at baseline in the resting state. We believe that these observations of elevated ongoing phase-amplitude coupling are first in amusia. They contribute to converging evidence that chronically elevated PAC levels could be brain signal indicators of neurophysiological dysfunction, as previously shown in e.g., Parkinson's disease [de Hemptinne et al., 2013; van Wijk et al., 2016], epilepsy [Amiri et al., 2016; Samiee et al., 2018] and autism spectrum disorders [Berman et al., 2015]).

Delta-to-beta coupling was stronger in auditory than inferior frontal cortices in both groups (Fig. 5.3G), which we interpret as caused by a more direct entrainment of auditory delta activity by the stimulus, than in downstream regions. Yet, another marking difference between groups was that there were modulations of delta-to-beta phase-amplitude coupling in the in-

Chapter 5: Neurophysiological network dynamics for pitch discrimination

ferior frontal cortex of controls depending on their perception of the target tone as deviant, regardless of accuracy. Such percept-dependent increases are compatible with the known involvement of the inferior frontal cortex in pitch detection [Doeller et al., 2003; Alain et al., 2001; Florin et al., 2017]. There was no such modulation in amusics, which is in line with the absence of P300 event-related responses in this group, generated in part in the IFG region [Florin et al., 2017].

We derived time-resolved measurements of phase-amplitude coupling (tPAC) over time windows around the occurrence of each of the tones in the sequence. In the auditory cortex of both groups, there was an increase of cross-frequency coupling immediately after the onset of the tone sequence (Fig. 5.3B), which culminated at the expected latency of the target tone presentation. This was confirmed by a time-resolved analysis of stimulus-to-beta coupling in the auditory cortex, which showed that stronger phasic beta activity occurred at the expected latency of the auditory tones in the sequence (Fig. 5.3H). These effects were observed both in controls and amusics. The measurement of such coupling between the timing of the tone presentations (i.e., the actual physical stimulus) and modulations of beta-band signal amplitude in auditory cortex is an approach that was used previously by Chang et al. [2018]. They showed that stimulus-to-beta coupling in right auditory cortex was associated with the predictability of pitch changes in a sequence. In our study, pitch changes occurred at the fourth tone of the sequence but only in 50% of the trials. Hence the predictability of the timing of pitch changes was high, but their actual occurrences were unpredictable from trial to trial. In that respect, our results are consistent with Chang et al. [2018]’s, as our participants presented lower levels of stimulus-to-beta coupling than their endogenous delta-to-beta counterparts, with no time modulations along the tone sequence presentation (Fig. 5.1H).

We interpret the lesser levels of stimulus-to-beta compared to delta-to-beta coupling as due to the fact that the dominant delta-band neurophysiological activity did not exactly match the tone presentation rate. This is indicative of phase and frequency jitters between the regular

Chapter 5: Neurophysiological network dynamics for pitch discrimination

auditory inputs of the tone sequence and the entrained neurophysiological responses. These fluctuations were similar between groups and were not related to accuracy.

Our observations of directed, frequency-specific connectivity between regions of interest provided further insight into both the neurophysiological processes of normal pitch discrimination and their alteration in amusia. During resting-state baseline, we found in both groups bilateral connections in the beta band issued from the precentral motor cortex and directed to the auditory and inferior frontal cortices. These connections persisted during task performance and were emphasized during the pre-target segment of each trial. These results are in line with reports of dynamically-structured and anatomically-organized beta-band activity in the resting state [Brookes et al., 2011; Florin and Baillet, 2015]. They are also concordant with strong emerging evidence that beta-band activity is a vehicle for top-down signalling in brain systems during sensory processing [Engel et al., 2001; Engel and Fries, 2010; Bressler and Richter, 2015; Bastos et al., 2015; Michalareas et al., 2016; Chao et al., 2018]. This body of experimental evidence is in support of the theoretical framework of predictive coding [Rao and Ballard, 1999; Friston and Kiebel, 2009] and predictive timing [Arnal and Giraud, 2012] in sensory perception. In this context, beta-band top-down activity would channel predictive information concerning the expected nature and temporal occurrence of incoming sensory information to primary systems [Fontolan et al., 2014; Baillet, 2017]. In essence, the theoretical principles posit sensory perception as an active sensing process, in which the motor system would play a key role [Schroeder et al., 2010]. In audition for instance, we previously showed that the lateral motor cortex directs beta-band connectivity towards the auditory cortices, even in the absence of overt movements, contributing to the temporal predictions of tone occurrences in complex sequences [Morillon and Baillet, 2017]. Our present data confirm and extend these observations: the modulations of beta-band activity in the auditory cortex peaked at the occurrences of the tones in the sequence, which is compatible with the involvement of the motor cortex in driving inter-regional signals for predictive sensory timing. This top-down signalling mechanism was not affected in amusics.

Chapter 5: Neurophysiological network dynamics for pitch discrimination

Symmetrically, during tone-sequence presentations, we found only in controls a bottom-up form of directed connectivity issued from the auditory cortices towards both the inferior frontal and motor cortices (Fig. 5.4A). These connections were not significantly expressed in amusics, and not present during the baseline resting state in controls. The delta band was that of maximum phase-amplitude coupling found at the regional level and encompassed the stimulus presentation rate of 2.85Hz. There was an hemispheric asymmetry of this connectivity transfer to the right hemisphere [Zatorre et al., 1992]. This bottom-up connectivity transfer is also compatible with the principles of predictive coding and timing that primary sensory regions propagate prediction-error signals downstream in brain systems networks, for ongoing updates of internal predictive and decision models [Rao and Ballard, 1999; Friston and Kiebel, 2009; Baillet, 2017].

This observation is consistent with published dynamical causal models of impaired directed connections between auditory and inferior frontal cortices in amusics [Albouy et al., 2013] and other neurophysiological disorders [Omgie et al., 2013]. These previous results were not frequency-specific as they were obtained from event-related signals in response to tone-sequence presentations. Our present findings are also in line with fMRI data showing reduced functional – not directed – connectivity between the same cortical regions of amusics [Hyde et al., 2010]. Loui et al. [2009] also reported lower anatomical connections via the arcuate fasciculus in amusics, using diffusion-imaging tractography, although these results were not reproduced [Chen et al., 2015]. In our data, the directed connectivity patterns were qualitatively similar between amusics and controls. The inter-individual variability of dPTE statistics was greater in amusics, which may explain why both the strength and directionality of connections were deemed not significant in this group. We are cognizant that our sample size was small. Yet the motifs of directed connectivity are compatible with the large effects observed in both behavior and local phase-amplitude coupling statistics.

In conclusion, the present study provides evidence that pitch discrimination from a sequence

Chapter 5: Neurophysiological network dynamics for pitch discrimination

of pure tones engages a distributed network of cortical regions comprising at least the auditory, inferior frontal and lateral motor cortices. Our results show that the motor cortex issues beta-band signals down to inferior frontal and auditory regions, which are present in the resting state, but which timing during auditory presentation mark the actual expected occurrences of tones in the sequence. The auditory cortex is entrained at a rate around the physical pace of the tone sequence, and this signal is propagated in a top-down fashion further downstream to the motor system and along the ventral pathway to the inferior frontal cortex. These poly-frequency phenomena interact locally through phase-amplitude coupling, which increases in auditory regions at the onset of the tone sequence and culminates at the expected occurrence of the target tone before returning to baseline levels.

This data identify two poly- and cross-frequency mechanisms as crucial to pitch-change detection, when contrasting amusics with controls. First, delta-to-beta phase-amplitude coupling is chronically elevated in the auditory and inferior frontal regions of amusics. Second, bottom-up signalling along the ventral auditory pathway and to the motor cortex is depressed in this group. In sum, these findings point at an alteration of pitch encoding in the auditory regions of amusics, leading to insufficient prediction error signalling driven to inferior frontal regions and poorer detection. The predictive timing functions seem to be preserved in amusics, at least in the present context of highly predictable and regular pacing of the tone sequence.

Taken together, we believe these findings advance the complete and dynamic view of tone sequence sensory processing in audition. We anticipate that some of these new observations would generalize to other sensory modalities and that the cross- and poly-frequency neurophysiological markers of impaired auditory processing would be pertinent to plain other functional deficits in sensory perception.

Acknowledgment

S.S. acknowledges the support from McGill University Integrated Program in Neuroscience. S.B. was supported a Discovery Grant from the National Science and Engineering Research Council of Canada (436355-13), the NIH (2R01EB009048-05) and a Platform Support Grant from the Brain Canada Foundation (PSG15-3755).

6

General discussion & conclusion

6.1 Summary of findings and discussions

The main objective of my thesis was to advance knowledge of the functional role of cross-frequency interactions between the phase and amplitude of neural oscillations at different frequencies. I also aimed at studying expressions of cross-frequency coupling in selected disease and behavior models. Cross-frequency coupling between rhythmic fluctuations of brain activity has been observed over the last couple of decades and has triggered a lot of interest and questioning in the integrative neuroscience community. However, there are still several unanswered questions related to this phenomenon. In this chapter, I summarize our findings and discuss their implications, limitations and the prospective of future research work beyond the present contributions.

The robust and reliable identification of phase-amplitude coupling in electrophysiological recordings was the foremost methodological step I have taken. I proposed tPAC as a new method for detection and quantification of cross-frequency phase-amplitude coupling in a time-resolved manner [Samiee and Baillet, 2017] (Chapter 3, Fig. 3.1). The method applies to all varieties of experimental designs, i.e. both for event-related and ongoing spontaneous

General discussion & conclusion

time series of brain activity. I ran a thorough evaluation and comparison of tPAC against four competing approaches using synthesized data, which confirmed its ability to resolve cross-frequency coupling strength and other parameters, even from short segments of signal (Fig. 3.4). The output of tPAC is a sparse three-dimensional array in time, frequency for phase and frequency for amplitude. I developed the analytical tools to project these tPAC parameters on three two-dimensional subspaces (Fig. 3.3). Hence, tPAC also provides the typical data representations (e.g., comodulograms), with improved sensitivity and temporal resolution (Fig. 3.5). I have made tPAC and the suite of such practical tools available in Brainstorm [Tadel et al., 2011], with extensive online documentation. The code is also publicly available via *GitHub* (<https://github.com/SoheilaSamiee/Phase-amplitude-coupling-estimation>). I conducted the empirical evaluation of tPAC with in-vivo LFP recordings from the entorhinal cortex of a freely-moving rat, in a linear-track experiment (Fig. 3.6).

Abnormal expressions of PAC in brain disorders have attracted a lot of attention over the past decade [Spencer et al., 2009; White et al., 2010; López-Azcárate et al., 2010; Allen et al., 2011; Miskovic et al., 2011; Kirihara et al., 2012; Goutagny et al., 2013; Shimamoto et al., 2013; de Hemptinne et al., 2013; Ibrahim et al., 2014; De Hemptinne et al., 2015; Zhang et al., 2016]. However, the actual alignment of these observations with pathophysiology is not entirely clear. In Chapter 4 of my dissertation, I investigated the disease model of Pilocarpine-induced MTLE, which affects the inhibitory-excitatory balance in the networks of the medial temporal cortex of a rat. I discussed how interactions between these networks can be marked by CFC in electrophysiological recordings. My hypothesis was confirmed by experimental data, which showed exaggerated expressions of PAC between the phase of slow-wave NREM oscillations and the amplitude of fast rhythms in the HFO band, with specific localization within the seizure onset zone (Fig. 4.3- 4.4, [Samiee et al., 2018]). This observation was consistent with a previous report on interactions between HFO and slow waves in epileptic patients [Amiri et al., 2016]. We did not analyze the direct relationship between the imbalance of excitatory and inhibitory activity and CFC. A follow-up study in the lab, also in collaboration with Prof Avoli,

General discussion & conclusion

is now using optogenetics to establish such causal link with the specific blockade of inhibitory interneurons.

Looking forward, using CFC with scalp or intracranial recordings during EEG monitoring of epilepsy patients could improve the delineation of the seizure onset zone before surgery, for severe forms of complex partial epilepsy.

I also observed that PAC strength in the SOZ was higher on days when epileptic seizure activity was also high (Fig. 4.4). To the best of our knowledge, this is the first report showing a positive correlation between PAC modulations and the frequency of seizure occurrences. Previous studies had measured PAC variations between different states: peri-ictal and ictal states [Nariai et al., 2011], or temporal changes of PAC in different sleep stages [Amiri et al., 2016]. Further investigation of such associations between PAC strength and seizure frequencies or occurrences could contribute to improved patient monitoring or even seizure forecasting for patient safety and interventions.

One limitation of our study was that we did not have access to surface (scalp) EEG recordings to determine with certainty the polarity of excitability cycles during sleep. The polarity of excitability cycles are important in determining the preferred phase angle of PAC with respect to these cycles. Song et al. [2017] and Frauscher et al. [2015] suggested that the preferred phase angle for coupling would help discriminating between pathological and healthy variants of HFOs. In my study, I grouped this phase across different recordings using the method suggested by [Ellenrieder et al., 2016], but access to surface EEG recording would have been optimal and should be considered in future studies.

I then proceeded to study a model of brain function and sensory integration using a pitch discrimination task. I used MEG data from human participants and extracted phase-amplitude coupling parameters from source imaging time-series distributed over the cortex. I reported observations of increased PAC between delta-phase (2-4 Hz) and beta-amplitude (15-35 Hz) during pitch discrimination, with respect to resting-state baseline levels in the auditory cortex

General discussion & conclusion

and inferior frontal gyrus (Fig. 5.3). These two regions are part of the ventral auditory pathway and have previously been reported to be involved in auditory pitch processing [Zatorre et al., 1992; Gaab et al., 2003]. My observation of transient augmentation of PAC strength is consistent with previous reports of increased PAC during task performance, for example in working memory [Axmacher et al., 2010], visual attention [Szczepanski et al., 2014] and associative learning [Tort et al., 2009; van Wingerden et al., 2014]. I propose that sensory entrainment (see section 2.2.1) – whereby a sensory stimulus drives both slow and fast oscillatory networks – emphasizes the phenomenon. In my study, the auditory stimulus was presented in sequences at a rate of 2.85 Hz, which is in the delta frequency range. I propose that the transient coupling of this slow oscillation with top-down beta bursts is compatible with the theoretical frameworks of active sensing [Morillon and Baillet, 2017] and general sensory de-multiplexing [Hyafil et al., 2015b] (see sec. 2.2.2). My analyses of effective connectivity, revealed that local PAC fluctuations co-occur with inter-regional communication, also in the same frequency ranges as those observed within PAC: delta and beta. Hence, we can think of these oscillatory manifestations as supports for information inter-regional transfer and local integration in brain networks. Whether my findings in auditory pitch perception generalize to other sensory modalities or even higher-order brain functions such as natural speech processing needs to be investigated.

Furthermore, we observed augmented PAC in amusics compared to controls in both auditory cortex and inferior frontal gyrus (Fig. 5.3). This alteration in PAC strength is in line with previous reports on PAC changes in other disorders including Parkinson’s disease [López-Azcárate et al., 2010; Shimamoto et al., 2013; de Hemptinne et al., 2013; De Hemptinne et al., 2015], Alzheimer’s disease [Goutagny et al., 2013; Zhang et al., 2016], and epilepsy [Ibrahim et al., 2014; Amiri et al., 2016; Samiee et al., 2018]. Additionally, increased coupling in amusics is observed in regions (Aud and IFG) previously reported to present thicker cortex in amusics than in controls [Hyde et al., 2007]. Hence, further analysis of the potential relationship between cortical thickness and PAC could be the topic of future studies in the field.

6.2 Future research

I hope the methods and data reported in my dissertation have advanced the tools and understanding of the possible functional role and mechanisms of oscillatory brain activity. I believe my contributions can inspire future research works over a wide spectrum of related topics.

6.2.1 Mechanisms

Although some computational [Hyafil et al., 2015b] and biological mechanisms [Wulff et al., 2009; Korotkova et al., 2010] have been hypothesized for CFC, there are still multiple aspects that require investigation and justification. In-vivo and in-vitro studies, potentially combined with optogenetics will nurture progress in that direction.

One of the basic aspects to be further investigated in my opinion, is the respective contribution of inhibitory vs. excitatory neural circuits in CFC, at distinct frequency bands (associated with different tasks or observed in different regions of the brain). This could only be achieved from analyzing the direct effects of silencing each circuitry on the CFC pattern. This would help improve the physiological understanding of empirical results when an altered pattern of CFC is observed in brain and mental disorder. Animals models and in-vitro preparations could contribute toward this aim. Targeting a particular group of cells via transgenic animal models can confirm how impairment of those cells would lead to alterations of CFC in different regions of the brain and for different tasks. Optogenetics is also a key tool for such investigation as it provides the opportunity to study the causal influence of activating or silencing a particular circuit or cell type, in a well-defined region of the brain, on PAC patterns, during rest and task, with observable consequences on behavior.

6.2.2 Inter-regional coupling

Interactions in brain networks, between regional neural assemblies, can in principle be mediated by and reflected in oscillatory rhythmic signalling. So far I have put the focus on local manifestations of cross-frequency coupling. Oscillatory coupling between regions is typically measured within a single narrow-band frequency e.g., using measures of temporal or amplitude-envelope correlations or spectral coherence [Srinivasan et al., 2007; Murias et al., 2007; Hipp et al., 2012; Meijer et al., 2014; La Rocca et al., 2014]. However, since different oscillatory rhythms may carry different dimensions of brain integration (both spatially and temporally), coupling of neural assemblies oscillating at different frequencies can be hypothesized to provide enhanced opportunities for communication at multiple spatial scales and for storing complex information [Buzsáki and Draguhn, 2004; Canolty and Knight, 2010; Fries, 2015]. Therefore, further studies of possible mechanisms for inter-regional cross-frequency coupling (IRCFC) and how it is affected in task performance and disorders is warranted. The proposed algorithm for PAC estimation in chapter 3 (tPAC) can also be used in this type of analysis for IRPAC estimation.

In terms of potential mechanism for IRCFC, one possibility is that inter-regional coupling is driven by local CFC, and long-range connections of slow rhythms [Hyafil et al., 2015b]; however, if inter-regional CFC is stronger than local CFC, as shown in [Fontolan et al., 2014], this mechanism may not explain the observed IRCFC adequately, and there could be other mechanisms involved, which would require further investigation.

In terms of applications, variations of IRCFC with task performance need to be documented so that we advance our understanding of complex brain functions. For example, in our pitch discrimination analysis (Chapter 5), strong PAC between delta and beta oscillations was found locally in both Aud and IFG. Symmetrically, our connectivity analysis revealed that delta is mainly originating from auditory cortex, and beta from motor cortex. Hence, inter-regional phase-amplitude coupling analysis between auditory and motor cortices could be an interesting topic for future works in this direction. This would involve analysis of whether and how IRPAC

General discussion & conclusion

is affected during pitch processing by amusics, and whether it would contribute new insights to our previous findings of alteration of local PAC and inter-regional single band connectivity. This type of analysis would also advance our understanding of brain network mechanisms at large.

6.2.3 PAC and epilepsy

Based on my investigations of PAC in an animal model of epilepsy, I consider there remain several open questions on the topic and opportunities for further research:

- Using disease models to register histology with electrophysiology: it would clarify the relation between PAC parameters and structural and morphological changes in epileptic tissues.
- Understanding the association between the inhibitory-excitatory balance and PAC parameters: Optogenetics can target and modulate selectively excitatory and inhibitory sub-networks in animal models of epilepsy [Krook-Magnuson et al., 2013; Kokaia et al., 2013]. The approach is presently investigated for controlling ictogenesis [Shiri et al., 2017; Lévesque and Avoli, 2018]. Such specific interventions would clarify which and how PAC parameters are related to the activity of inhibitory and excitatory neural sub-populations, at baseline and in epilepsy tissues.
- Analysis of time-resolved changes in transition between states (e.g., interictal, preictal, and ictal states): In Samiee et al. [2018], I have focused on inter-ictal periods between seizures and found stronger coupling between the phase of slow oscillations and the amplitude of bursts in the ripple band, especially when seizure daily activity was the strongest. I propose that tracking in time the coupling parameters during the transition from interictal to preictal and ictal states would provide considerable insight into the electrophysiological mechanisms of ictogenesis. I would anticipate that PAC may be a better (in sensitivity and specificity) marker of individual epilepsy phenotypes in patients

and predictor of seizure activity than current alternatives. CFC could also be used for better categorization of the various seizure onset patterns observed in models and patients e.g., low-voltage fast-onset (LVF) and hypersynchronous-onset (HYP).

6.3 Conclusion

In conclusion, cross-frequency phase-amplitude coupling is a rich signal marker of basic physiological mechanisms of neural population activity and interactions. It is sensitive to interactions between inhibitory and excitatory neural assemblies in all brain states, including rest, task-oriented behavior and sleep (Chapter 3 and 4). We also showed how sensory entrainment influences the rhythmicity of faster bursting activity according to this mechanism (Chapter 5). As such, CFC expands our insight into the mechanisms of electrophysiological signalling, and opens wide perspectives on applications to brain signal markers in healthy behavior and a range of chronic and neurodegenerative disorders. Further studies are warranted to transfer the findings into genuine clinical applications. For instance, CFC measures could potentially be used in neurostimulation approaches for functional recovery and therapeutic interventions. Frequency-tuned none-invasive brain stimulation [Albouy et al., 2018] could be an example approach for targeting a particular underlying oscillatory component – highlighted with PAC analysis – and enhancing it. This approach could be helpful in other applications than the present model of auditory working memory enhancements [Albouy et al., 2018] and abating ictogenesis [Shiri et al., 2017], for example in helping with the recovery of motor functions in stroke patients.

List of Publications

Published:

- Samiee, S. and Baillet, S. Time-resolved phase-amplitude coupling in neural oscillations. *NeuroImage*, 159:270–279, 2017
- Samiee, S., Lévesque, M., Avoli, M., and Baillet, S. Phase-amplitude coupling and epileptogenesis in an animal model of mesial temporal lobe epilepsy. *Neurobiology of disease*, 114:111–119, 2018

Submitted:

- Samiee, S., Florin, E., Vivan, D., Albouy, P., Peretz, I., and Baillet, S. Oscillatory network dynamics for pitch discrimination. *Submitted*

Bibliography

- Ackermann, R. F. and Moshé, S. L. Excitation/inhibition interactions and seizures: the brain's lifelong balancing act. In *Atlas of Epilepsies*, pages 177–184. Springer, 2010.
- Aftanas, L. and Golocheikine, S. Human anterior and frontal midline theta and lower alpha reflect emotionally positive state and internalized attention: high-resolution eeg investigation of meditation. *Neuroscience letters*, 310(1):57–60, 2001.
- Ahmed, R. E. et al. Comparison between pitch discrimination in normal children, children with hearing aids, and children with cochlear implant. *The Egyptian Journal of Otolaryngology*, 34(4):332, 2018.
- Akam, T. and Kullmann, D. M. Oscillations and filtering networks support flexible routing of information. *Neuron*, 67(2):308–320, 2010.
- Alain, C., Arnott, S. R., Hevenor, S., Graham, S., and Grady, C. L. "what" and "where" in the human auditory system. *Proceedings of the National Academy of Sciences*, 98(21):12301–12306, 2001.
- Albouy, P., Mattout, J., Bouet, R., Maby, E., Sanchez, G., Aguera, P.-E., Daligault, S., Delpuech, C., Bertrand, O., Caclin, A., et al. Impaired pitch perception and memory in congenital amusia: the deficit starts in the auditory cortex. *Brain*, 136(5):1639–1661, 2013.
- Albouy, P., Weiss, A., Baillet, S., and Zatorre, R. J. Selective entrainment of theta oscillations in the dorsal stream causally enhances auditory working memory performance. *Neuron*, 94(1):193–206, 2017.

BIBLIOGRAPHY

- Albouy, P., Baillet, S., and Zatorre, R. J. Driving working memory with frequency-tuned non-invasive brain stimulation. *Annals of the New York Academy of Sciences*, 1423(1):126–137, 2018.
- Allen, E. A., Liu, J., Kiehl, K. A., Gelernter, J., Pearlson, G. D., Perrone-Bizzozero, N. I., and Calhoun, V. D. Components of cross-frequency modulation in health and disease. *Frontiers in systems neuroscience*, 5, 2011.
- Alvarado-Rojas, C., Valderrama, M., Fouad-Ahmed, A., Feldwisch-Drentrup, H., Ihle, M., Teixeira, C., Sales, F., Schulze-Bonhage, A., Adam, C., Dourado, A., et al. Slow modulations of high-frequency activity (40–140 hz) discriminate preictal changes in human focal epilepsy. *Scientific reports*, 4, 2014.
- Amiri, M., Frauscher, B., and Gotman, J. Phase-amplitude coupling is elevated in deep sleep and in the onset zone of focal epileptic seizures. *Frontiers in Human Neuroscience*, 10, 2016.
- Andino-Pavlovsky, V., Souza, A. C., Scheffer-Teixeira, R., Tort, A. B., Etchenique, R., and Ribeiro, S. Dopamine modulates delta-gamma phase-amplitude coupling in the prefrontal cortex of behaving rats. *Frontiers in neural circuits*, 11, 2017.
- Arnal, L. H. and Giraud, A.-L. Cortical oscillations and sensory predictions. *Trends in cognitive sciences*, 16(7):390–398, 2012.
- Aru, J., Aru, J., Priesemann, V., Wibral, M., Lana, L., Pipa, G., Singer, W., and Vicente, R. Untangling cross-frequency coupling in neuroscience. *Current opinion in neurobiology*, 31: 51–61, 2015.
- Axmacher, N., Henseler, M. M., Jensen, O., Weinreich, I., Elger, C. E., and Fell, J. Cross-frequency coupling supports multi-item working memory in the human hippocampus. *Proceedings of the National Academy of Sciences*, 107(7):3228–3233, 2010.

BIBLIOGRAPHY

- Ayotte, J., Peretz, I., and Hyde, K. Congenital amusia: A group study of adults afflicted with a music-specific disorder. *Brain*, 125(2):238–251, 2002.
- Bahramisharif, A., Mazaheri, A., Levar, N., Schuurman, P. R., Figeer, M., and Denys, D. Deep brain stimulation diminishes cross-frequency coupling in obsessive-compulsive disorder. *Biological psychiatry*, 80(7):e57–e58, 2016.
- Baillet, S. Magnetoencephalography for brain electrophysiology and imaging. *Nature Neuroscience*, 20(3):327–339, 2017.
- Bair, W., Koch, C., Newsome, W., and Britten, K. Power spectrum analysis of bursting cells in area mt in the behaving monkey. *Journal of Neuroscience*, 14(5):2870–2892, 1994.
- Bao, W. and Wu, J.-y. Propagating wave and irregular dynamics: Spatiotemporal patterns of cholinergic theta oscillations in neocortex, in vitro. *Journal of neurophysiology*, 2003.
- Bastos, A. M., Vezoli, J., Bosman, C. A., Schoffelen, J.-M., Oostenveld, R., Dowdall, J. R., De Weerd, P., Kennedy, H., and Fries, P. Visual areas exert feedforward and feedback influences through distinct frequency channels. *Neuron*, 85(2):390–401, 2015.
- Beghi, M., Cornaggia, C. M., Frigeni, B., and Beghi, E. Learning disorders in epilepsy. *Epilepsia*, 47:14–18, 2006.
- Behr, C., Lévesque, M., Ragsdale, D., and Avoli, M. Lacosamide modulates interictal spiking and high-frequency oscillations in a model of mesial temporal lobe epilepsy. *Epilepsy research*, 115:8–16, 2015.
- Behr, C., Lévesque, M., Stroh, T., and Avoli, M. Time-dependent evolution of seizures in a model of mesial temporal lobe epilepsy. *Neurobiology of Disease*, 106:205–213, 2017.
- Belluscio, M. A., Mizuseki, K., Schmidt, R., Kempter, R., and Buzsáki, G. Cross-frequency phase–phase coupling between theta and gamma oscillations in the hippocampus. *The Journal of Neuroscience*, 32(2):423–435, 2012.

BIBLIOGRAPHY

- Berman, J. I., Liu, S., Bloy, L., Blaskey, L., Roberts, T. P., and Edgar, J. C. Alpha-to-gamma phase-amplitude coupling methods and application to autism spectrum disorder. *Brain connectivity*, 5(2):80–90, 2015.
- Bertram, E. H. Neuronal circuits in epilepsy: do they matter? *Experimental neurology*, 244: 67–74, 2013.
- Blume, W. and Parrent, A. Assessment of patients with intractable epilepsy for surgery. *Adv Neurol.*, 97:537–548, 2006.
- Börger, C. and Kopell, N. Effects of noisy drive on rhythms in networks of excitatory and inhibitory neurons. *Neural computation*, 17(3):557–608, 2005.
- Bosman, C. A., Schoffelen, J.-M., Brunet, N., Oostenveld, R., Bastos, A. M., Womelsdorf, T., Rubehn, B., Stieglitz, T., De Weerd, P., and Fries, P. Attentional stimulus selection through selective synchronization between monkey visual areas. *Neuron*, 75(5):875–888, 2012.
- Bragin, A., Engel Jr, J., Wilson, C. L., Fried, I., and Buzsáki, G. High-frequency oscillations in human brain. *Hippocampus*, 9(2):137–142, 1999.
- Brattico, E., Näätänen, R., and Tervaniemi, M. Context effects on pitch perception in musicians and nonmusicians: Evidence from event-related-potential recordings. *Music Perception: An Interdisciplinary Journal*, 19(2):199–222, 2001.
- Bressler, S. L. and Richter, C. G. Interareal oscillatory synchronization in top-down neocortical processing. *Current opinion in neurobiology*, 31:62–66, 2015.
- Brookes, M. J., Woolrich, M., Luckhoo, H., Price, D., Hale, J. R., Stephenson, M. C., Barnes, G. R., Smith, S. M., and Morris, P. G. Investigating the electrophysiological basis of resting state networks using magnetoencephalography. *Proceedings of the National Academy of Sciences*, page 201112685, 2011.

BIBLIOGRAPHY

- Bruns, A. and Eckhorn, R. Task-related coupling from high-to low-frequency signals among visual cortical areas in human subdural recordings. *International journal of psychophysiology*, 51(2):97–116, 2004.
- Buhl, E. H., Tamás, G., and Fisahn, A. Cholinergic activation and tonic excitation induce persistent gamma oscillations in mouse somatosensory cortex in vitro. *The Journal of physiology*, 513(1):117–126, 1998.
- Buschman, T. J., Denovellis, E. L., Diogo, C., Bullock, D., and Miller, E. K. Synchronous oscillatory neural ensembles for rules in the prefrontal cortex. *Neuron*, 76(4):838–846, 2012.
- Buzsáki, G. *Rhythms of the Brain*. Oxford University Press, 2006.
- Buzsáki, G. Neural syntax: cell assemblies, synapsembles, and readers. *Neuron*, 68(3):362–385, 2010.
- Buzsáki, G. and Draguhn, A. Neuronal oscillations in cortical networks. *Science*, 304(5679):1926–1929, 2004.
- Buzsáki, G. and Moser, E. I. Memory, navigation and theta rhythm in the hippocampal-entorhinal system. *Nature neuroscience*, 16(2):130, 2013.
- Buzsáki, G. and Schomburg, E. W. What does gamma coherence tell us about inter-regional neural communication? *Nature neuroscience*, 18(4):484–489, 2015.
- Buzsáki, G. and Wang, X.-J. Mechanisms of gamma oscillations. *Annual review of neuroscience*, 35:203–225, 2012.
- Buzsáki, G., Anastassiou, C. A., and Koch, C. The origin of extracellular fields and currents—EEG, ecog, lfp and spikes. *Nature Reviews Neuroscience*, 13(6):407–420, 2012.
- by Heinz-Gregor Wieser for the ILAE Commission on Neurosurgery of Epilepsy, C. Mesial temporal lobe epilepsy with hippocampal sclerosis. *Epilepsia*, 45(6):695–714, 2004.

BIBLIOGRAPHY

- Canolty, R. T. and Knight, R. T. The functional role of cross-frequency coupling. *Trends in cognitive sciences*, 14(11):506, 2010.
- Canolty, R. T., Edwards, E., Dalal, S. S., Soltani, M., Nagarajan, S. S., Kirsch, H. E., Berger, M. S., Barbaro, N. M., and Knight, R. T. High gamma power is phase-locked to theta oscillations in human neocortex. *science*, 313(5793):1626–1628, 2006.
- Cardin, J. A., Carlén, M., Meletis, K., Knoblich, U., Zhang, F., Deisseroth, K., Tsai, L.-H., and Moore, C. I. Driving fast-spiking cells induces gamma rhythm and controls sensory responses. *Nature*, 459(7247):663, 2009.
- Cassenaer, S. and Laurent, G. Hebbian stdp in mushroom bodies facilitates the synchronous flow of olfactory information in locusts. *Nature*, 448(7154):709, 2007.
- Cavalheiro, E., Santos, N., and Priel, M. The pilocarpine model of epilepsy in mice. *Epilepsia*, 37(10):1015–1019, 1996.
- Cavalheiro, E. A. The pilocarpine model of epilepsy. *The Italian Journal of Neurological Sciences*, 16(1-2):33–37, 1995.
- Cendes, F., Andermann, F., Dubeau, F., Gloor, P., Evans, A., Jones-Gotman, M., Olivier, A., Andermann, E., Robitaille, Y., Lopes-Cendes, I., et al. Early childhood prolonged febrile convulsions, atrophy and sclerosis of mesial structures, and temporal lobe epilepsy an mri volumetric study. *Neurology*, 43(6):1083–1083, 1993.
- Chan, S., Erickson, J. K., and Yoon, S. S. Limbic system abnormalities associated with mesial temporal sclerosis: a model of chronic cerebral changes due to seizures. *Radiographics*, 17(5):1095–1110, 1997.
- Chang, A., Bosnyak, D. J., and Trainor, L. J. Beta oscillatory power modulation reflects the predictability of pitch change. *Cortex*, 106:248–260, 2018.

BIBLIOGRAPHY

- Chao, Z. C., Takaura, K., Wang, L., Fujii, N., and Dehaene, S. Large-scale cortical networks for hierarchical prediction and prediction error in the primate brain. *Neuron*, 2018.
- Chen, J. L., Penhune, V. B., and Zatorre, R. J. Listening to musical rhythms recruits motor regions of the brain. *Cerebral cortex*, 18(12):2844–2854, 2008.
- Chen, J. L., Kumar, S., Williamson, V. J., Scholz, J., Griffiths, T. D., and Stewart, L. Detection of the arcuate fasciculus in congenital amusia depends on the tractography algorithm. *Frontiers in psychology*, 6:9, 2015.
- Chrobak, J. and Buzsáki, G. Gamma oscillations in the entorhinal cortex of the freely behaving rat. *The Journal of Neuroscience*, 18(1):388–398, 1998.
- Ciesielski, K. T., Hämäläinen, M. S., Geller, D. A., Wilhelm, S., Goldsmith, T. E., and Ahlfors, S. P. Dissociation between meg alpha modulation and performance accuracy on visual working memory task in obsessive compulsive disorder. *Human brain mapping*, 28(12):1401–1414, 2007.
- Cirelli, L. K., Bosnyak, D., Manning, F. C., Spinelli, C., Marie, C., Fujioka, T., Ghahremani, A., and Trainor, L. J. Beat-induced fluctuations in auditory cortical beta-band activity: using eeg to measure age-related changes. *Frontiers in psychology*, 5:742, 2014.
- Clark, A. Whatever next? predictive brains, situated agents, and the future of cognitive science. *Behavioral and brain sciences*, 36(3):181–204, 2013.
- Cohen, M. X. Assessing transient cross-frequency coupling in eeg data. *Journal of neuroscience methods*, 168(2):494–499, 2008.
- Cohen, M. X., Elger, C. E., and Fell, J. Oscillatory activity and phase–amplitude coupling in the human medial frontal cortex during decision making. *Journal of cognitive neuroscience*, 21(2):390–402, 2008.

BIBLIOGRAPHY

- Cohen, M. X., Axmacher, N., Lenartz, D., Elger, C. E., Sturm, V., and Schlaepfer, T. E. Good vibrations: cross-frequency coupling in the human nucleus accumbens during reward processing. *Journal of Cognitive Neuroscience*, 21(5):875–889, 2009.
- Cole, S. R. and Voytek, B. Brain oscillations and the importance of waveform shape. *Trends in cognitive sciences*, 21(2):137–149, 2017.
- Colgin, L. L. Rhythms of the hippocampal network. *Nature Reviews Neuroscience*, 17(4):239, 2016.
- Colgin, L. L., Denninger, T., Fyhn, M., Hafting, T., Bonnevie, T., Jensen, O., Moser, M.-B., and Moser, E. I. Frequency of gamma oscillations routes flow of information in the hippocampus. *Nature*, 462(7271):353–357, 2009.
- Colic, S., Lang, M., Wither, R. G., Eubanks, J. H., Liang, Z., and Bardakjian, B. L. Low frequency-modulated high frequency oscillations in seizure-like events recorded from in-vivo mecp2-deficient mice. In *Engineering in Medicine and Biology Society (EMBC), 2013 35th Annual International Conference of the IEEE*, pages 985–988. IEEE, 2013.
- Coppola, A. and Moshé, S. L. Animal models. In *Handbook of clinical neurology*, volume 107, pages 63–98. Elsevier, 2012.
- Cossart, R., Dinocourt, C., Hirsch, J., Merchan-Perez, A., De Felipe, J., Ben-Ari, Y., Esclapez, M., and Bernard, C. Dendritic but not somatic gabaergic inhibition is decreased in experimental epilepsy. *Nature neuroscience*, 4(1):52, 2001.
- Curia, G., Longo, D., Biagini, G., Jones, R. S., and Avoli, M. The pilocarpine model of temporal lobe epilepsy. *Journal of neuroscience methods*, 172(2):143–157, 2008.
- Darvas, F., Miller, K. J., Rao, R. P., and Ojemann, J. G. Nonlinear phase–phase cross-frequency coupling mediates communication between distant sites in human neocortex. *Journal of Neuroscience*, 29(2):426–435, 2009.

BIBLIOGRAPHY

- de Hemptinne, C., Ryapolova-Webb, E. S., Air, E. L., Garcia, P. A., Miller, K. J., Ojemann, J. G., Ostrem, J. L., Galifianakis, N. B., and Starr, P. A. Exaggerated phase–amplitude coupling in the primary motor cortex in parkinson disease. *Proceedings of the National Academy of Sciences*, 110(12):4780–4785, 2013.
- De Hemptinne, C., Swann, N. C., Ostrem, J. L., Ryapolova-Webb, E. S., San Luciano, M., Galifianakis, N. B., and Starr, P. A. Therapeutic deep brain stimulation reduces cortical phase-amplitude coupling in parkinson’s disease. *Nature neuroscience*, 18(5):779–786, 2015.
- De Tisi, J., Bell, G. S., Peacock, J. L., McEvoy, A. W., Harkness, W. F., Sander, J. W., and Duncan, J. S. The long-term outcome of adult epilepsy surgery, patterns of seizure remission, and relapse: a cohort study. *The Lancet*, 378(9800):1388–1395, 2011.
- De Vos, M., Vergult, A., De Lathauwer, L., De Clercq, W., Van Huffel, S., Dupont, P., Palmieri, A., and Van Paesschen, W. Canonical decomposition of ictal scalp eeg reliably detects the seizure onset zone. *NeuroImage*, 37(3):844–854, 2007.
- Del Felice, A., Beghi, E., Boero, G., La Neve, A., Bogliun, G., De Palo, A., and Specchio, L. M. Early versus late remission in a cohort of patients with newly diagnosed epilepsy. *Epilepsia*, 51(1):37–42, 2010.
- Demiralp, T., Bayraktaroglu, Z., Lenz, D., Junge, S., Busch, N. A., Maess, B., Ergen, M., and Herrmann, C. S. Gamma amplitudes are coupled to theta phase in human eeg during visual perception. *International journal of psychophysiology*, 64(1):24–30, 2007.
- Destexhe, A. and Sejnowski, T. Interactions between membrane conductances underlying thalamocortical slow-wave oscillations. *Physiological reviews*, 83(4):1401–1453, 2003.
- Dimitriadis, S. I., Laskaris, N. A., Bitzidou, M. P., Tarnanas, I., and Tsolaki, M. N. A novel biomarker of amnesic mci based on dynamic cross-frequency coupling patterns during cognitive brain responses. *Frontiers in neuroscience*, 9:350, 2015.

BIBLIOGRAPHY

- Doeller, C. F., Opitz, B., Mecklinger, A., Krick, C., Reith, W., and Schröger, E. Prefrontal cortex involvement in preattentive auditory deviance detection: neuroimaging and electrophysiological evidence. *Neuroimage*, 20(2):1270–1282, 2003.
- Doelling, K. B. and Poeppel, D. Cortical entrainment to music and its modulation by expertise. *Proceedings of the National Academy of Sciences*, 112(45):E6233–E6242, 2015.
- Doesburg, S. M., Green, J. J., McDonald, J. J., and Ward, L. M. Rhythms of consciousness: binocular rivalry reveals large-scale oscillatory network dynamics mediating visual perception. *PloS one*, 4(7):e6142, 2009.
- Dümpelmann, M., Jacobs, J., and Schulze-Bonhage, A. Temporal and spatial characteristics of high frequency oscillations as a new biomarker in epilepsy. *Epilepsia*, 56(2):197–206, 2015.
- Duncan, J. S., Sander, J. W., Sisodiya, S. M., and Walker, M. C. Adult epilepsy. *The Lancet*, 367(9516):1087–1100, 2006.
- Düzel, E., Penny, W. D., and Burgess, N. Brain oscillations and memory. *Current opinion in neurobiology*, 20(2):143–149, 2010.
- Dvorak, D. and Fenton, A. A. Toward a proper estimation of phase–amplitude coupling in neural oscillations. *Journal of neuroscience methods*, 225:42–56, 2014.
- Ellenrieder, N., Frauscher, B., Dubeau, F., and Gotman, J. Interaction with slow waves during sleep improves discrimination of physiologic and pathologic high-frequency oscillations (80–500 Hz). *Epilepsia*, 57(6):869–878, 2016.
- Engel, A. K. and Fries, P. Beta-band oscillations—signalling the status quo? *Current opinion in neurobiology*, 20(2):156–165, 2010.
- Engel, A. K., Fries, P., and Singer, W. Dynamic predictions: oscillations and synchrony in top–down processing. *Nature Reviews Neuroscience*, 2(10):704, 2001.

BIBLIOGRAPHY

- Engel, E., Fischer, R., and Galetovic, A. Highway franchising: pitfalls and opportunities. *The American Economic Review*, 87(2):68–72, 1997.
- Engel, J., McDermott, M. P., Wiebe, S., Langfitt, J. T., Stern, J. M., Dewar, S., Sperling, M. R., Gardiner, I., Erba, G., Fried, I., et al. Early surgical therapy for drug-resistant temporal lobe epilepsy: a randomized trial. *Jama*, 307(9):922–930, 2012.
- Engel Jr, J. Introduction to temporal lobe epilepsy. *Epilepsy research*, 26(1):141–150, 1996.
- Engel Jr, J. Mesial temporal lobe epilepsy: what have we learned? *The Neuroscientist*, 7(4): 340–352, 2001.
- Engel Jr, J., Pitkänen, A., Loeb, J. A., Edward Dudek, F., Bertram III, E. H., Cole, A. J., Moshé, S. L., Wiebe, S., Jensen, F. E., Mody, I., et al. Epilepsy biomarkers. *Epilepsia*, 54:61–69, 2013.
- Fell, J. and Axmacher, N. The role of phase synchronization in memory processes. *Nature Reviews Neuroscience*, 12(2):105–118, 2011.
- Fisher, R. S., Boas, W. V. E., Blume, W., Elger, C., Genton, P., Lee, P., and Engel Jr, J. Epileptic seizures and epilepsy: definitions proposed by the international league against epilepsy (ilae) and the international bureau for epilepsy (ibe). *Epilepsia*, 46(4):470–472, 2005.
- Fisher, R. S., Acevedo, C., Arzimanoglou, A., Bogacz, A., Cross, J. H., Elger, C. E., Engel Jr, J., Forsgren, L., French, J. A., Glynn, M., et al. Ilae official report: a practical clinical definition of epilepsy. *Epilepsia*, 55(4):475–482, 2014.
- Florin, E. and Baillet, S. The brain’s resting-state activity is shaped by synchronized cross-frequency coupling of neural oscillations. *NeuroImage*, 111:26–35, 2015.
- Florin, E. and Baillet, S. Commentary: Evaluation of phase-amplitude coupling in resting state magnetoencephalographic signals: Effect of surrogates and evaluation approach. *Frontiers in computational neuroscience*, 12:26, 2018.

BIBLIOGRAPHY

- Florin, E., Vuvan, D., Peretz, I., and Baillet, S. Pre-target neural oscillations predict variability in the detection of small pitch changes. *PLoS one*, 12(5):e0177836, 2017.
- Fontolan, L., Krupa, M., Hyafil, A., and Gutkin, B. Analytical insights on theta-gamma coupled neural oscillators. *The Journal of Mathematical Neuroscience*, 3(1):16, 2013.
- Fontolan, L., Morillon, B., Liegeois-Chauvel, C., and Giraud, A.-L. The contribution of frequency-specific activity to hierarchical information processing in the human auditory cortex. *Nature communications*, 5:4694, 2014.
- Frauscher, B., von Ellenrieder, N., Ferrari-Marinho, T., Avoli, M., Dubeau, F., and Gotman, J. Facilitation of epileptic activity during sleep is mediated by high amplitude slow waves. *Brain*, 138(6):1629–1641, 2015.
- Freeman, W. J. Origin, structure, and role of background eeg activity. part 2. analytic phase. *Clinical Neurophysiology*, 115(9):2089–2107, 2004.
- Freeman, W. J. et al. *Mass action in the nervous system*, volume 2004. Citeseer, 1975.
- French, J., Williamson, P., Thadani, V., Darcey, T., Mattson, R., Spencer, S., and Spencer, D. Characteristics of medial temporal lobe epilepsy: I. results of history and physical examination. *Annals of neurology*, 34(6):774–780, 1993.
- Friedrich, R., Genoud, C., and Wanner, A. A. Analyzing the structure and function of neuronal circuits in zebrafish. *Frontiers in neural circuits*, 7:71, 2013.
- Fries, P. A mechanism for cognitive dynamics: neuronal communication through neuronal coherence. *Trends in cognitive sciences*, 9(10):474–480, 2005.
- Fries, P. Neuronal gamma-band synchronization as a fundamental process in cortical computation. *Annual review of neuroscience*, 32:209–224, 2009.
- Fries, P. Rhythms for cognition: communication through coherence. *Neuron*, 88(1):220–235, 2015.

BIBLIOGRAPHY

- Fries, P., Nikolić, D., and Singer, W. The gamma cycle. *Trends in neurosciences*, 30(7):309–316, 2007.
- Friston, K. A theory of cortical responses. *Philosophical Transactions of the Royal Society of London B: Biological Sciences*, 360(1456):815–836, 2005.
- Friston, K. and Kiebel, S. Predictive coding under the free-energy principle. *Philosophical Transactions of the Royal Society of London B: Biological Sciences*, 364(1521):1211–1221, 2009.
- Fründ, I., Ohl, F. W., and Herrmann, C. S. Spike-timing-dependent plasticity leads to gamma band responses in a neural network. *Biological cybernetics*, 101(3):227–240, 2009.
- Fujioka, T., Trainor, L. J., Large, E. W., and Ross, B. Internalized timing of isochronous sounds is represented in neuromagnetic beta oscillations. *Journal of Neuroscience*, 32(5):1791–1802, 2012.
- Gaab, N., Gaser, C., Zaehle, T., Jancke, L., and Schlaug, G. Functional anatomy of pitch memory—An fmri study with sparse temporal sampling. *Neuroimage*, 19(4):1417–1426, 2003.
- Galanopoulou, A. S. Developmental patterns in the regulation of chloride homeostasis and gabaa receptor signaling by seizures. *Epilepsia*, 48:14–18, 2007.
- Galanopoulou, A. S. Mutations affecting gabaergic signaling in seizures and epilepsy. *Pflügers Archiv-European Journal of Physiology*, 460(2):505–523, 2010.
- Galanopoulou, A. S. and Moshé, S. L. Neuronal network mechanisms—sex and development. In *Neuronal Networks in Brain Function, CNS Disorders, and Therapeutics*, pages 145–155. Elsevier, 2014.
- Gerber, E. M., Sadeh, B., Ward, A., Knight, R. T., and Deouell, L. Y. Non-sinusoidal activity

BIBLIOGRAPHY

- can produce cross-frequency coupling in cortical signals in the absence of functional interaction between neural sources. *PloS one*, 11(12):e0167351, 2016.
- Gerstein, G. L. and Kirkland, K. L. Neural assemblies: technical issues, analysis, and modeling. *Neural Networks*, 14(6-7):589–598, 2001.
- Gevins, A. and Smith, M. E. Neurophysiological measures of working memory and individual differences in cognitive ability and cognitive style. *Cerebral cortex*, 10(9):829–839, 2000.
- Gevins, A., Zeitlin, G., Doyle, J., Yingling, C., Schaffer, R., Callaway, E., and Yeager, C. Electroencephalogram correlates of higher cortical functions. *Science*, 203(4381):665–668, 1979.
- Gips, B., Eerden, J. P., and Jensen, O. A biologically plausible mechanism for neuronal coding organized by the phase of alpha oscillations. *European Journal of Neuroscience*, 44(4): 2147–2161, 2016.
- Gloor, P. *The temporal lobe and limbic system*. Oxford University Press, USA, 1997.
- Gloveli, T., Dugladze, T., Rotstein, H. G., Traub, R. D., Monyer, H., Heinemann, U., Whittington, M. A., and Kopell, N. J. Orthogonal arrangement of rhythm-generating microcircuits in the hippocampus. *Proceedings of the National Academy of Sciences*, 102(37):13295–13300, 2005.
- Gok, B., Jallo, G., Hayeri, R., Wahl, R., and Aygun, N. The evaluation of fdg-pet imaging for epileptogenic focus localization in patients with mri positive and mri negative temporal lobe epilepsy. *Neuroradiology*, 55(5):541–550, 2013.
- Goldman, R. I., Stern, J. M., Engel Jr, J., and Cohen, M. S. Simultaneous eeg and fmri of the alpha rhythm. *Neuroreport*, 13(18):2487, 2002.
- Goutagny, R., Gu, N., Cavanagh, C., Jackson, J., Chabot, J.-G., Quirion, R., Krantic, S., and Williams, S. Alterations in hippocampal network oscillations and theta–gamma coupling

BIBLIOGRAPHY

- arise before $\alpha\beta$ overproduction in a mouse model of alzheimer's disease. *European Journal of Neuroscience*, 37(12):1896–1902, 2013.
- Gray, C. M. Synchronous oscillations in neuronal systems: mechanisms and functions. *Journal of computational neuroscience*, 1(1-2):11–38, 1994.
- Gray, C. M. and Singer, W. Stimulus-specific neuronal oscillations in orientation columns of cat visual cortex. *Proceedings of the National Academy of Sciences*, 86(5):1698–1702, 1989.
- Gray, C. M., König, P., Engel, A. K., and Singer, W. Oscillatory responses in cat visual cortex exhibit inter-columnar synchronization which reflects global stimulus properties. *Nature*, 338(6213):334, 1989.
- Griesmayr, B., Gruber, W. R., Klimesch, W., and Sauseng, P. Human frontal midline theta and its synchronization to gamma during a verbal delayed match to sample task. *Neurobiology of learning and memory*, 93(2):208–215, 2010.
- Gross, J., Baillet, S., Barnes, G. R., Henson, R. N., Hillebrand, A., Jensen, O., Jerbi, K., Litvak, V., Maess, B., Oostenveld, R., et al. Good practice for conducting and reporting meg research. *Neuroimage*, 65:349–363, 2013a.
- Gross, J., Hoogenboom, N., Thut, G., Schyns, P., Panzeri, S., Belin, P., and Garrod, S. Speech rhythms and multiplexed oscillatory sensory coding in the human brain. *PLoS biology*, 11(12):e1001752, 2013b.
- Guerrini, R. Epilepsy in children. *The Lancet*, 367(9509):499–524, 2006.
- Guirgis, M., Chinvarun, Y., del Campo, M., Carlen, P. L., and Bardakjian, B. L. Defining regions of interest using cross-frequency coupling in extratemporal lobe epilepsy patients. *Journal of neural engineering*, 12(2):026011, 2015.
- Haider, B., Duque, A., Hasenstaub, A. R., and McCormick, D. A. Neocortical network activity

BIBLIOGRAPHY

- in vivo is generated through a dynamic balance of excitation and inhibition. *The Journal of neuroscience*, 26(17):4535–4545, 2006.
- Hamid, H., Blackmon, K., Cong, X., Dziura, J., Atlas, L. Y., Vickrey, B. G., Berg, A. T., Bazil, C. W., Langfitt, J. T., Walczak, T. S., et al. Mood, anxiety, and incomplete seizure control affect quality of life after epilepsy surgery. *Neurology*, pages 10–1212, 2014.
- Hari, R. and Salmelin, R. Human cortical oscillations: a neuromagnetic view through the skull. *Trends in neurosciences*, 20(1):44–49, 1997.
- Harris, K. D., Csicsvari, J., Hirase, H., Dragoi, G., and Buzsáki, G. Organization of cell assemblies in the hippocampus. *Nature*, 424(6948):552, 2003.
- Hasselmo, M. E., Bodelón, C., and Wyble, B. P. A proposed function for hippocampal theta rhythm: separate phases of encoding and retrieval enhance reversal of prior learning. *Neural computation*, 14(4):793–817, 2002.
- He, B. J., Zempel, J. M., Snyder, A. Z., and Raichle, M. E. The temporal structures and functional significance of scale-free brain activity. *Neuron*, 66(3):353–369, 2010.
- Hermann, B. P., Seidenberg, M., Schoenfeld, J., and Davies, K. Neuropsychological characteristics of the syndrome of mesial temporal lobe epilepsy. *Archives of neurology*, 54(4):369–376, 1997.
- Hillebrand, A., Tewarie, P., Van Dellen, E., Yu, M., Carbo, E. W., Douw, L., Gouw, A. A., Van Straaten, E. C., and Stam, C. J. Direction of information flow in large-scale resting-state networks is frequency-dependent. *Proceedings of the National Academy of Sciences*, 113(14):3867–3872, 2016.
- Hipp, J. F., Hawellek, D. J., Corbetta, M., Siegel, M., and Engel, A. K. Large-scale cortical correlation structure of spontaneous oscillatory activity. *Nature neuroscience*, 15(6):884, 2012.

BIBLIOGRAPHY

- Hohmann, A., Loui, P., Li, C. H., and Schlaug, G. Reverse engineering tone-deafness: Disrupting pitch-matching by creating temporary dysfunctions in the auditory-motor network. *Frontiers in human neuroscience*, 12:9, 2018.
- Holz, E. M., Glennon, M., Prendergast, K., and Sauseng, P. Theta–gamma phase synchronization during memory matching in visual working memory. *Neuroimage*, 52(1):326–335, 2010.
- Hutcheon, B. and Yarom, Y. Resonance, oscillation and the intrinsic frequency preferences of neurons. *Trends in neurosciences*, 23(5):216–222, 2000.
- Hyafil, A., Fontolan, L., Kabdebon, C., Gutkin, B., and Giraud, A.-L. Speech encoding by coupled cortical theta and gamma oscillations. *Elife*, 4:e06213, 2015a.
- Hyafil, A., Giraud, A.-L., Fontolan, L., and Gutkin, B. Neural cross-frequency coupling: connecting architectures, mechanisms, and functions. *Trends in neurosciences*, 38(11):725–740, 2015b.
- Hyde, K. L. and Peretz, I. Brains that are out of tune but in time. *Psychological Science*, 15(5): 356–360, 2004.
- Hyde, K. L., Lerch, J. P., Zatorre, R. J., Griffiths, T. D., Evans, A. C., and Peretz, I. Cortical thickness in congenital amusia: when less is better than more. *Journal of Neuroscience*, 27(47):13028–13032, 2007.
- Hyde, K. L., Zatorre, R. J., and Peretz, I. Functional mri evidence of an abnormal neural network for pitch processing in congenital amusia. *Cerebral Cortex*, 21(2):292–299, 2010.
- Ibrahim, G. M., Wong, S. M., Anderson, R. A., Singh-Cadieux, G., Akiyama, T., Ochi, A., Osubo, H., Okanishi, T., Valiante, T. A., Donner, E., et al. Dynamic modulation of epileptic high frequency oscillations by the phase of slower cortical rhythms. *Experimental neurology*, 251:30–38, 2014.

BIBLIOGRAPHY

- Isomura, Y., Sirota, A., Özen, S., Montgomery, S., Mizuseki, K., Henze, D. A., and Buzsáki, G. Integration and segregation of activity in entorhinal-hippocampal subregions by neocortical slow oscillations. *Neuron*, 52(5):871–882, 2006.
- Izhikevich, E. M. Polychronization: computation with spikes. *Neural computation*, 18(2): 245–282, 2006.
- Jacobs, J., Kahana, M. J., Ekstrom, A. D., and Fried, I. Brain oscillations control timing of single-neuron activity in humans. *Journal of Neuroscience*, 27(14):3839–3844, 2007.
- Jacobs, J., LeVan, P., Chander, R., Hall, J., Dubeau, F., and Gotman, J. Interictal high-frequency oscillations (80–500 Hz) are an indicator of seizure onset areas independent of spikes in the human epileptic brain. *Epilepsia*, 49(11):1893–1907, 2008.
- Jacobs, J., Vogt, C., LeVan, P., Zelmann, R., Gotman, J., and Kobayashi, K. The identification of distinct high-frequency oscillations during spikes delineates the seizure onset zone better than high-frequency spectral power changes. *Clinical Neurophysiology*, 127(1):129–142, 2016.
- Jallon, P. Epilepsy in developing countries. *Epilepsia*, 38(10):1143–1151, 1997.
- Jensen, O. Information transfer between rhythmically coupled networks: reading the hippocampal phase code. *Neural computation*, 13(12):2743–2761, 2001.
- Jensen, O. and Colgin, L. L. Cross-frequency coupling between neuronal oscillations. *Trends in cognitive sciences*, 11(7):267–269, 2007.
- Jensen, O. and Lisman, J. E. An oscillatory short-term memory buffer model can account for data on the sternberg task. *Journal of Neuroscience*, 18(24):10688–10699, 1998.
- Jensen, O. and Lisman, J. E. Hippocampal sequence-encoding driven by a cortical multi-item working memory buffer. *Trends in neurosciences*, 28(2):67–72, 2005.

BIBLIOGRAPHY

- Jensen, O. and Mazaheri, A. Shaping functional architecture by oscillatory alpha activity: gating by inhibition. *Frontiers in human neuroscience*, 4:186, 2010.
- Jensen, O., Gips, B., Bergmann, T. O., and Bonnefond, M. Temporal coding organized by coupled alpha and gamma oscillations prioritize visual processing. *Trends in neurosciences*, 37(7):357–369, 2014.
- Jensen, O., Spaak, E., and Park, H. Discriminating valid from spurious indices of phase-amplitude coupling. *eNeuro*, 3(6):ENEURO–0334, 2016.
- Jiang, H., Bahramisharif, A., van Gerven, M. A., and Jensen, O. Measuring directionality between neuronal oscillations of different frequencies. *Neuroimage*, 118:359–367, 2015.
- Jobst, B. C. and Cascino, G. D. Resective epilepsy surgery for drug-resistant focal epilepsy: a review. *Jama*, 313(3):285–293, 2015.
- Jones, M. W. and Wilson, M. A. Theta rhythms coordinate hippocampal–prefrontal interactions in a spatial memory task. *PLoS biology*, 3(12):e402, 2005.
- Kahana, M. J., Seelig, D., and Madsen, J. R. Theta returns. *Current opinion in neurobiology*, 11(6):739–744, 2001.
- Karunakaran, S., Grasse, D. W., and Moxon, K. A. Role of ca3 theta-modulated interneurons during the transition to spontaneous seizures. *Experimental neurology*, 283:341–352, 2016.
- Kirihara, K., Rissling, A. J., Swerdlow, N. R., Braff, D. L., and Light, G. A. Hierarchical organization of gamma and theta oscillatory dynamics in schizophrenia. *Biological psychiatry*, 71(10):873–880, 2012.
- Kishon-Rabin, L., Amir, O., Vexler, Y., and Zaltz, Y. Pitch discrimination: Are professional musicians better than non-musicians? *Journal of basic and clinical physiology and pharmacology*, 12(2):125–144, 2001.

BIBLIOGRAPHY

- Klimesch, W. Eeg alpha and theta oscillations reflect cognitive and memory performance: a review and analysis. *Brain research reviews*, 29(2):169–195, 1998.
- Kokaia, M., Andersson, M., and Ledri, M. An optogenetic approach in epilepsy. *Neuropharmacology*, 69:89–95, 2013.
- Korotkova, T., Fuchs, E. C., Ponomarenko, A., von Engelhardt, J., and Monyer, H. Nmda receptor ablation on parvalbumin-positive interneurons impairs hippocampal synchrony, spatial representations, and working memory. *Neuron*, 68(3):557–569, 2010.
- Kramer, M. and Eden, U. Assessment of cross-frequency coupling with confidence using generalized linear models. *Journal of neuroscience methods*, 220(1):64–74, 2013.
- Kramer, M. A., Tort, A. B., and Kopell, N. J. Sharp edge artifacts and spurious coupling in eeg frequency comodulation measures. *Journal of neuroscience methods*, 170(2):352–357, 2008.
- Kreiter, A. and Singer, W. Oscillatory neuronal responses in the visual cortex of the awake macaque monkey. *European Journal of Neuroscience*, 4(4):369–375, 1992.
- Krook-Magnuson, E., Armstrong, C., Oijala, M., and Soltesz, I. On-demand optogenetic control of spontaneous seizures in temporal lobe epilepsy. *Nature communications*, 4:1376, 2013.
- La Fougère, C., Rominger, A., Förster, S., Geisler, J., and Bartenstein, P. Pet and spect in epilepsy: a critical review. *Epilepsy & Behavior*, 15(1):50–55, 2009.
- La Rocca, D., Campisi, P., Vegso, B., Cserti, P., Kozmann, G., Babiloni, F., and Fallani, F. D. V. Human brain distinctiveness based on eeg spectral coherence connectivity. *IEEE transactions on Biomedical Engineering*, 61(9):2406–2412, 2014.
- Lachaux, J.-P., Rodriguez, E., Martinerie, J., and Varela, F. J. Measuring phase synchrony in brain signal. *Human brain mapping*, 8(4):194–208, 1999.

BIBLIOGRAPHY

- Lakatos, P., Shah, A. S., Knuth, K. H., Ulbert, I., Karmos, G., and Schroeder, C. E. An oscillatory hierarchy controlling neuronal excitability and stimulus processing in the auditory cortex. *Journal of neurophysiology*, 94(3):1904–1911, 2005.
- Lakatos, P., Karmos, G., Mehta, A. D., Ulbert, I., and Schroeder, C. E. Entrainment of neuronal oscillations as a mechanism of attentional selection. *science*, 320(5872):110–113, 2008.
- Lakatos, P., Musacchia, G., O’Connell, M. N., Falchier, A. Y., Javitt, D. C., and Schroeder, C. E. The spectrotemporal filter mechanism of auditory selective attention. *Neuron*, 77(4):750–761, 2013.
- Laurent, G. Dynamical representation of odors by oscillating and evolving neural assemblies. *Trends in neurosciences*, 19(11):489–496, 1996.
- Lévesque, M. and Avoli, M. Carbachol-induced theta-like oscillations in the rodent brain limbic system: Underlying mechanisms and significance. *Neuroscience & Biobehavioral Reviews*, 2018.
- Lévesque, M., Bortel, A., Gotman, J., and Avoli, M. High-frequency (80–500hz) oscillations and epileptogenesis in temporal lobe epilepsy. *Neurobiology of disease*, 42(3):231–241, 2011.
- Lévesque, M., Salami, P., Gotman, J., and Avoli, M. Two seizure-onset types reveal specific patterns of high-frequency oscillations in a model of temporal lobe epilepsy. *Journal of Neuroscience*, 32(38):13264–13272, 2012.
- Lévesque, M., Behr, C., and Avoli, M. The anti-ictogenic effects of levetiracetam are mirrored by interictal spiking and high-frequency oscillation changes in a model of temporal lobe epilepsy. *Seizure*, 25:18–25, 2015.
- Levine, D. S., Brown, V. R., and Shirey, T. *Oscillations in neural systems*. Psychology Press, 1999.

BIBLIOGRAPHY

- Lisman, J. The theta/gamma discrete phase code occurring during the hippocampal phase precession may be a more general brain coding scheme. *Hippocampus*, 15(7):913–922, 2005.
- Lisman, J. and Buzsáki, G. A neural coding scheme formed by the combined function of gamma and theta oscillations. *Schizophrenia bulletin*, 34(5):974–980, 2008.
- Lisman, J. E. and Idiart, M. Storage of 7 ± 2 short-term memories in oscillatory subcycles. *Science*, 267:10, 1995.
- Liu, S., Sha, Z., Sencer, A., Aydoseli, A., Bebek, N., Abosch, A., Henry, T., Gurses, C., and Ince, N. F. Exploring the time–frequency content of high frequency oscillations for automated identification of seizure onset zone in epilepsy. *Journal of neural engineering*, 13(2): 026026, 2016.
- Liu, Y., Lopez-Santiago, L. F., Yuan, Y., Jones, J. M., Zhang, H., O’malley, H. A., Patino, G. A., O’Brien, J. E., Rusconi, R., Gupta, A., et al. Dravet syndrome patient-derived neurons suggest a novel epilepsy mechanism. *Annals of neurology*, 74(1):128–139, 2013.
- Lobier, M., Siebenhühner, F., Palva, S., and Palva, J. M. Phase transfer entropy: a novel phase-based measure for directed connectivity in networks coupled by oscillatory interactions. *Neuroimage*, 85:853–872, 2014.
- López-Azcárate, J., Tainta, M., Rodríguez-Oroz, M. C., Valencia, M., González, R., Guridi, J., Iriarte, J., Obeso, J. A., Artieda, J., and Alegre, M. Coupling between beta and high-frequency activity in the human subthalamic nucleus may be a pathophysiological mechanism in parkinson’s disease. *Journal of Neuroscience*, 30(19):6667–6677, 2010.
- López-Azcárate, J., Nicolás, M. J., Cordon, I., Alegre, M., Valencia, M., and Artieda, J. Delta-mediated cross-frequency coupling organizes oscillatory activity across the rat cortico-basal ganglia network. *Frontiers in neural circuits*, 7, 2013.

BIBLIOGRAPHY

- Loui, P., Alsop, D., and Schlaug, G. Tone deafness: a new disconnection syndrome? *Journal of Neuroscience*, 29(33):10215–10220, 2009.
- Loup, F., Wieser, H.-G., Yonekawa, Y., Aguzzi, A., and Fritschy, J.-M. Selective alterations in gabaa receptor subtypes in human temporal lobe epilepsy. *Journal of Neuroscience*, 20(14): 5401–5419, 2000.
- Lozano-Soldevilla, D., ter Huurne, N., and Oostenveld, R. Neuronal oscillations with non-sinusoidal morphology produce spurious phase-to-amplitude coupling and directionality. *Frontiers in computational neuroscience*, 10, 2016.
- Lu, N., Xing, D., Sheng, T., and Lu, W. The mechanism and function of hippocampal neural oscillation. *Sheng li xue bao:[Acta physiologica Sinica]*, 69(5):647–656, 2017.
- Luo, H. and Poeppel, D. Phase patterns of neuronal responses reliably discriminate speech in human auditory cortex. *Neuron*, 54(6):1001–1010, 2007.
- Malerba, P. and Kopell, N. Phase resetting reduces theta–gamma rhythmic interaction to a one-dimensional map. *Journal of mathematical biology*, 66(7):1361–1386, 2013.
- Mazaheri, A. and Jensen, O. Asymmetric amplitude modulations of brain oscillations generate slow evoked responses. *Journal of Neuroscience*, 28(31):7781–7787, 2008.
- Mazaheri, A., van Schouwenburg, M. R., Dimitrijevic, A., Denys, D., Cools, R., and Jensen, O. Region-specific modulations in oscillatory alpha activity serve to facilitate processing in the visual and auditory modalities. *Neuroimage*, 87:356–362, 2014.
- Mazzoni, A., Panzeri, S., Logothetis, N. K., and Brunel, N. Encoding of naturalistic stimuli by local field potential spectra in networks of excitatory and inhibitory neurons. *PLoS computational biology*, 4(12):e1000239, 2008.
- McCulloch, W. S. and Pitts, W. A logical calculus of the ideas immanent in nervous activity. *The bulletin of mathematical biophysics*, 5(4):115–133, 1943.

BIBLIOGRAPHY

- McGinn, R. J. and Valiante, T. A. Phase–amplitude coupling and interlaminar synchrony are correlated in human neocortex. *Journal of Neuroscience*, 34(48):15923–15930, 2014.
- Medvedev, A. V., Murro, A. M., and Meador, K. J. Abnormal interictal gamma activity may manifest a seizure onset zone in temporal lobe epilepsy. *International journal of neural systems*, 21(02):103–114, 2011.
- Mehta, M. R. Neuronal dynamics of predictive coding. *The Neuroscientist*, 7(6):490–495, 2001.
- Meijer, E., Hermans, K., Zwanenburg, A., Jennekens, W., Niemarkt, H., Cluitmans, P., Van Pul, C., Wijn, P., and Andriessen, P. Functional connectivity in preterm infants derived from eeg coherence analysis. *European journal of paediatric neurology*, 18(6):780–789, 2014.
- Michalareas, G., Vezoli, J., Van Pelt, S., Schoffelen, J.-M., Kennedy, H., and Fries, P. Alpha-beta and gamma rhythms subserve feedback and feedforward influences among human visual cortical areas. *Neuron*, 89(2):384–397, 2016.
- Micheyl, C., Delhommeau, K., Perrot, X., and Oxenham, A. J. Influence of musical and psychoacoustical training on pitch discrimination. *Hearing research*, 219(1-2):36–47, 2006.
- Miskovic, V., Moscovitch, D. A., Santesso, D. L., McCabe, R. E., Antony, M. M., and Schmidt, L. A. Changes in eeg cross-frequency coupling during cognitive behavioral therapy for social anxiety disorder. *Psychological science*, 22(4):507–516, 2011.
- Mizuseki, K., Sirota, A., Pastalkova, E., and Buzsáki, G. Theta oscillations provide temporal windows for local circuit computation in the entorhinal-hippocampal loop. *Neuron*, 64(2):267–280, 2009.
- Monto, S., Palva, S., Voipio, J., and Palva, J. M. Very slow eeg fluctuations predict the dynamics of stimulus detection and oscillation amplitudes in humans. *Journal of Neuroscience*, 28(33):8268–8272, 2008.

BIBLIOGRAPHY

- Moran, L. V. and Hong, L. E. High vs low frequency neural oscillations in schizophrenia. *Schizophrenia bulletin*, 37(4):659–663, 2011.
- Morillon, B. and Baillet, S. Motor origin of temporal predictions in auditory attention. *Proceedings of the National Academy of Sciences*, 114(42):E8913–E8921, 2017.
- Moshé, S. L., Perucca, E., Ryvlin, P., and Tomson, T. Epilepsy: new advances. *The Lancet*, 385(9971):884–898, 2015.
- Murias, M., Webb, S. J., Greenson, J., and Dawson, G. Resting state cortical connectivity reflected in eeg coherence in individuals with autism. *Biological psychiatry*, 62(3):270–273, 2007.
- Nakamura, T., Small, M., and Hirata, Y. Testing for nonlinearity in irregular fluctuations with long-term trends. *Physical Review E*, 74(2):026205, 2006.
- Nariai, H., Matsuzaki, N., Juhász, C., Nagasawa, T., Sood, S., Chugani, H. T., and Asano, E. Ictal high-frequency oscillations at 80–200 hz coupled with delta phase in epileptic spasms. *Epilepsia*, 52(10), 2011.
- Nazer, F. and Dickson, C. T. Slow oscillation state facilitates epileptiform events in the hippocampus. *Journal of neurophysiology*, 102(3):1880–1889, 2009.
- Neal, E. G., Chaffe, H., Schwartz, R. H., Lawson, M. S., Edwards, N., Fitzsimmons, G., Whitney, A., and Cross, J. H. The ketogenic diet for the treatment of childhood epilepsy: a randomised controlled trial. *The Lancet Neurology*, 7(6):500–506, 2008.
- Ng, B. S. W., Schroeder, T., and Kayser, C. A precluding but not ensuring role of entrained low-frequency oscillations for auditory perception. *Journal of Neuroscience*, 32(35):12268–12276, 2012.
- Niell, C. M. and Stryker, M. P. Modulation of visual responses by behavioral state in mouse visual cortex. *Neuron*, 65(4):472–479, 2010.

BIBLIOGRAPHY

- Nir, Y., Staba, R. J., Andrillon, T., Vyazovskiy, V. V., Cirelli, C., Fried, I., and Tononi, G. Regional slow waves and spindles in human sleep. *Neuron*, 70(1):153–169, 2011.
- Norman-Haignere, S., Kanwisher, N., and McDermott, J. H. Cortical pitch regions in humans respond primarily to resolved harmonics and are located in specific tonotopic regions of anterior auditory cortex. *Journal of Neuroscience*, 33(50):19451–19469, 2013.
- Nowotny, T., Huerta, R., and Rabinovich, M. I. Neuronal synchrony: peculiarity and generality. *Chaos: An Interdisciplinary Journal of Nonlinear Science*, 18(3):5692, 2008.
- O’Keefe, J. Hippocampus, theta, and spatial memory. *Current opinion in neurobiology*, 3(6): 917–924, 1993.
- Omigie, D., Pearce, M. T., Williamson, V. J., and Stewart, L. Electrophysiological correlates of melodic processing in congenital amusia. *Neuropsychologia*, 51(9):1749–1762, 2013.
- Onitsuka, T., Oribe, N., and Kanba, S. Neurophysiological findings in patients with bipolar disorder. In *Supplements to Clinical neurophysiology*, volume 62, pages 197–206. Elsevier, 2013.
- Ono, T. and Galanopoulou, A. S. Epilepsy and epileptic syndrome. In *Neurodegenerative Diseases*, pages 99–113. Springer, 2012.
- Onslow, A. C., Bogacz, R., and Jones, M. W. Quantifying phase–amplitude coupling in neuronal network oscillations. *Progress in biophysics and molecular biology*, 105(1-2):49–57, 2011.
- Onslow, A. C., Jones, M. W., and Bogacz, R. A canonical circuit for generating phase-amplitude coupling. *PLoS One*, 9(8):e102591, 2014.
- Osipova, D., Hermes, D., and Jensen, O. Gamma power is phase-locked to posterior alpha activity. *PloS one*, 3(12):e3990, 2008.

BIBLIOGRAPHY

- Ozkurt, T. E. Statistically reliable and fast direct estimation of phase-amplitude cross-frequency coupling. *Biomedical Engineering, IEEE Transactions on*, 59(7):1943–1950, 2012.
- Palva, J. M. and Palva, S. Roles of multiscale brain activity fluctuations in shaping the variability and dynamics of psychophysical performance. In *Progress in brain research*, volume 193, pages 335–350. Elsevier, 2011.
- Palva, J. M., Palva, S., and Kaila, K. Phase synchrony among neuronal oscillations in the human cortex. *The Journal of Neuroscience*, 25(15):3962–3972, 2005.
- Palva, J. M., Monto, S., Kulashekhar, S., and Palva, S. Neuronal synchrony reveals working memory networks and predicts individual memory capacity. *Proceedings of the National Academy of Sciences*, 107(16):7580–7585, 2010.
- Pantazis, D., Nichols, T. E., Baillet, S., and Leahy, R. M. A comparison of random field theory and permutation methods for the statistical analysis of meg data. *NeuroImage*, 25(2):383–394, 2005.
- Panzeri, S., Ince, R. A., Diamond, M. E., and Kayser, C. Reading spike timing without a clock: intrinsic decoding of spike trains. *Philosophical Transactions of the Royal Society B: Biological Sciences*, 369(1637):20120467, 2014.
- Pasley, B. N., David, S. V., Mesgarani, N., Flinker, A., Shamma, S. A., Crone, N. E., Knight, R. T., and Chang, E. F. Reconstructing speech from human auditory cortex. *PLoS biology*, 10(1):e1001251, 2012.
- Peng, Z., Huang, C. S., Stell, B. M., Mody, I., and Houser, C. R. Altered expression of the δ subunit of the gabaa receptor in a mouse model of temporal lobe epilepsy. *Journal of Neuroscience*, 24(39):8629–8639, 2004.
- Penny, W., Duzel, E., Miller, K., and Ojemann, J. Testing for nested oscillation. *Journal of neuroscience methods*, 174(1):50–61, 2008.

BIBLIOGRAPHY

- Peretz, I. Neurobiology of congenital amusia. *Trends in cognitive sciences*, 20(11):857–867, 2016.
- Peretz, I., Ayotte, J., Zatorre, R. J., Mehler, J., Ahad, P., Penhune, V. B., and Jutras, B. Congenital amusia: a disorder of fine-grained pitch discrimination. *Neuron*, 33(2):185–191, 2002.
- Peretz, I., Champod, A. S., and Hyde, K. Varieties of musical disorders: the montreal battery of evaluation of amusia. *Annals of the New York Academy of Sciences*, 999(1):58–75, 2003.
- Peretz, I., Brattico, E., and Tervaniemi, M. Abnormal electrical brain responses to pitch in congenital amusia. *Annals of neurology*, 58(3):478–482, 2005.
- Peretz, I., Cummings, S., and Dubé, M.-P. The genetics of congenital amusia (tone deafness): a family-aggregation study. *The American Journal of Human Genetics*, 81(3):582–588, 2007.
- Perucca, E. Introduction to the choice of antiepileptic drugs. *The treatment of epilepsy*, 3: 389–98, 2009.
- Perucca, E. and Tomson, T. The pharmacological treatment of epilepsy in adults. *The lancet neurology*, 10(5):446–456, 2011.
- Petkar, S., Hamid, T., Iddon, P., Clifford, A., Rice, N., Claire, R., McKee, D., Curtis, N., Cooper, P. N., and Fitzpatrick, A. P. Prolonged implantable electrocardiographic monitoring indicates a high rate of misdiagnosis of epilepsy—revisé study. *Europace*, 14(11):1653–1660, 2012.
- Pittman-Polletta, B., Hsieh, W.-H., Kaur, S., Lo, M.-T., and Hu, K. Detecting phase-amplitude coupling with high frequency resolution using adaptive decompositions. *Journal of neuroscience methods*, 226:15–32, 2014.
- Poulter, M. O., Brown, L. A., Tynan, S., Willick, G., William, R., and McIntyre, D. C. Differential expression of $\alpha 1$, $\alpha 2$, $\alpha 3$, and $\alpha 5$ gabaa receptor subunits in seizure-prone and seizure-resistant rat models of temporal lobe epilepsy. *Journal of Neuroscience*, 19(11):4654–4661, 1999.

BIBLIOGRAPHY

- Rao, R. P. and Ballard, D. H. Predictive coding in the visual cortex: a functional interpretation of some extra-classical receptive-field effects. *Nature neuroscience*, 2(1):79, 1999.
- Rizzuto, D. S., Madsen, J. R., Bromfield, E. B., Schulze-Bonhage, A., and Kahana, M. J. Human neocortical oscillations exhibit theta phase differences between encoding and retrieval. *Neuroimage*, 31(3):1352–1358, 2006.
- Rosen, S. Temporal information in speech: acoustic, auditory and linguistic aspects. *Phil. Trans. R. Soc. Lond. B*, 336(1278):367–373, 1992.
- Roux, F. and Uhlhaas, P. J. Working memory and neural oscillations: alpha–gamma versus theta–gamma codes for distinct wm information? *Trends in cognitive sciences*, 18(1):16–25, 2014.
- Roux, F., Wibrals, M., Singer, W., Aru, J., and Uhlhaas, P. J. The phase of thalamic alpha activity modulates cortical gamma-band activity: evidence from resting-state meg recordings. *Journal of Neuroscience*, 33(45):17827–17835, 2013.
- Saalmann, Y. B., Pinsk, M. A., Wang, L., Li, X., and Kastner, S. The pulvinar regulates information transmission between cortical areas based on attention demands. *Science*, 337(6095):753–756, 2012.
- Salami, P., Lévesque, M., Benini, R., Behr, C., Gotman, J., and Avoli, M. Dynamics of interictal spikes and high-frequency oscillations during epileptogenesis in temporal lobe epilepsy. *Neurobiology of disease*, 67:97–106, 2014.
- Salanova, V., Quesney, L., Rasmussen, T., Andermann, F., and Olivier, A. Reevaluation of surgical failures and the role of reoperation in 39 patients with frontal lobe epilepsy. *Epilepsia*, 35(1):70–80, 1994a.
- Salanova, V., Markand, O. N., and Worth, R. Clinical characteristics and predictive factors in 98

BIBLIOGRAPHY

- patients with complex partial seizures treated with temporal resection. *Archives of neurology*, 51(10):1008–1013, 1994b.
- Saleh, M., Reimer, J., Penn, R., Ojakangas, C. L., and Hatsopoulos, N. G. Fast and slow oscillations in human primary motor cortex predict oncoming behaviorally relevant cues. *Neuron*, 65(4):461–471, 2010.
- Sameiro-Barbosa, C. M. and Geiser, E. Sensory entrainment mechanisms in auditory perception: neural synchronization cortico-striatal activation. *Frontiers in neuroscience*, 10:361, 2016.
- Samiee, S. and Baillet, S. Time-resolved phase-amplitude coupling in neural oscillations. *NeuroImage*, 159:270–279, 2017.
- Samiee, S., Florin, E., Vivan, D., Albouy, P., Peretz, I., and Baillet, S. Oscillatory network dynamics for pitch discrimination. *Submitted*.
- Samiee, S., Lévesque, M., Avoli, M., and Baillet, S. Phase-amplitude coupling and epileptogenesis in an animal model of mesial temporal lobe epilepsy. *Neurobiology of disease*, 114: 111–119, 2018.
- Sams, M., Paavilainen, P., Alho, K., and Näätänen, R. Auditory frequency discrimination and event-related potentials. *Electroencephalography and Clinical Neurophysiology/Evoked Potentials Section*, 62(6):437–448, 1985.
- Sauseng, P., Klimesch, W., Gruber, W. R., and Birbaumer, N. Cross-frequency phase synchronization: a brain mechanism of memory matching and attention. *Neuroimage*, 40(1): 308–317, 2008.
- Schack, B., Vath, N., Petsche, H., Geissler, H.-G., and Möller, E. Phase-coupling of theta–gamma eeg rhythms during short-term memory processing. *International Journal of Psychophysiology*, 44(2):143–163, 2002.

BIBLIOGRAPHY

- Schall, K. P., Kerber, J., and Dickson, C. T. Rhythmic constraints on hippocampal processing: state and phase-related fluctuations of synaptic excitability during theta and the slow oscillation. *Journal of neurophysiology*, 99(2):888–899, 2008.
- Scheffer-Teixeira, R. and Tort, A. B. On cross-frequency phase-phase coupling between theta and gamma oscillations in the hippocampus. *Elife*, 5:e20515, 2016.
- Schevon, C. A., Weiss, S. A., McKhann Jr, G., Goodman, R. R., Yuste, R., Emerson, R. G., and Trevelyan, A. J. Evidence of an inhibitory restraint of seizure activity in humans. *Nature communications*, 3:1060, 2012.
- Schroeder, C. E. and Lakatos, P. The gamma oscillation: master or slave? *Brain topography*, 22(1):24–26, 2009a.
- Schroeder, C. E. and Lakatos, P. Low-frequency neuronal oscillations as instruments of sensory selection. *Trends in neurosciences*, 32(1):9–18, 2009b.
- Schroeder, C. E., Wilson, D. A., Radman, T., Scharfman, H., and Lakatos, P. Dynamics of active sensing and perceptual selection. *Current opinion in neurobiology*, 20(2):172–176, 2010.
- Schutter, D. J. and Knyazev, G. G. Cross-frequency coupling of brain oscillations in studying motivation and emotion. *Motivation and emotion*, 36(1):46–54, 2012.
- Seeck, M., Lazeyras, F., Michel, C. M., Blanke, O., Gericke, C., Ives, J., Delavelle, J., Golay, X., Haenggeli, C.-A., De Tribolet, N., et al. Non-invasive epileptic focus localization using eeg-triggered functional mri and electromagnetic tomography. *Electroencephalography and clinical Neurophysiology*, 106(6):508–512, 1998.
- Seiam, A.-H. R., Dhaliwal, H., and Wiebe, S. Determinants of quality of life after epilepsy surgery: systematic review and evidence summary. *Epilepsy & Behavior*, 21(4):441–445, 2011.

BIBLIOGRAPHY

- Shimamoto, S. A., Ryapolova-Webb, E. S., Ostrem, J. L., Galifianakis, N. B., Miller, K. J., and Starr, P. A. Subthalamic nucleus neurons are synchronized to primary motor cortex local field potentials in parkinson's disease. *Journal of Neuroscience*, 33(17):7220–7233, 2013.
- Shiri, Z., Lévesque, M., Etter, G., Manseau, F., Williams, S., and Avoli, M. Optogenetic low-frequency stimulation of specific neuronal populations abates ictogenesis. *Journal of Neuroscience*, 37(11):2999–3008, 2017.
- Smith, M. E., McEvoy, L. K., and Gevins, A. Neurophysiological indices of strategy development and skill acquisition. *Cognitive Brain Research*, 7(3):389–404, 1999.
- Solomon, E., Kragel, J., Sperling, M. R., Sharan, A., Worrell, G., Kucewicz, M., Inman, C., Lega, B., Davis, K., Stein, J., et al. Widespread theta synchrony and high-frequency desynchronization underlies enhanced cognition. *Nature communications*, 8(1):1704, 2017.
- Somers, D. and Kopell, N. Rapid synchronization through fast threshold modulation. *Biological cybernetics*, 68(5):393–407, 1993.
- Song, I., Orosz, I., Chervoneva, I., Waldman, Z. J., Fried, I., Wu, C., Sharan, A., Salamon, N., Gorniak, R., Dewar, S., et al. Bimodal coupling of ripples and slower oscillations during sleep in patients with focal epilepsy. *Epilepsia*, 58(11):1972–1984, 2017.
- Spaak, E., Zeitler, M., and Gielen, S. Hippocampal theta modulation of neocortical spike times and gamma rhythm: a biophysical model study. *PloS one*, 7(10):e45688, 2012.
- Spencer, K. M., Niznikiewicz, M. A., Nestor, P. G., Shenton, M. E., and McCarley, R. W. Left auditory cortex gamma synchronization and auditory hallucination symptoms in schizophrenia. *BMC neuroscience*, 10(1):85, 2009.
- Spencer, S. S. The relative contributions of mri, spect, and pet imaging in epilepsy. *Epilepsia*, 35:S72–S89, 1994.

BIBLIOGRAPHY

- Spencer, S. S. and Spencer, D. D. Entorhinal-hippocampal interactions in medial temporal lobe epilepsy. *Epilepsia*, 35(4):721–727, 1994.
- Spiegel, M. F. and Watson, C. S. Performance on frequency-discrimination tasks by musicians and nonmusicians. *The Journal of the Acoustical Society of America*, 76(6):1690–1695, 1984.
- Srinivasan, R., Winter, W. R., Ding, J., and Nunez, P. L. Eeg and meg coherence: measures of functional connectivity at distinct spatial scales of neocortical dynamics. *Journal of neuroscience methods*, 166(1):41–52, 2007.
- Steriade, M. Impact of network activities on neuronal properties in corticothalamic systems. *Journal of neurophysiology*, 86(1):1–39, 2001.
- Steriade, M., McCormick, D. A., and Sejnowski, T. J. Thalamocortical oscillations in the sleeping and aroused brain. *Science*, 262(5134):679–685, 1993.
- Steriade, M., Amzica, F., and Contreras, D. Synchronization of fast (30–40 hz) spontaneous cortical rhythms during brain activation. *Journal of Neuroscience*, 16(1):392–417, 1996.
- Stief, F., Zusratter, W., Hartmann, K., Schmitz, D., and Draguhn, A. Enhanced synaptic excitation–inhibition ratio in hippocampal interneurons of rats with temporal lobe epilepsy. *European Journal of Neuroscience*, 25(2):519–528, 2007.
- Szczepanski, S. M., Crone, N. E., Kuperman, R. A., Auguste, K. I., Parvizi, J., and Knight, R. T. Dynamic changes in phase-amplitude coupling facilitate spatial attention control in fronto-parietal cortex. *PLoS biology*, 12(8):e1001936, 2014.
- Tadel, F., Baillet, S., Mosher, J. C., Pantazis, D., and Leahy, R. M. Brainstorm: a user-friendly application for meg/eeg analysis. *Computational intelligence and neuroscience*, 2011:8, 2011.

BIBLIOGRAPHY

- Takeuchi, S., Mima, T., Murai, R., Shimazu, H., Isomura, Y., and Tsujimoto, T. Gamma oscillations and their cross-frequency coupling in the primate hippocampus during sleep. *Sleep*, 38(7):1085–1091, 2015.
- Tallon-Baudry, C. and Bertrand, O. Oscillatory gamma activity in humans and its role in object representation. *Trends in cognitive sciences*, 3(4):151–162, 1999.
- Tervaniemi, M., Alho, K., Paavilainen, P., Sams, M., and Näätänen, R. Absolute pitch and event-related brain potentials. *Music Perception: An Interdisciplinary Journal*, 10(3):305–316, 1993.
- Tervaniemi, M., Just, V., Koelsch, S., Widmann, A., and Schröger, E. Pitch discrimination accuracy in musicians vs nonmusicians: an event-related potential and behavioral study. *Experimental brain research*, 161(1):1–10, 2005.
- Tesche, C. and Karhu, J. Theta oscillations index human hippocampal activation during a working memory task. *Proceedings of the National Academy of Sciences*, 97(2):919–924, 2000.
- Thivierge, J.-P. and Cisek, P. Nonperiodic synchronization in heterogeneous networks of spiking neurons. *Journal of Neuroscience*, 28(32):7968–7978, 2008.
- Thurman, D. J., Beghi, E., Begley, C. E., Berg, A. T., Buchhalter, J. R., Ding, D., Hesdorffer, D. C., Hauser, W. A., Kazis, L., Kobau, R., et al. Standards for epidemiologic studies and surveillance of epilepsy. *Epilepsia*, 52:2–26, 2011.
- Tort, A. B., Rotstein, H. G., Dugladze, T., Gloveli, T., and Kopell, N. J. On the formation of gamma-coherent cell assemblies by oriens lacunosum-moleculare interneurons in the hippocampus. *Proceedings of the National Academy of Sciences*, 104(33):13490–13495, 2007.
- Tort, A. B., Kramer, M. A., Thorn, C., Gibson, D. J., Kubota, Y., Graybiel, A. M., and Kopell, N. J. Dynamic cross-frequency couplings of local field potential oscillations in rat striatum

BIBLIOGRAPHY

- and hippocampus during performance of a t-maze task. *Proceedings of the National Academy of Sciences*, 105(51):20517–20522, 2008.
- Tort, A. B., Komorowski, R. W., Manns, J. R., Kopell, N. J., and Eichenbaum, H. Theta–gamma coupling increases during the learning of item–context associations. *Proceedings of the National Academy of Sciences*, 106(49):20942–20947, 2009.
- Tort, A. B., Komorowski, R., Eichenbaum, H., and Kopell, N. Measuring phase-amplitude coupling between neuronal oscillations of different frequencies. *Journal of neurophysiology*, 104(2):1195–1210, 2010.
- Toyoda, I., Bower, M. R., Leyva, F., and Buckmaster, P. S. Early activation of ventral hippocampus and subiculum during spontaneous seizures in a rat model of temporal lobe epilepsy. *Journal of Neuroscience*, 33(27):11100–11115, 2013.
- Toyoda, I., Fujita, S., Thamattoor, A. K., and Buckmaster, P. S. Unit activity of hippocampal interneurons before spontaneous seizures in an animal model of temporal lobe epilepsy. *Journal of Neuroscience*, 35(16):6600–6618, 2015.
- Uhlhaas, P. J. and Singer, W. High-frequency oscillations and the neurobiology of schizophrenia. *Dialogues in clinical neuroscience*, 15(3):301, 2013.
- Uhlhaas, P. J., Pipa, G., Neuenschwander, S., Wibral, M., and Singer, W. A new look at gamma? high-(> 60 Hz) γ -band activity in cortical networks: function, mechanisms and impairment. *Progress in biophysics and molecular biology*, 105(1-2):14–28, 2011.
- Urrestarazu, E., Chander, R., Dubeau, F., and Gotman, J. Interictal high-frequency oscillations (100–500 Hz) in the intracerebral EEG of epileptic patients. *Brain*, 130(9):2354–2366, 2007.
- Valentino, D. A., Arruda, J., and Gold, S. Comparison of qEEG and response accuracy in good vs poorer performers during a vigilance task. *International Journal of Psychophysiology*, 15(2):123–133, 1993.

BIBLIOGRAPHY

- van der Meij, R., Kahana, M., and Maris, E. Phase–amplitude coupling in human electrocortigraphy is spatially distributed and phase diverse. *Journal of Neuroscience*, 32(1): 111–123, 2012.
- van Wijk, B., Jha, A., Penny, W., and Litvak, V. Parametric estimation of cross-frequency coupling. *Journal of neuroscience methods*, 243:94–102, 2015.
- van Wijk, B. C., Beudel, M., Jha, A., Oswal, A., Foltynie, T., Hariz, M. I., Limousin, P., Zrinzo, L., Aziz, T. Z., Green, A. L., et al. Subthalamic nucleus phase–amplitude coupling correlates with motor impairment in parkinson’s disease. *Clinical Neurophysiology*, 127(4):2010–2019, 2016.
- van Wingerden, M., van der Meij, R., Kalenscher, T., Maris, E., and Pennartz, C. M. Phase–amplitude coupling in rat orbitofrontal cortex discriminates between correct and incorrect decisions during associative learning. *The Journal of Neuroscience*, 34(2):493–505, 2014.
- VanRullen, R. and Koch, C. Is perception discrete or continuous? *Trends in cognitive sciences*, 7(5):207–213, 2003.
- VanRullen, R. and Macdonald, J. S. Perceptual echoes at 10 hz in the human brain. *Current biology*, 22(11):995–999, 2012.
- Varela, F., Lachaux, J.-P., Rodriguez, E., and Martinerie, J. The brainweb: phase synchronization and large-scale integration. *Nature reviews neuroscience*, 2(4):229, 2001.
- Vierling-Claassen, D., Cardin, J., Moore, C. I., and Jones, S. R. Computational modeling of distinct neocortical oscillations driven by cell-type selective optogenetic drive: separable resonant circuits controlled by low-threshold spiking and fast-spiking interneurons. *Frontiers in human neuroscience*, 4:198, 2010.
- Von Stein, A. and Sarnthein, J. Different frequencies for different scales of cortical integra-

BIBLIOGRAPHY

- tion: from local gamma to long range alpha/theta synchronization. *International Journal of Psychophysiology*, 38(3):301–313, 2000.
- Voytek, B., D’Esposito, M., Crone, N., and Knight, R. T. A method for event-related phase/amplitude coupling. *Neuroimage*, 64:416–424, 2013.
- Wang, S., Wang, I. Z., Bulacio, J. C., Mosher, J. C., Gonzalez-Martinez, J., Alexopoulos, A. V., Najm, I. M., and So, N. K. Ripple classification helps to localize the seizure-onset zone in neocortical epilepsy. *Epilepsia*, 54(2):370–376, 2013.
- Wang, X.-J. Neurophysiological and computational principles of cortical rhythms in cognition. *Physiological reviews*, 90(3):1195–1268, 2010.
- Ward, L. M. Synchronous neural oscillations and cognitive processes. *Trends in cognitive sciences*, 7(12):553–559, 2003.
- Weiss, S. A., Banks, G. P., McKhann, G. M., Goodman, R. R., Emerson, R. G., Trevelyan, A. J., and Schevon, C. A. Ictal high frequency oscillations distinguish two types of seizure territories in humans. *Brain*, page awt276, 2013.
- Weiss, S. A., Orosz, I., Salamon, N., Moy, S., Wei, L., Van’t Klooster, M. A., Knight, R. T., Harper, R. M., Bragin, A., Fried, I., et al. Ripples on spikes show increased phase-amplitude coupling in mesial temporal lobe epilepsy seizure-onset zones. *Epilepsia*, 57(11):1916–1930, 2016.
- Wendling, A.-S., Hirsch, E., Wisniewski, I., Davanture, C., Ofer, I., Zentner, J., Bilic, S., Scholly, J., Staack, A. M., Valenti, M.-P., et al. Selective amygdalohippocampectomy versus standard temporal lobectomy in patients with mesial temporal lobe epilepsy and unilateral hippocampal sclerosis. *Epilepsy research*, 104(1-2):94–104, 2013.
- Wendling, F., Chauvel, P., Biraben, A., and Bartolomei, F. From intracerebral eeg signals to

BIBLIOGRAPHY

- brain connectivity: identification of epileptogenic networks in partial epilepsy. *Frontiers in systems neuroscience*, 4:154, 2010.
- White, T. P., Joseph, V., O'Regan, E., Head, K. E., Francis, S. T., and Liddle, P. F. Alpha-gamma interactions are disturbed in schizophrenia: a fusion of electroencephalography and functional magnetic resonance imaging. *Clinical Neurophysiology*, 121(9):1427–1437, 2010.
- Whittington, M. A. and Traub, R. D. Interneuron diversity series: inhibitory interneurons and network oscillations in vitro. *Trends in neurosciences*, 26(12):676–682, 2003.
- Wiebe, S. Effectiveness and safety of epilepsy surgery: what is the evidence? *CNS spectrums*, 9(2):120–132, 2004.
- Wiebe, S., Blume, W. T., Girvin, J. P., and Eliasziw, M. A randomized, controlled trial of surgery for temporal-lobe epilepsy. *New England Journal of Medicine*, 345(5):311–318, 2001.
- Winson, J. Loss of hippocampal theta rhythm results in spatial memory deficit in the rat. *Science*, 201(4351):160–163, 1978.
- Wolansky, T., Clement, E. A., Peters, S. R., Palczak, M. A., and Dickson, C. T. Hippocampal slow oscillation: a novel eeg state and its coordination with ongoing neocortical activity. *Journal of Neuroscience*, 26(23):6213–6229, 2006.
- Worrell, G. A., Lagerlund, T. D., Sharbrough, F. W., Brinkmann, B. H., Busacker, N. E., Cicora, K. M., and O'Brien, T. J. Localization of the epileptic focus by low-resolution electromagnetic tomography in patients with a lesion demonstrated by mri. *Brain topography*, 12(4):273–282, 2000.
- Wulff, P., Ponomarenko, A. A., Bartos, M., Korotkova, T. M., Fuchs, E. C., Böhner, F., Both, M., Tort, A. B., Kopell, N. J., Wisden, W., et al. Hippocampal theta rhythm and its coupling

BIBLIOGRAPHY

- with gamma oscillations require fast inhibition onto parvalbumin-positive interneurons. *Proceedings of the National Academy of Sciences*, 106(9):3561–3566, 2009.
- Zarate, J. M. and Zatorre, R. J. Experience-dependent neural substrates involved in vocal pitch regulation during singing. *Neuroimage*, 40(4):1871–1887, 2008.
- Zatorre, R. J., Evans, A. C., Meyer, E., and Gjedde, A. Lateralization of phonetic and pitch discrimination in speech processing. *Science*, 256(5058):846–849, 1992.
- Zhan, R.-Z., Timofeeva, O., and Nadler, J. V. High ratio of synaptic excitation to synaptic inhibition in hilar ectopic granule cells of pilocarpine-treated rats. *Journal of neurophysiology*, 104(6):3293–3304, 2010.
- Zhang, H., Watrous, A. J., Patel, A., and Jacobs, J. Theta and alpha oscillations are traveling waves in the human neocortex. *Neuron*, 98(6):1269–1281, 2018.
- Zhang, R., Ren, Y., Liu, C., Xu, N., Li, X., Cong, F., Ristaniemi, T., and Wang, Y. Temporal-spatial characteristics of phase-amplitude coupling in electrocorticogram for human temporal lobe epilepsy. *Clinical Neurophysiology*, 2017.
- Zhang, X., Zhong, W., Brankačk, J., Weyer, S. W., Müller, U. C., Tort, A. B., and Draguhn, A. Impaired theta-gamma coupling in app-deficient mice. *Scientific reports*, 6:21948, 2016.
- Zhang, Y., Yoshida, T., Katz, D. B., and Lisman, J. E. Nmdar antagonist action in thalamus imposes delta oscillations on the hippocampus. *Journal of neurophysiology*, 107(11):3181–3189, 2012.
- Zheng, C. and Zhang, T. Alteration of phase–phase coupling between theta and gamma rhythms in a depression-model of rats. *Cognitive neurodynamics*, 7(2):167–172, 2013.
- Zijlmans, M., Jacobs, J., Zelmann, R., Dubeau, F., and Gotman, J. High-frequency oscillations mirror disease activity in patients with epilepsy. *Neurology*, 72(11):979–986, 2009.